# MODELING BUILDING ENERGY USE AND HVAC EFFICIENCY IMPROVEMENTS IN EXTREME HOT AND HUMID REGIONS

A Thesis

by

MITCHELL RYAN BIBLE

Submitted to the Office of Graduate Studies of
Texas A&M University
in partial fulfillment of the requirements for the degree of

MASTER OF SCIENCE

August 2011

Major Subject: Mechanical Engineering

Modeling Building Energy Use and HVAC Efficiency Improvements in Extreme Hot and Humid Regions

Copyright 2011 Mitchell Ryan Bible

# MODELING BUILDING ENERGY USE AND HVAC EFFICIENCY IMPROVEMENTS IN EXTREME HOT AND HUMID REGIONS

A Thesis

by

MITCHELL RYAN BIBLE

Submitted to the Office of Graduate Studies of
Texas A&M University
in partial fulfillment of the requirements for the degree of

MASTER OF SCIENCE

Approved by:

| | |
|---|---|
| Co-Chairs of Committee, | Dennis O'Neal |
| | John Bryant |
| Committee Members, | Warren Heffington |
| | Charles Culp |
| Head of Department, | Jerald Caton |

August 2011

Major Subject: Mechanical Engineering

# ABSTRACT

Modeling Building Energy Use and HVAC Efficiency Improvements in Extreme Hot and Humid Regions. (August 2011)

Mitchell Ryan Bible, B.S., Texas A&M University

Co-Chairs of Advisory Committee: Dr. Dennis O'Neal
Dr. John Bryant

An energy analysis was performed on the Texas A&M University at Qatar building in Doha, Qatar. The building and its HVAC systems were modeled using EnergyPlus. Building chilled water and electrical data were collected to validate the computer simulation. The simulated monthly electricity consumption was within ±5% of the metered building data. Ninety-five percent of simulated hourly electricity data in a day were within ±10% of metered data. Monthly chilled water demand was within ±18% of measurements, and simulated monthly demand was correlated to metered monthly values with an R-squared correlation coefficient of 0.95.

Once the simulation was verified with the metered data, an optimization of the building's HVAC systems was performed. Better utilizing the building's variable speed fans at part loads showed potential annual electricity savings of 16% over the base case, with another 22% savings in chilled water energy. After converting chilled water savings to equivalent chiller electricity savings, the potential utility cost savings over the base case were found to be $90,000/yr at local utility rates.

Reducing outdoor air intake to ASHRAE indoor air quality minimums yielded an additional 17% in potential chilled water savings and brought total monetary savings over the base case to $110,000/yr. Using a dedicated outside air system to precisely control individual zone ventilation showed potential for an additional 12% chilled water savings and $14,000 in yearly utility savings, while also eliminating cases of under-ventilation.

A hypothetical retrofit of fan powered terminal units (FPTU's) resulted in energy savings only at very low minimum flow rates, below ventilation standards. Savings were never more than 20% over the no-fan case. Series FPTU's showed no savings at any flow setting and negligible difference was found between ECM and SCR motor control.

Finally, the dependence on climate of each improvement was studied. Simulations were run in the relatively milder climates of Houston and Phoenix and compared to those found for Doha. It was found that variable speed fan operation is a more cost effective option for milder climates, while outside air control is more cost effective in extreme hot and humid climates such as Doha. Future study is needed to make the FPTU model valid for different climates and flow ranges.

# ACKNOWLEDGEMENTS

I would like to thank my committee co-chair, Dr. O'Neal, for his guidance in directing me to the project, and also my other co-chair Dr. Bryant for his hands on assistance in Qatar. Thanks also to my committee members, Dr. Heffington and Dr. Culp for their assistance throughout the writing process, and to TAMUQ and Qatar Foundation for their financial and logistical support.

Finally, thanks to my mother and father, and to my wife for her love and willingness to follow me to the ends of the earth.

# TABLE OF CONTENTS

CHAPTER Page

# LIST OF FIGURES

Page

Page

Page

Page

# LIST OF TABLES

Page

# CHAPTER I

# INTRODUCTION

Building energy consumption makes up over a third of total energy use in the United States (Hunn 2010). In the Middle East, new building construction is increasing, and per capita energy use and carbon emissions are now among the highest in the world (Crawford-Brown 2009). Following the oil embargo of 1973 and ensuing energy crisis, building energy codes were put into place to curb consumption in the building sector and promote energy sustainability. These codes evolved and remain today with the American Society of Heating Refrigeration and Air-conditioning Engineer's (ASHRAE) standard 90.1 for commercial buildings. With the recent advent of standard 90.1-2010, baseline building energy consumption will have been reduced by nearly 50% from 1973 when the first standards were introduced (Hunn 2010), but potential for further savings still exists.

Of the total energy used in the building sector, as much as 45% goes toward heating, ventilating, and air-conditioning (HVAC) systems (Kreider et. al 2002). The primary function of these systems is to supply conditioned air to a building space to promote the comfort and health of its occupants. Sub-functions of this goal include cooling or heating the air to within a specified temperature range, filtering out particulate matter, providing fresh outside air, and moving the conditioned air throughout the building. The subsystems performing these functions interact with one another, and all

---

This thesis follows the style of *HVAC&R Research Journal*.

require energy in some form. Ideally, an HVAC system should *just* fulfill each of these needs using the least possible energy.

Unfortunately, coupling of multiple building spaces, along with transient external and internal heating and cooling loads on the building, make this difficult. The problem is more exaggerated in hot and humid climates, where cooling is more critical, latent loads are higher, and fresh air requirements greatly increase total cooling and dehumidification demand.

One tool engineers use to better understand and control HVAC systems is computer simulation. Building energy models, when carefully constructed and verified using building energy data, can help identify system deficiencies. They can also quickly and inexpensively test possible solutions, while giving quantitative estimates of the solutions' results. EnergyPlus is one energy simulation software commonly used in the industry, and as such it was chosen for this research.

The Texas A&M University at Qatar (TAMUQ) engineering building in Doha, Qatar, was studied as an example of a building in an extremely hot and humid region. Dry bulb temperatures in Doha can reach up to 52°C (125°F) in the summer, with dew point temperatures reaching 32°C (90°F) (OTBD Weather Station 2011). The TAMUQ building has both an academic and research wing. Analysis for this study focused on the academic wing. The academic wing has over 30,000 $m^2$ (300,000 $ft^2$) of floor area, and is served by 46 air handlers equipped with variable speed supply and return fans. A single chilled water pump room receives chilled water from an off-site central chilled water plant and distributes it throughout the building. Most of the building's HVAC

systems are newly installed, but many suffer from inefficient operation. The objective of this project is to quantify the potential savings from energy efficiency improvements by using an EnergyPlus model of the TAMUQ engineering building that has been verified with metered building energy data.

The remainder of this thesis presents a review of the relevant literature, followed by the methodology used to achieve the project objective. Results are presented, along with a discussion of their significance. Finally, general conclusions are drawn to serve as a guide for TAMUQ facilities and for future efficient HVAC design in extreme hot and humid environments.

# CHAPTER II

# LITERATURE REVIEW

Since building energy codes were first implemented, entities such as ASHRAE and the Energy Systems Laboratory (ESL) at Texas A&M University have researched building systems and performed building case studies to develop and improve methods for saving energy without compromising occupant comfort or air quality (ASHRAE 2010a). Some of these methods often only involve changing system settings. For example reducing fan static pressures where possible and varying cooling coil outlet temperature set points with ambient weather conditions can save around 5% on annual energy bills, with minimum capital input (Cho et al. 2007). Chilled water temperature resets during off-peak periods can also yield savings at the central plant by increasing the chiller coefficient of performance (COP) (Gidwani 1984).

Larger savings can often be realized from equipment retrofits. Replacing constant volume pumps and fans with variable frequency drives (VFD's) is a common recommendation, and has been shown to reduce yearly fan power consumption by over 70% (Cho et al. 2009). Even after these retrofits however, proper commissioning is essential to their efficient operation (Zhu et al. 2001). In the case of variable speed pumping for a chilled water system, Zhu et al. (2000) showed that proper balancing of the individual air handler unit (AHU) manual chilled water valves can improve chilled water pump power savings by 40% over baseline VFD operation.

To maximize the savings of a variable air volume (VAV) system at part-load, an effective control strategy is important for tracking cooling demand and optimizing cooling supply (Mathews et al. 2001; Kumar and Kar 2010; Ning and Zaheeruddin 2010; Platt et al. 2010; Wemhoff 2010). Even a simple night-time reset of air flow can reduce air volume by 40% and yield nearly 80% fan power savings during unoccupied hours (Liu et al. 2002). More complex control schemes aim to reduce air volumes and thus fan powers to their necessary minimums during all hours. Ning and Zaheeruddin (2010) used a neural network based control strategy to show more than 10% energy reductions compared to a standard night reset scheme. Wemhoff (2010) used multi-dimensional interpolation to determine optimal PID controller coefficients for varying zone load combinations, showing 6% savings over standard fixed coefficient control. These theoretical studies optimized control where the loads on the zones, and thus the AHU cooling requirements, were known a-priori. In reality, the building cooling load is time dependent and difficult to measure directly. Kumar and Kar (2010) proposed an optimized control scheme that used, along with other measurable quantities, human thermal comfort as a system input, in the form of the predicted mean vote (PMV). PMV is an internationally standardized index proposed by Fanger (1972). The scheme again showed savings over a base case, with the added benefit that adjusting set points via a human operator would be unnecessary.

A limiting factor in optimizing VAV control is indoor air quality (IAQ). A specified volume of fresh outdoor air must be supplied at all times to a space according to ASHRAE standard 62.1 (ASHRAE 2010b). Compromising IAQ in some cases has

been shown to cost more to occupant productivity than it gains in energy savings (Sterling et al. 1994; Mathews et al. 2001), meaning airflow cannot be modulated below a given point, limiting the controllability of the system. Cho and Liu (2009) developed an algorithm that incorporated IAQ standards along with allowances for less ventilation at higher outside temperatures. The algorithm reset the allowable minimum flow rates according to ambient conditions, thus maximizing energy savings while maintaining adequate ventilation.

Complying with outside air requirements also puts an additional strain on building cooling equipment. In hot and humid climates such as Doha, Qatar, the latent load on AHU cooling coils can equal or exceed the sensible load (Walker and Sherman 2006). The high latent loads can be mitigated through use of a desiccant wheel to exchange moisture with the dryer return air, at least partially decoupling the latent and sensible loads and decreasing the demand on the cooling coil (Fischer 2000). Utilizing return air to outside air heat recovery is required by ASHRAE standard 90.1 for systems using 2360 L/s (5000 CFM) or more of outside air (ASHRAE 2010c). A more efficient method for supplying fresh air in hot and humid climates is to precondition it with a single large air handler and distribute it to other AHU's for mixing with return air and supplying to the building zones. Such a dedicated outside air handler has been shown to decrease cooling energy use by over 20% (Zhao et al. 2010). Outside air intake is often larger than necessary in buildings, and proper adjustment to IAQ minimums can show immediate savings. Unfortunately, a large part of the IAQ requirement – as well as its intended benefit – depends on building occupancy levels, which are seldom known

exactly. Therefore, overestimation and inherent energy overuse are commonplace. Dong and Andrews (2009) developed a data mining technique to accurately predict occupancy levels from a variety of sensor data. Integrating this technique with the HVAC control system yielded total cooling and lighting energy savings of 30% compared to a fixed set point system with night reset, while maintaining occupant comfort and IAQ compliance.

Another issue in hot and humid climates is overcooling. In the summer, supply air must be cooled well below its dew point, usually to around 55°F (12.8°C), to dehumidify it sufficiently and meet comfort requirements. Often, this overcooling can make a space uncomfortably cold for occupants, even at the minimum airflow. To maintain occupant comfort without dropping the airflow below IAQ requirements, the air must be reheated, either by reheat coils in terminal units or by personal space heaters. This reheating of previously cooled air is a significant waste of energy that can be avoided through use of fan powered terminal units (FPTU's). FPTU's induce warmer return air to mix with the cold supply air when in heating mode (Furr et al. 2008; Cho and Liu 2009). Davis et al. (2009) developed a computer model to simulate FPTU performance using experimental data from several FPTU models (Furr et al. 2008; Cramlet 2008; Bryant et al. 2009).

To predict and quantify the potential savings from these changes, engineers often use computer simulations. EnergyPlus is a well known energy simulation tool with extensive development history with building energy professionals (Crawley et al. 2005). Architectural, occupancy, and other known data from the building and its systems are entered into these models. Any unknowns such as precise plug loads or building

infiltration are adjusted within reason, known in the industry as “calibrating”, until simulation data matches measured data. Lavigne (2009) outlined those parameters most often unknown and in the realm of “calibrate-able”, while Raftery et al. (2009) proposed general rules for keeping the calibration process evidence based. During this process, certain inputs can be assumed to be at or near the program’s default value, while others require extra effort on the modeler’s part to find an accurate on-site value (Wasilowski and Reinhart 2009). Shrestha (2006) tested the accuracy of individual elements within the EnergyPlus program. Zone level parameters such as duct outlet temperatures and flow rates were found to vary by up to ±17%. System level parameters such as chilled water return temperatures, outside air flow rate, and supply fan power were found to vary up to ±16%. Plant level parameters such as chiller compressor power and chilled water energy consumption had errors of up to ±29%. Given these inherent uncertainties, a model within ±15% of metered data should be considered valid.

Many of the studies presented above focused on a single method of improving building efficiency. Moreover, they were mostly theoretical in nature, being tested on a simplified single-zone model. This study integrates many approaches on a whole-building level, in an attempt to maximize potential savings. Those studies presented that were more comprehensive and performed on real buildings, were performed in climates much milder than experienced in Doha, Qatar. A larger goal for this project is to note which strategies have more pronounced effects in more extreme conditions, to serve as a guideline for future sustainable building in the Middle East and other hot and humid regions.

# CHAPTER III

# BUILDING ENERGY DATA

Two critical components to creating a valid and justified building energy model are evidenced based model inputs and model verification with measured data. Both of these rely on collecting energy data from the building being studied. This chapter summarizes the TAMUQ building and its systems, provides a discussion of the experimental apparatuses and procedures used to collect energy data from the building, and presents results of the data collection and what they mean in terms of inputs to the model.

## 3.1 TAMUQ Building Summary

Figure 1 shows a plan view of the TAMUQ building, with the academic section highlighted. The academic wing has four floors, one below ground and three above, each with a 5 m (15 ft) floor to floor height. The outer perimeter consists mostly of labs and classrooms. The inner core is occupied by a student lounge, computer labs, and a library, on the first, second, and third floors, respectively. An additional library floor occupies a fourth floor tower in the core section. There is no core section on the basement level. The hallways leading from perimeter to core hold offices. A small atrium is found at the east side entrance, and a larger one is found at the west end, linking the academic and research sides. Both atriums span the first, second, and third floors. Large lecture halls

occupy the south end. In total, the academic section studied has 30,800 $m^2$ (332,000 $ft^2$) of floor space. The window to above-ground exterior wall ratio is approximately 25%. The building has thick, 750 mm (30 in.) exterior walls, and has extensive exterior shading.

Weekends in Qatar are on Fridays and Saturdays, thus the building's hours of operation are approximately 8:00AM to 5:00PM Sundays through Thursdays. As it is a university, the building is occupied primarily by students. Enrollment at TAMUQ is approximately 450 students, and along with faculty and staff, the peak occupancy for the academic wing is estimated at around 600 people. Although there are summer classes offered, the student population decreases significantly in mid-May when the spring semester ends. Several breaks also occur during the main school year when both the student *and* non-student populations decrease. The Muslim holidays Eid Al-Fitr and Eid Al-Adha follow a lunar calendar, and resulted in week-long breaks in occupancy during mid-September and mid-November of 2010, respectively. A semester break occurs from mid-December to mid-January, and there is a week-long spring break in early March.

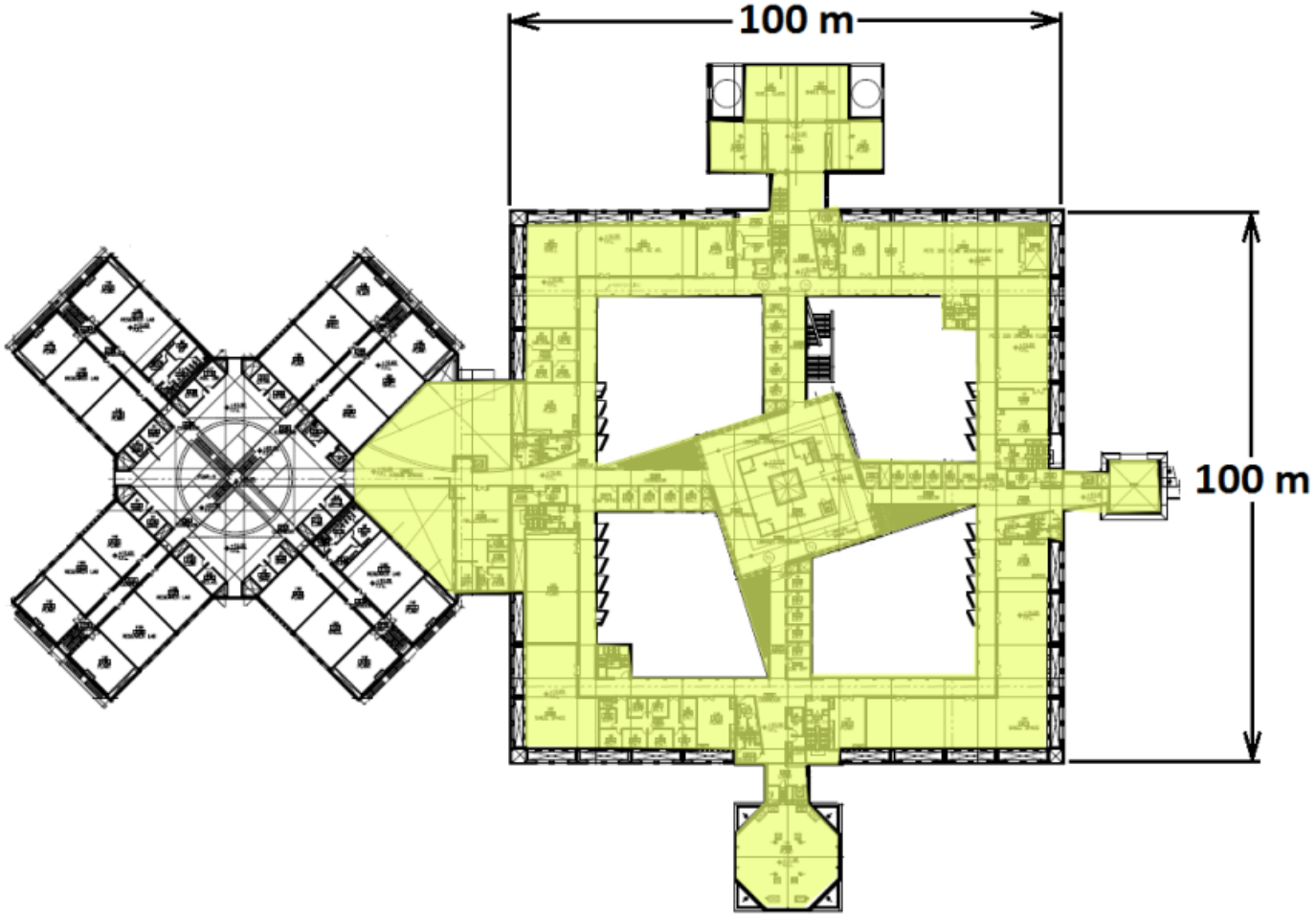


Figure 1. TAMUQ building plan view with highlighted academic wing.

Forty-six AHU's serve over 300 thermal zones around the building. Zones were considered as areas served by separate VAV terminal units. The AHU's are located in the positions shown in Figure 2. All AHU's have both supply and return fans equipped with VFD's, and the fans range in capacity from 800 L/s (1700 CFM) up to 7400 L/s (16000 CFM), several of which use 100% outside air. Cooling coils range in capacity from 10kW (3 tons) up to 580kW (170 tons), and all have heat pipe pre-cooling to recover energy from the exhaust air stream. Those AHU's using 100% outside air, 12 in total, are also equipped with a run-around coil for further exhaust air energy exchange. A run-around coil is an active system, as opposed to the passive heat pipes, that pumps water in a loop from the exhaust air stream to the outside air stream. Figure 3 shows a schematic with design specifications of a representative AHU in the building with run-around coil. No heating ability is installed in any AHU; instead, terminal unit reheat is used to maintain set points during cooler months. A detailed schedule of all academic side air handlers can be found in the appendix. The building's cooling needs are also supplemented by 67 fan coil units (FCU's) found primarily in stair wells, plant rooms, and certain zones in the basement level. Each floor also has four electrical and intermediate distribution frame (IDF) rooms that are served by individual direct expansion (DX) split units with chilled water cooled condensers.

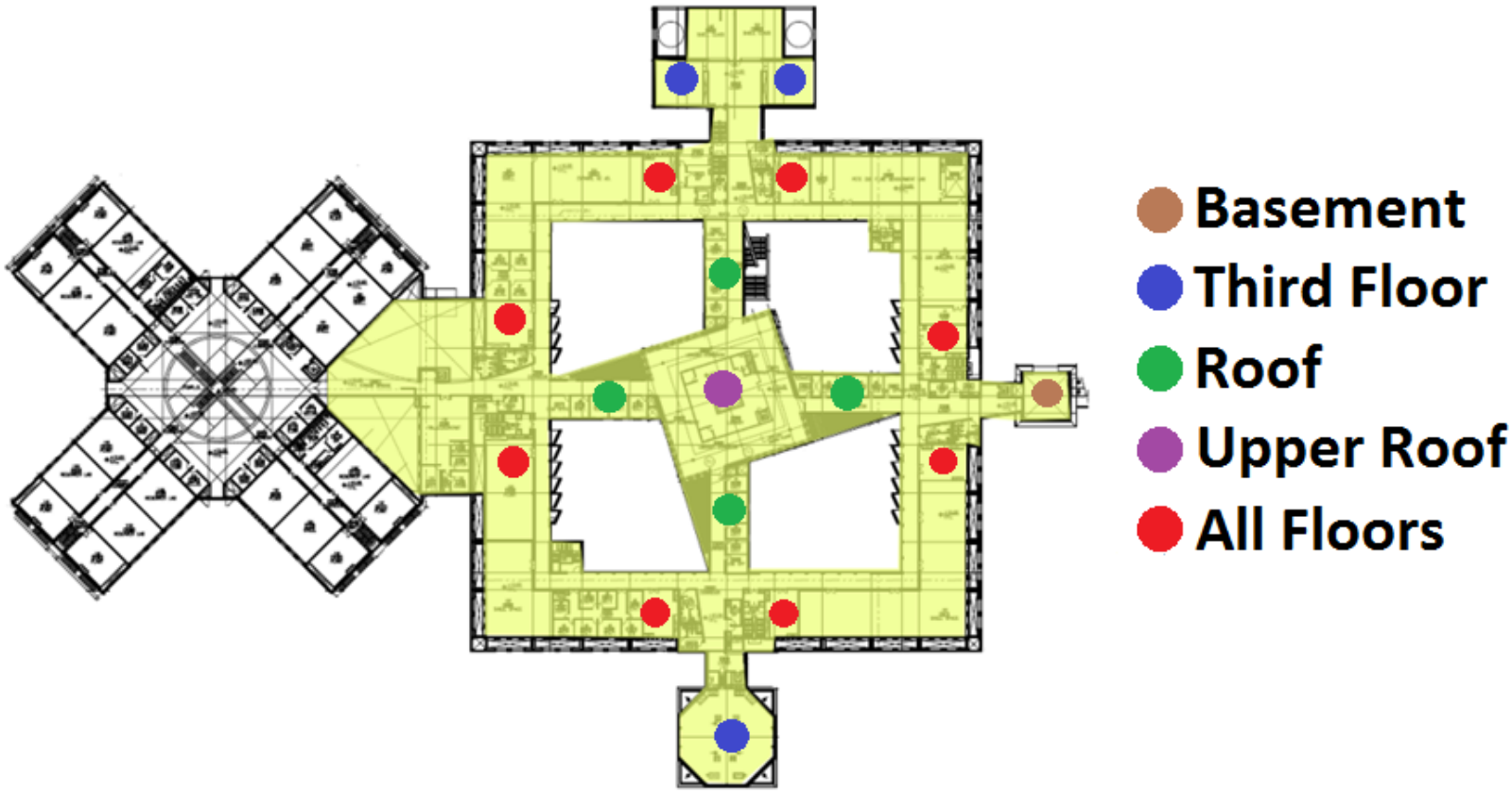


Figure 2. Locations of academic side air handlers around building.

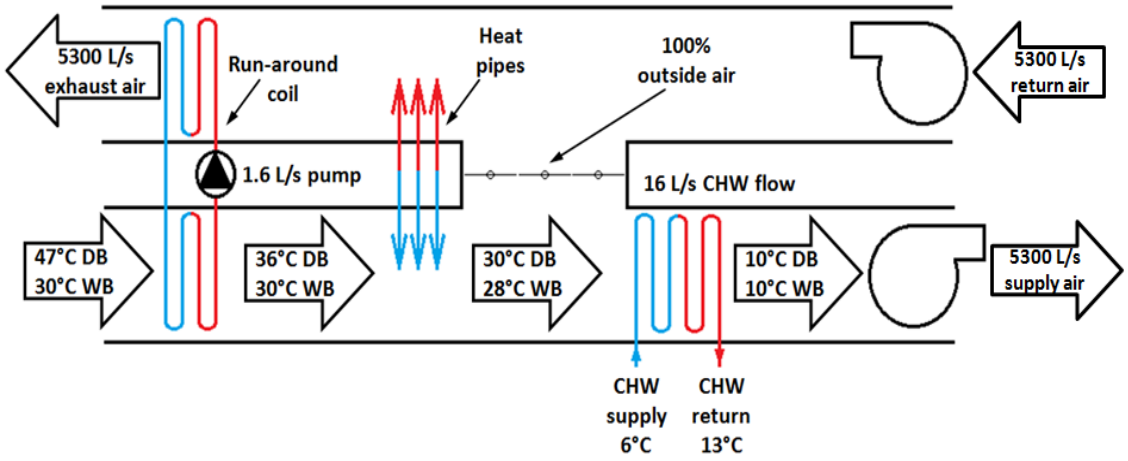


Figure 3. Schematic of 100% outside air-handler with run-around coil.

The chilled water pump room occupies the northeast corner of the basement floor, and distributes chilled water to all building AHU's, FCU's, and split unit condensers. Figure 4 shows a schematic of the pumps and heat exchangers in the pump room. Building return chilled water is circulated through four plate and frame heat exchangers where it exchanges energy with primary chilled water supplied from an off-site central chilled water plant. Three 250 L/s (4000 gpm), 55 kW (74 hp) constant speed pumps circulate this return building chilled water. Three 290 L/s (4600 gpm), 185 kW (250 hp) variable speed pumps are used to distribute the supply chilled water throughout the building.

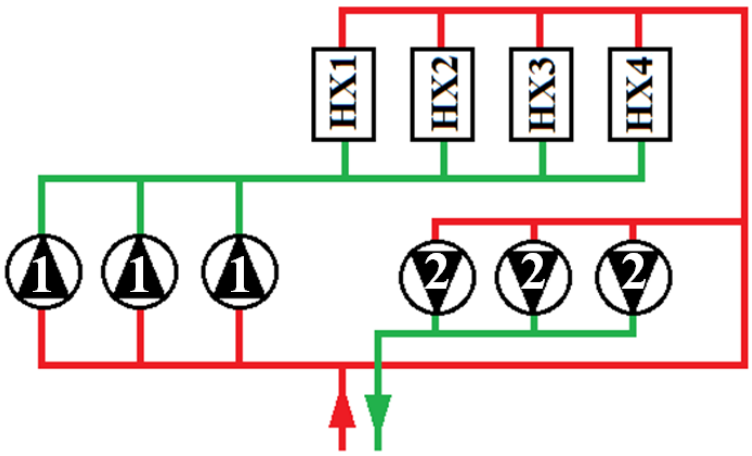


Figure 4. Pump room pump and heat exchanger schematic. Primary pumps are labeled 1, secondary pumps are labeled 2. Red lines denote low pressure sides and green lines denote high pressure sides.

The TAMUQ building has two power substations, one serving the research side, and one serving the academic side. The academic side substation is located in the north end of the academic wing on the basement level. Inside, four switchgear receive electricity from Qatar's power grid and distribute it to the building. Each switchgear is also equipped with 200 kVAR power factor correction equipment. Figure 5 is a photograph of the four switchgear in the academic power substation. A 500kW diesel generator is also present for emergency situations.

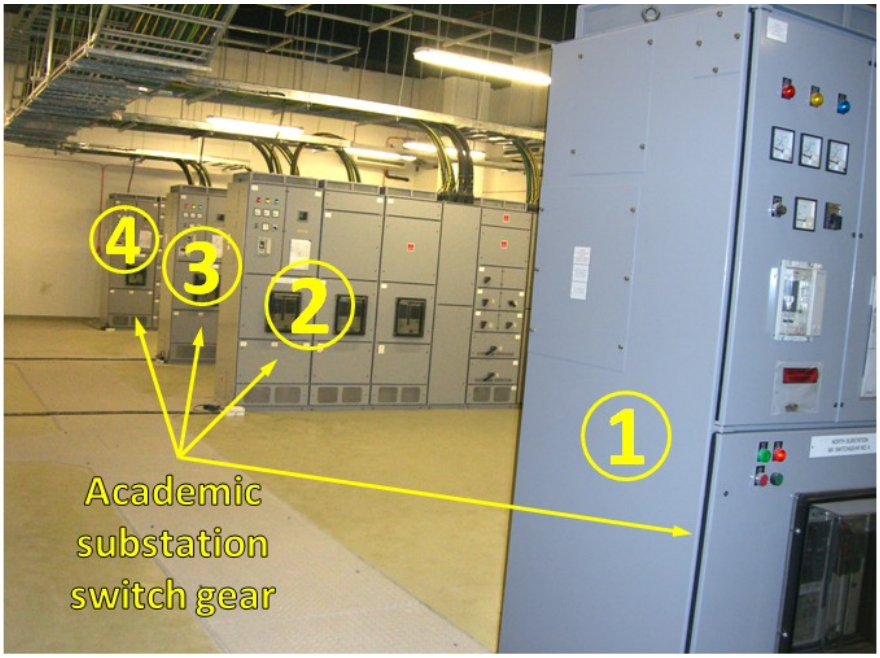


Figure 5. Switchgear supply power to academic wing of TAMUQ building.

The TAMUQ building was finished in 2005. Therefore, its systems and equipment are relatively new. The building was observed to be very well maintained and in good working condition. However, it appeared to be neither well commissioned nor optimally operated, which inspired the bulk of this research.

### 3.2 Data Collection

Two types of building energy data were collected to better define the model and aid in eventual validation. These were building electricity consumption and building chilled water usage. The following sections detail the equipment and procedures used to collect these data.

### *3.2.1 Electricity Consumption Metering*

Electricity metering took place in the academic power substation in Figure 5. Power distribution design drawings were analyzed to ensure that *only* power routed through the academic substation was used in the academic side on which the energy simulation was based, and that *all* the power routed through the academic substation was used in the academic side. Once this was verified, metering on all four academic switchgear using three-phase power meters began. Figure 6 shows one of the power meters set up in a switchgear. The meter's leads were connected to the line one (L1), line two (L2), line three (L3), and neutral (N) bus bars and the voltage and current across each phase was measured by the meter. The meters were set to calculate the average of measurements taken throughout every 15 minute interval, and record it to onboard flash memory. Onboard memory at this logging interval lasted around 45 days, at which point the data were uploaded to a computer, the flash memory was cleared, and logging began again.


Figure 6. Three-phase power metering setup on an academic switchgear.

For logistical reasons, there were times when the data could not be downloaded within the 45 day onboard memory limit. In some cases, days to weeks of data were lost during these periods. The percentage of data collected during each month for each switchgear is summarized in Table 1. Because EnergyPlus limits runtime to 12 months, only months in bold were chosen for direct comparison with simulation results. For cases where multiple months in different years were available, one was selected according to data completeness, minimal estimations needed to account for missing data, and runtime continuity.

Table 1. Electrical Metering Summary with Bold Months Compared to Simulated Data.

| Metered Month | SG1 Data Collected | SG2 Data Collected | SG3 Data Collected | SG4 Data Collected |
|---|---|---|---|---|
| **October-09** | **50%** | **50%** | **50%** | **50%** |
| **November-09** | **98%** | **98%** | **98%** | **98%** |
| **December-09** | **97%** | **97%** | **97%** | **97%** |
| **January-10** | **48%** | **48%** | **48%** | **48%** |
| **February-10** | **63%** | **63%** | **63%** | **2%** |
| **March-10** | **89%** | **89%** | **89%** | **0%** |
| **April-10** | **21%** | **21%** | **21%** | **21%** |
| **May-10** | **100%** | **100%** | **100%** | **100%** |
| **June-10** | **84%** | **84%** | **84%** | **84%** |
| **July-10** | **0%** | **0%** | **0%** | **0%** |
| **August-10** | **46%** | **46%** | **0%** | **46%** |
| **September-10** | **100%** | **100%** | **0%** | **100%** |
| October-10 | 2% | 2% | 0% | 2% |
| November-10 | 0% | 0% | 0% | 0% |
| December-10 | 46% | 46% | 46% | 46% |
| January-11 | 99% | 99% | 69% | 99% |

To reduce the effect of the data gaps, electrical data from the simulation and the building were compared month to month. The monthly metered electricity consumption was estimated from an average of the hourly consumption that *was* recorded within that month. Because the consumption was relatively constant, as will be seen in the results, and because the weather in Qatar generally changes only slightly day-to-day and even week to week, the intra-month averaging strategy was not expected to introduce significant error. Figure 7 shows a test of this error using May 2010 and November 2009

data that were 100% and 98% complete, respectively. The two smallest fractions of data gathered within a month were 21% and 46% of the month. Figure 7 simulates the effects of using the partial data to estimate the total monthly electricity consumption. The resulting averaged estimation is plotted as a function of position in the month that the partial data was available. The error when using only 21% of the month's electrical data was less than ±2.4% and ±3.5% for the May and November tests, respectively, with 90% confidence. The error when using 46% of the month's data was ±0.6% and ±1.7%. All other partially metered months had more than 46% of data available, so these errors represent upper limits.

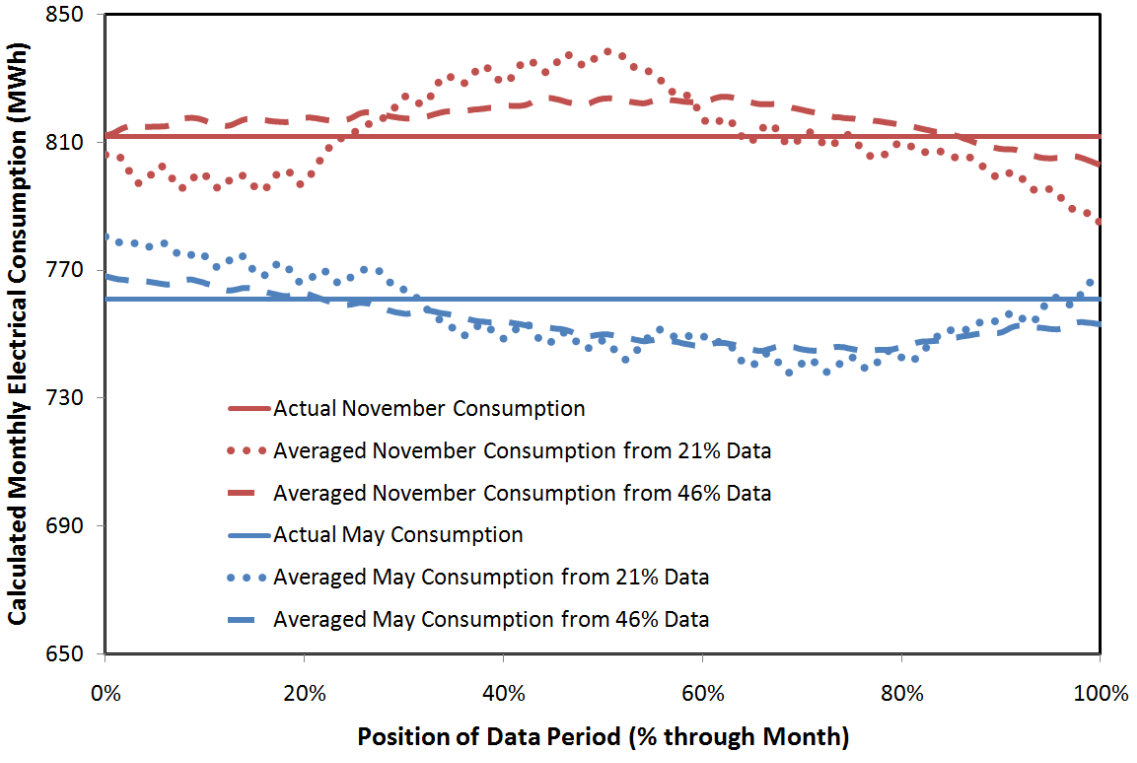


Figure 7. Error when estimating monthly consumption from partial month data.

The power meters were supplied with 220V mains electricity from a nearby outlet. While collecting data, a single meter became unplugged four times, twice from switchgear three and twice from switchgear four, and over a month of data was lost for that period. For such periods, the missing switchgear's power was estimated from existing data. The amount of data that had to be estimated during each metered month is also shown in Table 1.

When the power data from all switchgear were available, the fraction of one switchgear power out of the remaining three was calculated from

$$\beta_3 = \frac{P_3}{P_1+P_2+P_4}, \tag{1a}$$

$$\beta_4 = \frac{P_4}{P_1+P_2+P_3}. \tag{1b}$$

$P$ is the metered electric power and the subscripts denote the switchgear number as designated in Figure 5. During periods of missing data, the total power could then be estimated from

$$P_{total} = \begin{cases} \left(1+\overline{\beta_3}\right)(P_1+P_2+P_4), & switchgear\ 3\ missing \\ \left(1+\overline{\beta_4}\right)(P_1+P_2+P_3), & switchgear\ 4\ missing \end{cases}. \tag{2}$$

$\overline{\beta_3}$ and $\overline{\beta_4}$ are the time averaged values of $\beta_3$ and $\beta_4$ during the time all meters were operational. Only switchgear 3 and 4 were disconnected during metering.

Figure 8 shows $\beta_3$ and $\beta_4$ throughout the metering period when data from all four switchgear were available. The solid lines across the plot show the averaged values $\overline{\beta_3}$ and $\overline{\beta_4}$ that were used in estimating the total power. The dashed lines show the uncertainty of $\overline{\beta_3}$ and $\overline{\beta_4}$ with 90% confidence assuming a normal distribution. $\overline{\beta_3}$ was

found to be 0.4±0.08, while $\overline{\beta_4}$ was found to be 0.23±0.04. The resultant uncertainty in the total power is given by the equation from Kline and McClintock (1953):

$$\mu_{P_{total}} = \sqrt{\left(\frac{\partial P_{total}}{\partial \overline{\beta_3}}\mu_{\overline{\beta_3}}\right)^2 + \left(\frac{\partial P_{total}}{\partial P_1}\mu_{P_1}\right)^2 + \left(\frac{\partial P_{total}}{\partial P_2}\mu_{P_2}\right)^2 + \left(\frac{\partial P_{total}}{\partial P_4}\mu_{P_4}\right)^2}. \quad (3)$$

$\mu$ is the absolute uncertainty in each variable. A similar equation was used when switchgear 4 was estimated. $\mu_{P_{total}}$ was the uncertainty introduced when estimating one of the switchgear power readings. Because the inherent uncertainties of the other switchgear values remained the same in this case, they could be eliminated from Equation 3. Taking the partial derivative of $P_{total}$ from Equation 2 and dividing both sides by $P_{total}$ yielded the relative uncertainty:

$$\frac{\mu_{P_{total}}}{P_{total}} = \begin{cases} \frac{\mu_{\overline{\beta_3}}}{1+\overline{\beta_3}}, & switchgear\ 3\ missing \\ \frac{\mu_{\overline{\beta_4}}}{1+\overline{\beta_4}}, & switchgear\ 4\ missing \end{cases}. \quad (4)$$

Substituting the values found above, the relative uncertainty in total power when switchgear 3 was missing was ±5.7%. When switchgear 4 was missing it was ±3.2%. This was well within the inherent uncertainties of the individual components of EnergyPlus as measured by Shrestha (2006), and thus was considered acceptable.

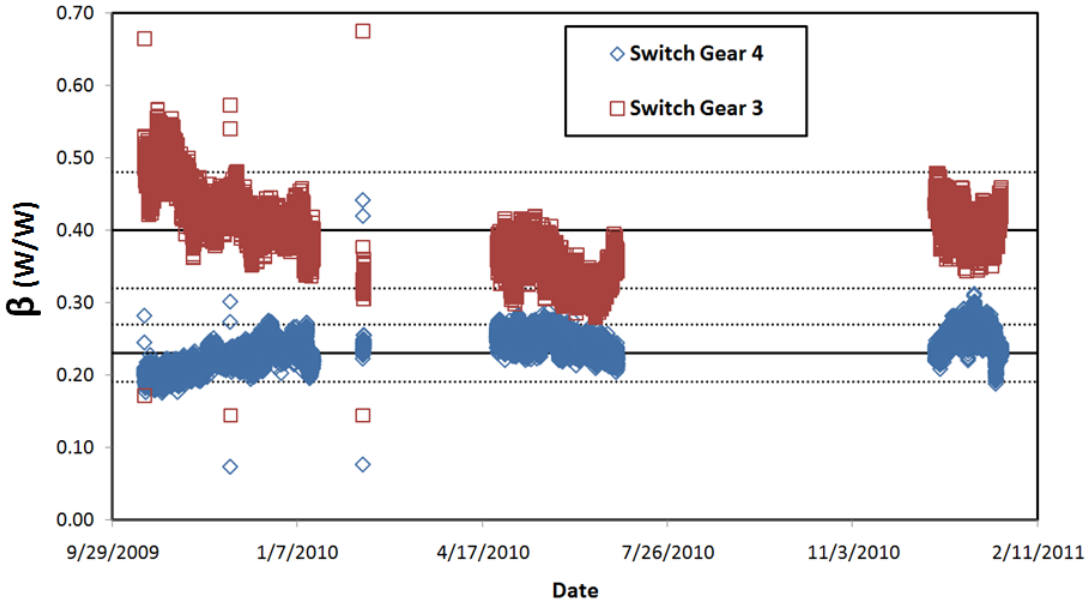


Figure 8. Measured $\beta_3$ and $\beta_4$ when all meters were operational. Solid lines show $\overline{\beta_3}$ and $\overline{\beta_4}$. Dashed lines show uncertainty in $\overline{\beta_3}$ and $\overline{\beta_4}$ with 90% confidence.

Power factor was also metered from the switchgear. TAMUQ power factor was quite high throughout the metering period, averaging around 0.97, and never falling below 0.95. Because of the high power factor due to the power factor correction equipment, its effects were in general neglected in this analysis.

### *3.2.2 Chilled Water Consumption Metering*

The chilled water supply for both research and academic wings originates from a single pump room. Isolating the academic load was therefore more difficult than it was with electrical metering. Figure 9 shows a diagram of the main chilled water branches from the pump room. The supply splits east and west immediately with the east branch

serving only the academic wing. The west branch splits again at the research/academic link, where one sub-branch serves the entire research wing, and the other serves the academic wing. The return branches follow the same paths in reverse back to the pump room.

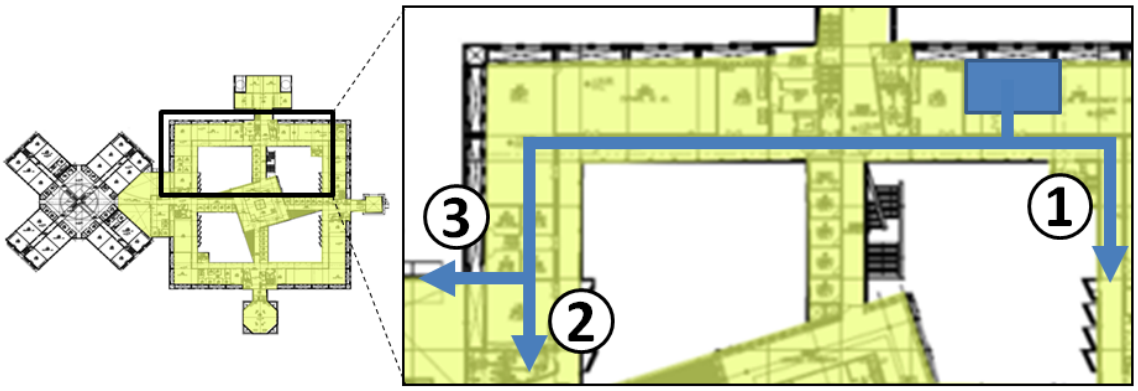


Figure 9. Main chilled water branches from the pump room. (1) and (2) serve the academic side only while (3) serves research side only. Return branches follow same paths back to pump room in reverse.

Originally, chilled water metering was placed at points A and B in Figure 10. When the scope of the project was focused on the academic wing, additional metering was added at point C to isolate the separate research and academic loads.

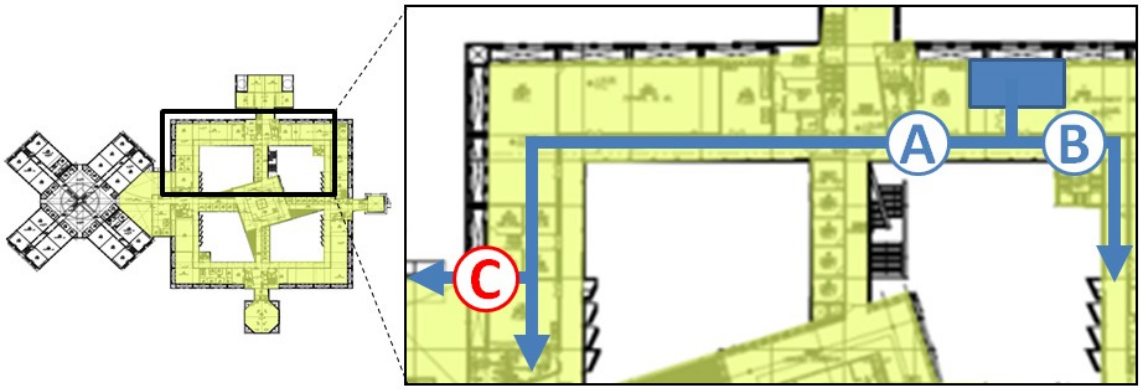


Figure 10. Original (A and B) and later added (C) chilled water metering positions.

After all chilled water metering was in place, the academic side load was determined from

$$Q_{academic} = Q_B + Q_A - Q_C, \quad (5)$$

where $Q$ was the cooling load. The cooling load at each metering position was calculated from

$$Q = \rho_w \dot{V} c_{p,w} (T_{r,w} - T_{s,w}), \quad (6)$$

where $\rho_w$ was the density of water, $c_{p,w}$ was the specific heat of water, $\dot{V}$ was the volume flow rate, and $T_R$ and $T_S$ were the supply and return temperatures, respectively. Density and specific heat were assumed constant over the temperature ranges measured. Therefore, flow rate and supply/return temperatures were the only quantities to be metered.

Flow rates were measured using ultrasonic flow meters. Ultrasonic flow meters directly measure the velocity of a fluid in a pipe from disturbances in sound wave propagation due to the flow. The meters were attached to their respective pipe sections

as shown in Figure 11, where the transducer spacing was a function of the pipe diameter. Conversions from velocity to volume flow were calculated automatically by the meters once the pipe diameter was specified. The flow meters used had accuracies of ±1% for flow velocities between 0 and 12 m/s (0 and 40 ft/s).

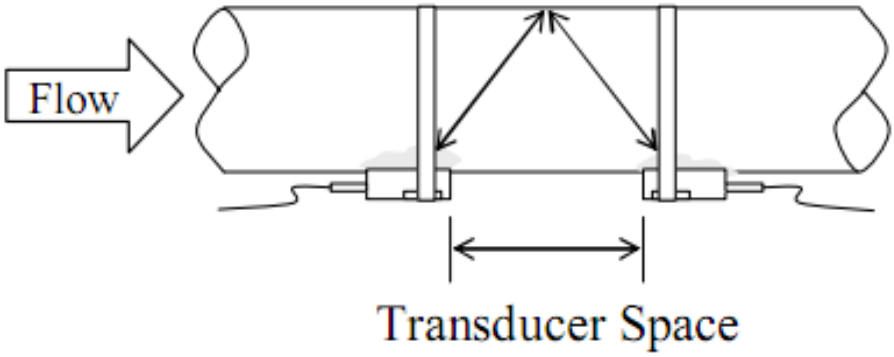


Figure 11. Ultrasonic flow metering setup (Sierra 2009).

Supply and return temperatures were metered using 1000Ω platinum resistive temperature devices (RTD's), with a ±0.1% accuracy at 0°C (32°F). The RTD leads were bonded to bare pipe on both supply and return sides using thermal grease, and the pipe's insulation was replaced, making the outer pipe temperature a close approximation of the internal fluid temperature. The temperature difference between supply and return ($\Delta T_{CHW}$) was the value of interest for determining energy use. Thus, any temperature rise across the pipe wall due to heat loss would apply to both supply and return sides, thereby having a negligible effect on the load calculation. An audit of the AHU cooling coil inlet temperature sensors in the TAMUQ building was conducted. Functioning inlet

temperature readouts were verified to be within ±1°C (±1.8°F) of the metered chilled water supply pipe temperature at that time. Similar to the electrical metering, flow and temperature data were measured every minute, averaged over a 15 minute interval, and logged to an external data logger.

As with the electrical metering, problems arose due to power outages, equipment malfunction, and data logger memory shortage. This led to missing data periods for some of the flow and temperature meters. Table 2 summarizes the percentage of each month that complete data were collected at each metering point labeled in Figure 10, as well as the percentage of each month where at least some data were collected while one sensor was malfunctioning.

Table 2. Chilled Water Metering Summary with Bold Months Compared to Simulated Data.

| Metered Month | Complete Data at A | At Least Partial Data at A | Complete Data at B | At Least Partial Data at B | Complete Data at C | At Least Partial Data at C |
|---|---|---|---|---|---|---|
| **October-09** | **53%** | **53%** | **53%** | **53%** | **0%** | **0%** |
| **November-09** | **44%** | **44%** | **44%** | **44%** | **0%** | **0%** |
| **December-09** | **97%** | **97%** | **97%** | **97%** | **0%** | **0%** |
| **January-10** | **54%** | **79%** | **54%** | **79%** | **0%** | **0%** |
| **February-10** | **63%** | **80%** | **63%** | **80%** | **0%** | **0%** |
| **March-10** | **15%** | **15%** | **15%** | **15%** | **0%** | **0%** |
| **April-10** | **21%** | **21%** | **21%** | **21%** | **0%** | **0%** |
| **May-10** | **72%** | **72%** | **72%** | **72%** | **0%** | **0%** |
| **June-10** | **100%** | **100%** | **100%** | **100%** | **0%** | **0%** |
| **July-10** | **4%** | **100%** | **4%** | **100%** | **0%** | **0%** |
| **August-10** | **0%** | **100%** | **0%** | **100%** | **0%** | **0%** |
| **September-10** | **62%** | **100%** | **62%** | **100%** | **0%** | **0%** |
| October-10 | 100% | 100% | 100% | 100% | 0% | 0% |
| November-10 | 100% | 100% | 100% | 100% | 0% | 0% |
| December-10 | 100% | 100% | 14% | 100% | 47% | 47% |
| January-11 | 53% | 100% | 0% | 100% | 100% | 100% |

Figure 12 shows a plot of $\Delta T_{CHW}$ measured over time at metering points A and B. Note that the values fluctuate more frequently from month to month than in the case of the electricity data. Note also that the magnitudes of the fluctuations are much more significant, up to 60% up or down from the mean value. Taking a global average of all metered $\Delta T_A$'s and $\Delta T_B$'s would yield estimated values for missing periods of 4.0±1.2 °C (7.2±2.2 °F) and 2.4±1.4 °C (4.3±2.5 °F), respectively, at 90% confidence assuming normal distribution. Because $Q$ is directly proportional to $\Delta T_{CHW}$, and therefore the uncertainty in $\Delta T_{CHW}$, this could mean possible errors in the estimated loads of 43% for meter A and 140% for meter B. To help reduce the uncertainty, more local averages were used to estimate missing data points. For periods where data were missing, an estimate for $\Delta T_{CHW}$ was used that averaged all existing data points within the same month as the missing period or the months immediately before or after. This helped both in decreasing the uncertainty itself in most cases, and also in providing a more seasonally accurate mean value around which to center the uncertainties. The results of the local averaging are given in Table 3. As with the electrical data, the monthly chilled water consumption that was compared with simulation results was calculated by taking the average hourly consumption for existing data points within that month and multiplying by the number of hours in that month. This also helped to average the data and minimize any error introduced by the missing temperature estimates.

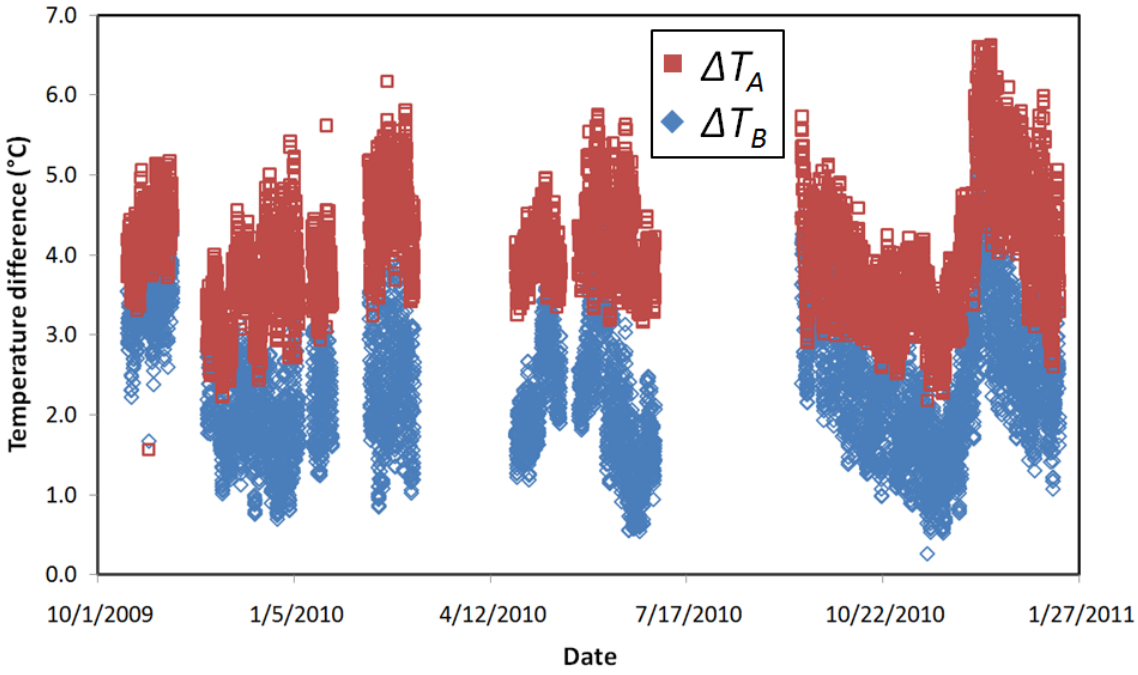


Figure 12. Chilled water temperature rises at metering points A and B.

Table 3. Local $\Delta T$ Values Used to Estimate Missing Temperature Data.

| Month | Average $\Delta T_A$ (°C) | Average $\Delta T_B$ (°C) |
|---|---|---|
| January | 4.2 ± 1.1 | 2.3 ± 1.1 |
| February | 4.2 ± 1.1 | 2.3 ± 1.1 |
| March | 4.4 ± 1.0 | 2.3 ± 1.1 |
| April | 4.1 ± 0.7 | 2.3 ± 1.0 |
| May | 4.1 ± 0.8 | 2.2 ± 1.3 |
| June | 4.1 ± 0.8 | 2.2 ± 1.3 |
| July | 4.1 ± 0.9 | 2.0 ± 1.5 |
| August | 4.1 ± 1.0 | 3.2 ± 1.3 |
| September | 3.8 ± 0.9 | 2.8 ± 1.3 |
| October | 3.7 ± 1.0 | 2.5 ± 1.4 |
| November | 3.9 ± 1.3 | 2.4 ± 1.5 |
| December | 4.0 ± 1.5 | 2.3 ± 1.5 |

Chilled water metering at point C in Figure 10 was only operational for the last two months of data collection, December of 2010 to January of 2011. During this time, the academic chilled water load was calculated using Equation 5. The academic load before this time was estimated by assuming the percentage contribution of $Q_C$ to $Q_A$ was approximately constant. $Q_{academic}$ when $Q_C$ is unknown could then be calculated from

$$Q_{academic} = Q_A + Q_B - \overline{\left(\frac{Q_C}{Q_A}\right)} Q_A, \qquad (7)$$

where the bracketed term represented the average percentage contribution of $Q_C$ to $Q_A$ throughout the time $Q_C$ was metered directly. Figure 13 shows $Q_C/Q_A$ as a function of time for the period $Q_C$ was metered. It can be seen that while not strictly constant, $Q_C/Q_A$

follows a periodic relationship with time throughout each day. Each peak seen in Figure 13 occurs on consecutive days between 12:00 and 14:00 in the afternoon. A higher resolution view in Figure 14 shows the mid-day peaks for December 19 and 20. The average daily peak amplitude over the metered days was 12.1%±7.3% with 90% confidence assuming a normal distribution. From an uncertainty equation analogous to Equation 3, the maximum relative uncertainty for the total academic load introduced by using Equation 7 was ±8%. While uncertainty was larger than in the case of the electrical metering, it was again minimized by comparing chilled water usage across month-long time scales.

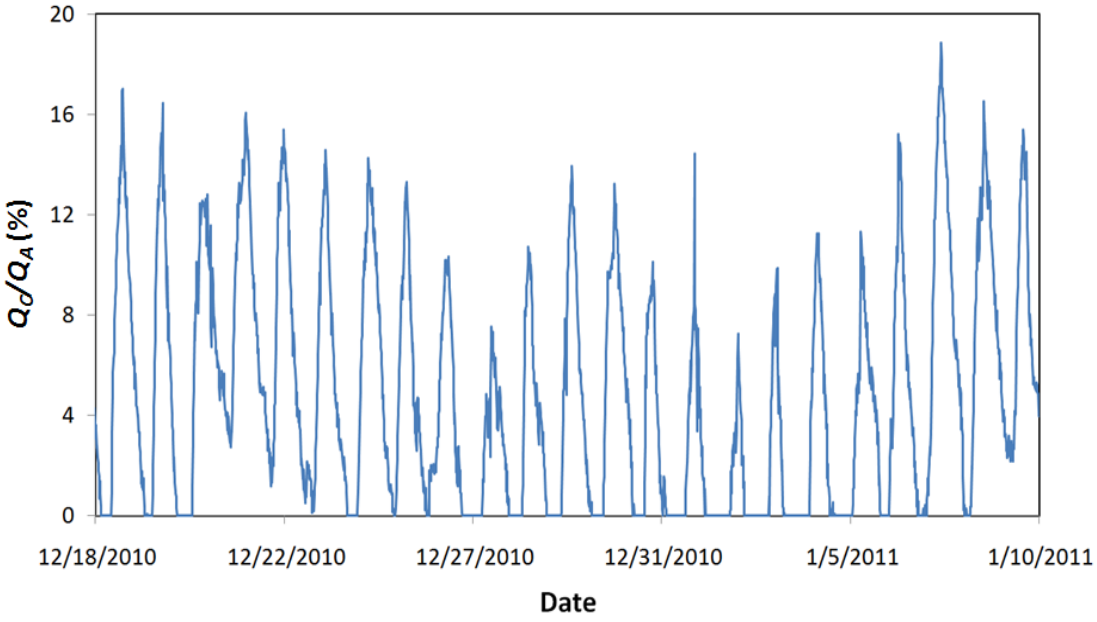


Figure 13. $Q_C$ as a percentage of $Q_A$ when metering at point C.

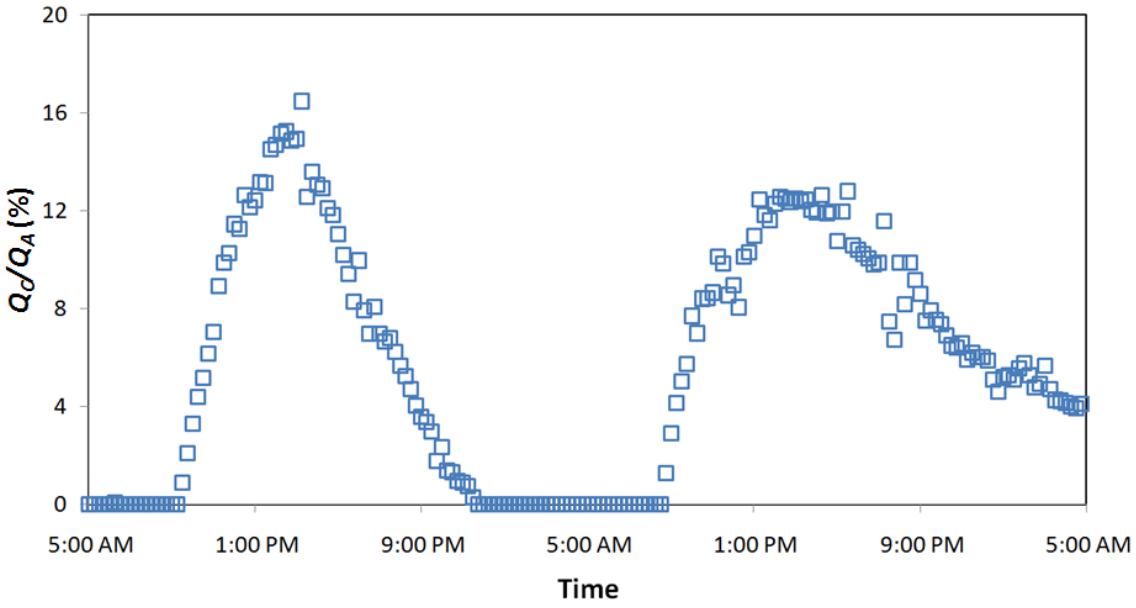


Figure 14. Example of $Q_C/Q_A$ peaking mid-day on December 19 and 20.

### 3.3 Metering Results and Discussion

After the electricity and chilled water consumption data were collected they were analyzed for use in modeling the building, and again for validating the simulation results. Figure 15 shows the total metered or partially estimated electricity consumption for each bold month in Table 1. Because July data were unavailable, the consumption value for July in Figure 15 was interpolated linearly from values in June and August. The monthly electricity consumption shown remained relatively constant throughout the year, despite significant changes in ambient weather conditions. The seasonal effect on the TAMUQ electrical bill should be less pronounced than for a typical building because

the chillers were in this case off-site. The effects of weather changes on the TAMUQ airside HVAC components were notably absent.

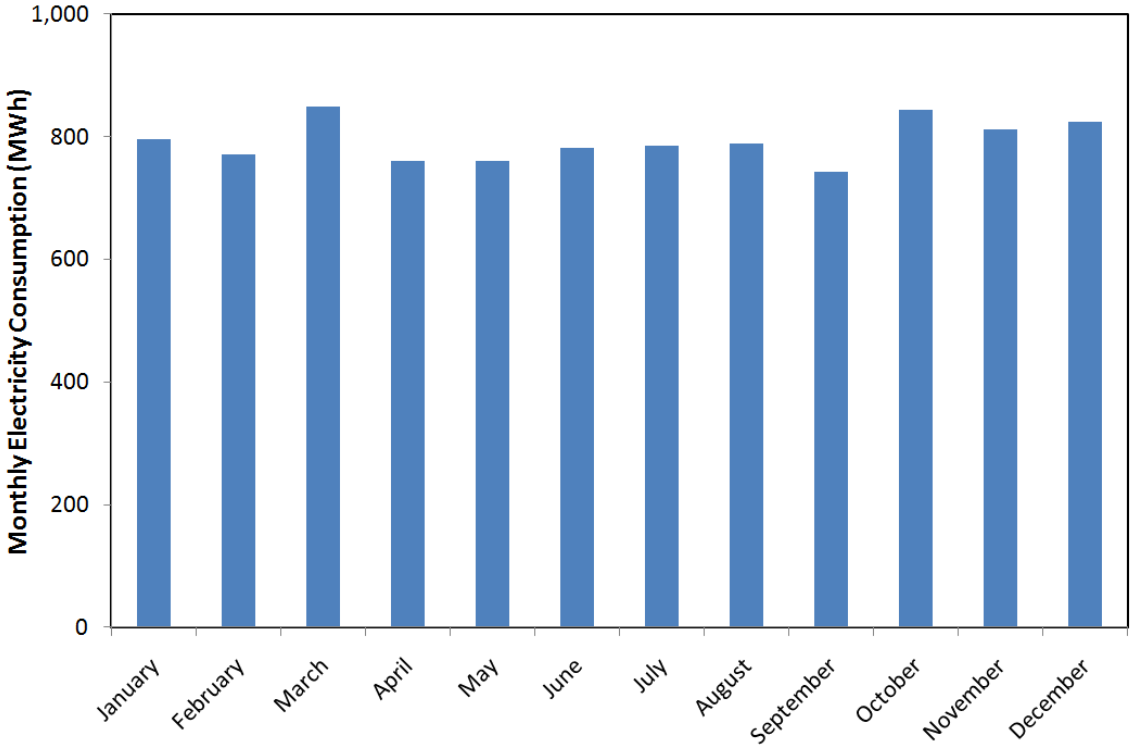


Figure 15. Monthly electricity consumption. The value for July is interpolated.

Figure 16 shows the total metered or partially estimated chilled water consumption for each bold month in Table 2. Recall that the $\overline{Q_C / Q_A}$ term in Equation 7 was an average taken over a month-long time scale to minimize the daily oscillations seen in Figure 13. Therefore, only monthly values for chilled water consumption were analyzed and compared to the simulation results. The chilled water depended on the season, unlike the electrical consumption.

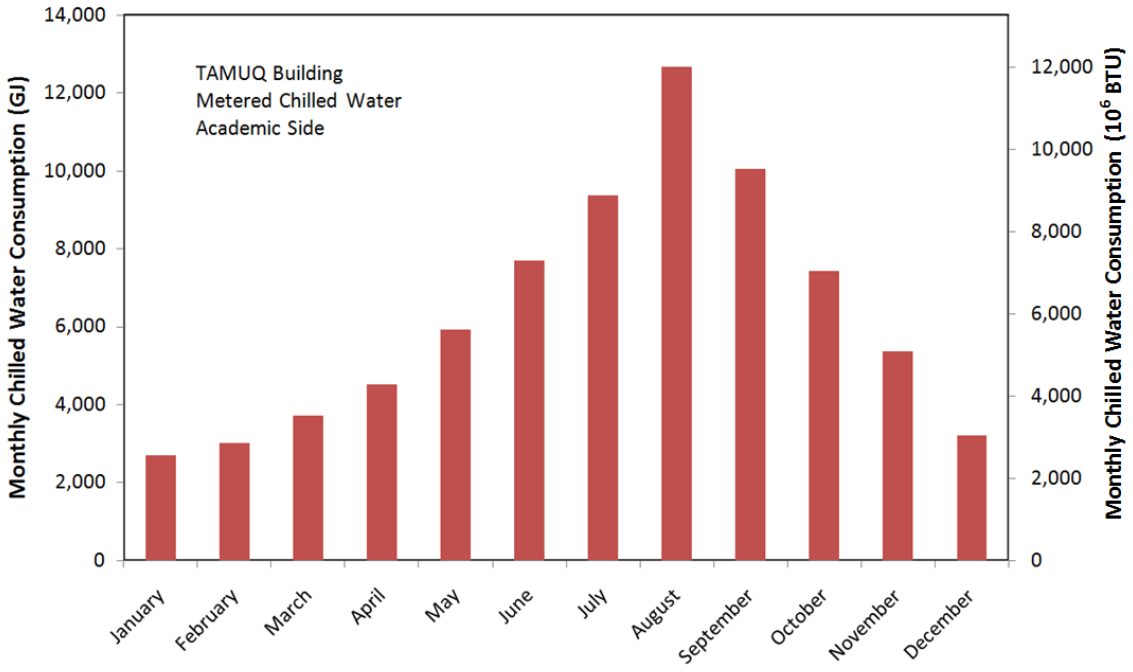


Figure 16. Monthly chilled water consumption.

To further demonstrate the counterintuitive constant electrical usage, the first week of spring semester classes, in the winter when conditions are among the mildest of the year, was compared to the first week of fall classes, in summer when conditions are still quite hot. The results are shown in Figure 17, along with the associated building loads over those periods, normalized to the maximum seen during the year. Note that the total load in winter is near zero and even negative at times, meaning heating was required. Though not as extreme as the sensible loads seen earlier in the summer, the summer loads shown are still considerably higher than in winter. In contrast, the summer and winter electricity usages are essentially identical.

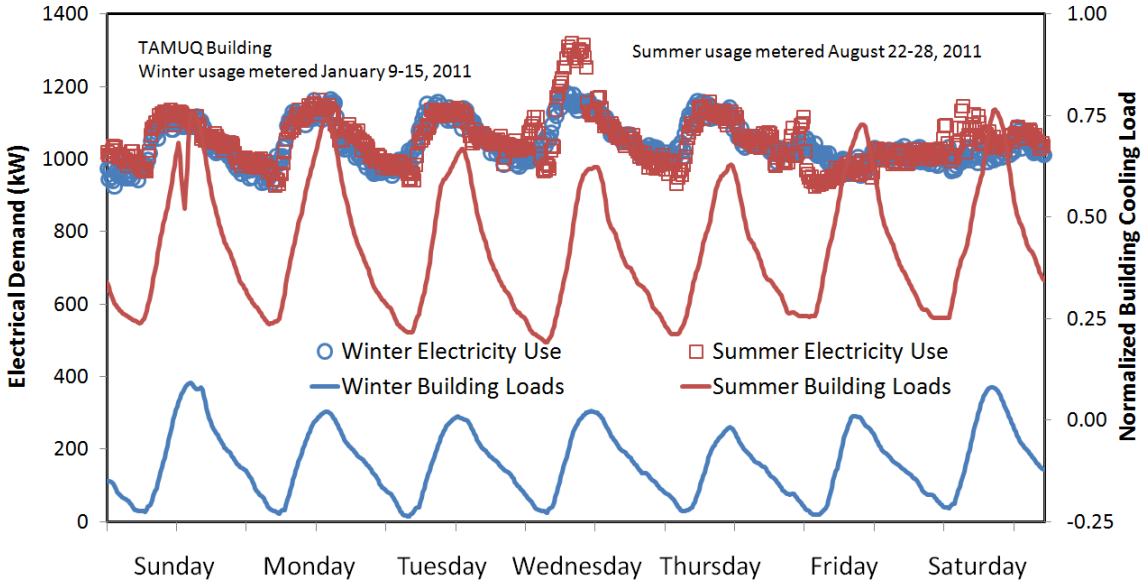


Figure 17. First week of spring classes vs. first week of fall classes with associated cooling loads at TAMUQ.

For comparing the average hourly consumption throughout a day, the data were placed into six categories. First they were separated by season, either hot or mild. Figure 18 shows the monthly mean temperatures for Doha, Qatar, during the bold months in Table 1 (OTBD Weather Station 2011). The ASHRAE Standard 55 indoor thermal comfort temperature limit is plotted as a measure of what is considered hot or mild (ASHRAE 2004). Days from April through October were deemed "hot", while all others were deemed "mild". Within the seasons the data were separated by occupancy: either a weekday with full occupancy, a weekend with minimal occupancy, or a student break with medium staff-and-faculty-only occupancy. All days within each category were overlaid and their electricity consumptions at each time step were averaged together. An average day's power usage for each category is shown in Figure 19.

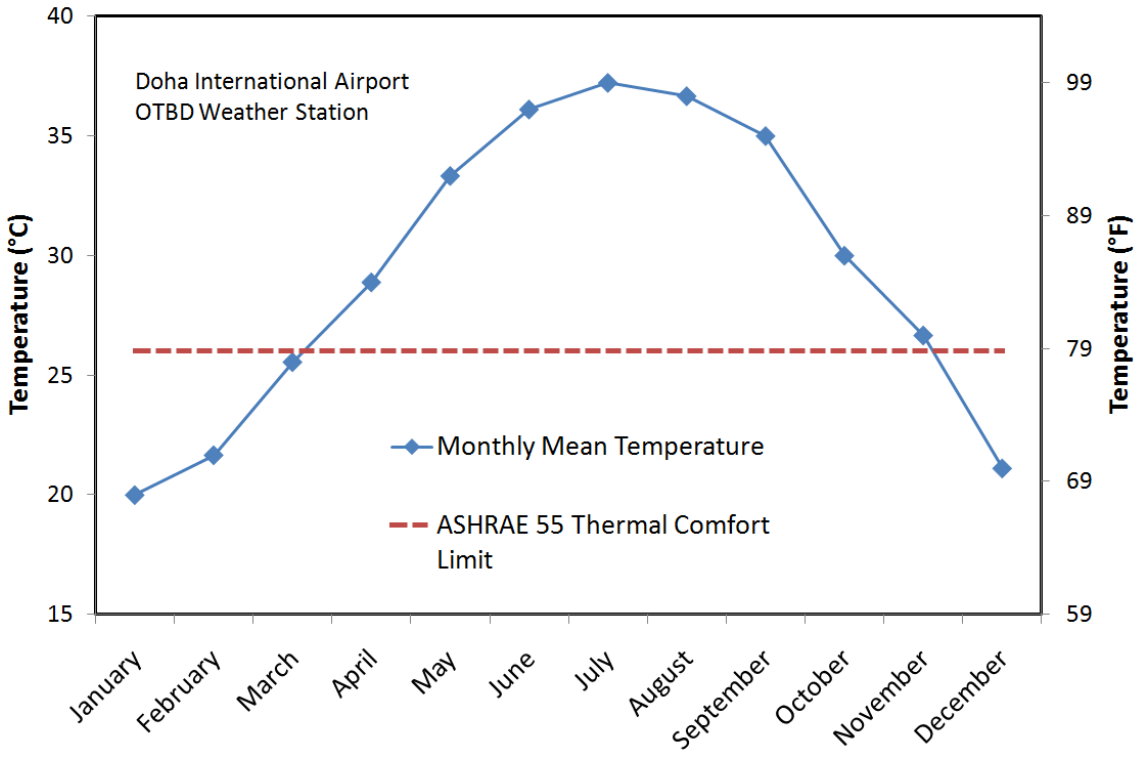


Figure 18. Doha monthly mean temperatures.

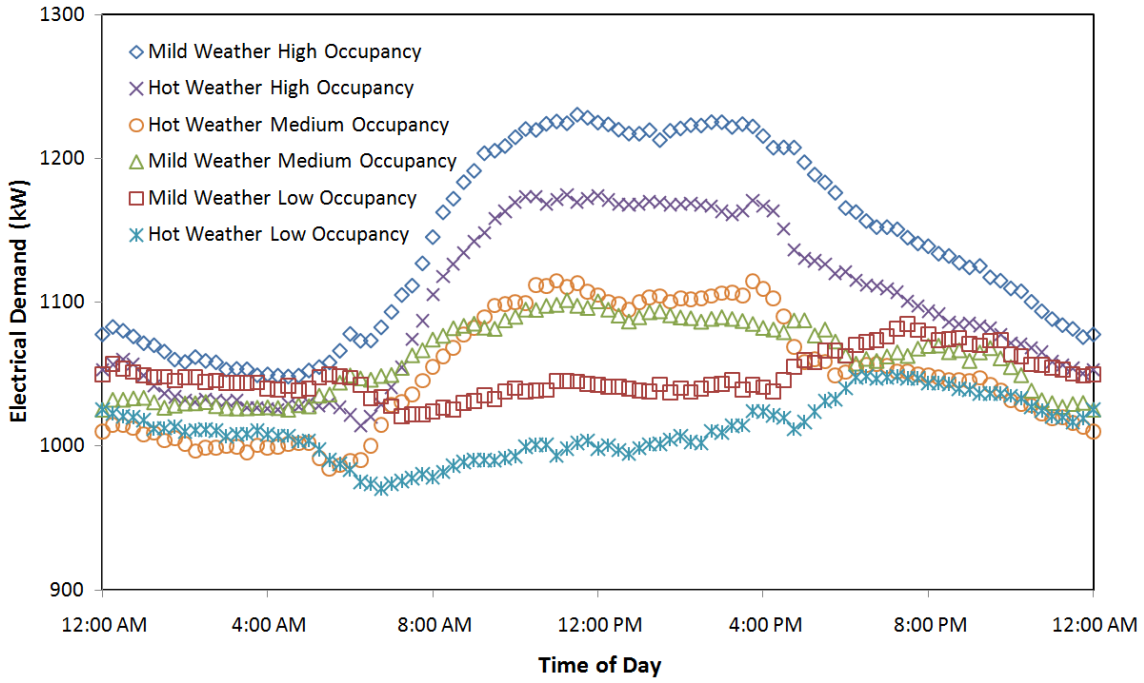


Figure 19. Electrical demand throughout day by occupancy and weather.

The electrical demand at any time in the building can be simplified to consist of a base load and an occupancy load. The base load results from constantly running machinery, the HVAC system, and constant plug loads such as computers, copiers, etc. It can be assumed constant for time scales as short as a day. The occupancy load is due to people using the building, turning on lights, and operating equipment. The base load made up approximately 85% of the total peak load for the TAMUQ building, while the occupancy load accounted for the remaining 15%.

Applying this simplification to the metered electrical data, the minimum load experienced within a single day can be assumed to be the building's base load for that day. Any additional demand can be taken as the occupancy load at that time step. The maximum occupancy load across *all* days represents an estimate of the installed

occupancy load capacity in the building. Dividing the calculated occupancy load at a given time step by this upper limit yields a normalized occupancy load. This parameter is useful for modeling the many transient loads of the building in EnergyPlus by expressing the real-time transient demand as a fraction of the installed capacity. The normalized occupancy loads for the six day categories are shown in Figure 20.

The normalized occupancy loads begin near zero, indicating almost pure base load and no activity. Starting around 6:00 AM, they begin to rise and reach their maximum for the day by around 10:00 AM. Building activity remains at this peak until approximately 4:00 PM, after which it decreases as the building begins to shut down for the day. A slight decrease can even be seen in Figure 20 around 12:00 PM when many occupants presumably leave for lunch.

A greater variation is seen between the hot and mild medium occupancy curves for the occupancy load than for the total load in Figure 19. This is likely because medium occupancy periods during hot months, namely summer school session, still have nearly the same faculty and staff presence. Medium periods during mild months, such as winter and spring breaks, have reduced levels of both students and faculty/staff.

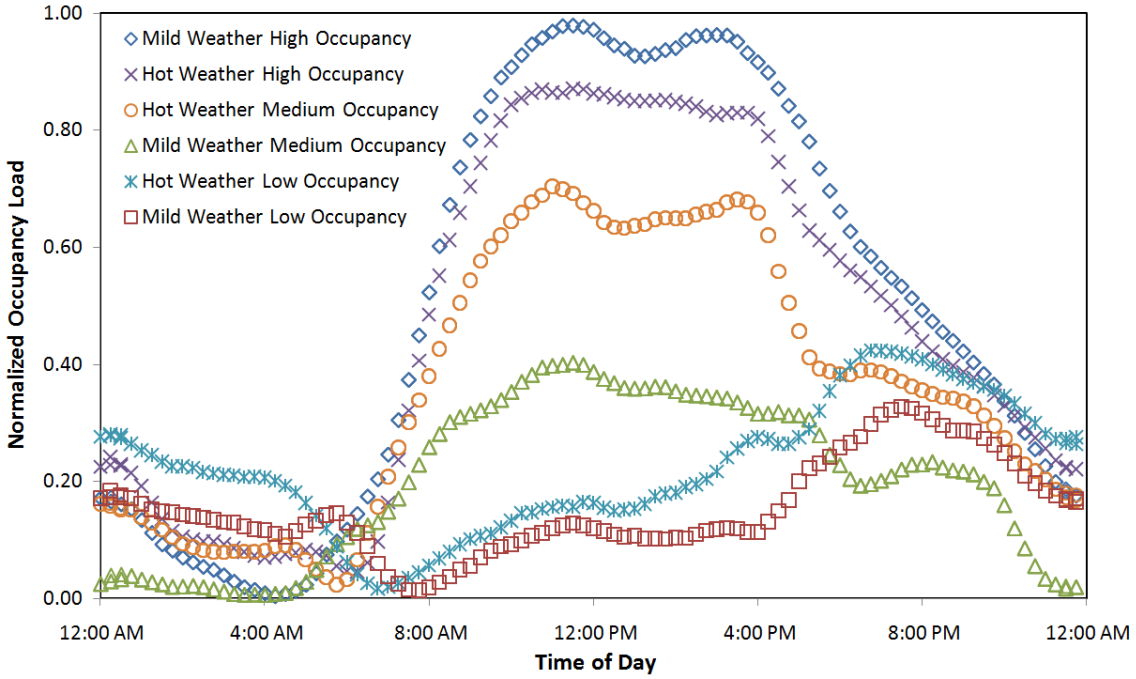


Figure 20. Normalized occupancy load throughout day by occupancy and weather.

The base load accounts for the majority of the total building load, around 85% during peak periods. Most of this base load goes toward running the many AHU and FCU fans that serve the building's cooling needs. The primary external source of these cooling needs can be described by

$$Q_{cl} = U_{total}(T_{\infty} - T_{SP}), \qquad (8)$$

where $Q_{cl}$ is the sensible conduction and convection load on a building space in Watts. $U_{total}$ is the overall heat transfer coefficient that accounts for wall area, materials and thickness, as well as internal and external convection. $T_{\infty}$ and $T_{SP}$ are the ambient temperature and space temperature set points, respectively. The total load on the space would also include terms due to radiation, as well as internal heat generation from plug loads and occupants, but the load calculated from Equation 8 comprises the majority of

the total. This was especially true in the TAMUQ building, where external and internal shading significantly decrease direct solar radiation loads.

$Q_{cl}$ represents the cooling energy required of the air handler to maintain the space set point, given by

$$Q_{AHU} = Q_{cl} = \rho_{air} c_{p,air} \dot{V} (T_{SP} - T_{s,air}), \qquad (9)$$

where $T_{s,air}$ is the supply temperature of the air from the AHU. $\rho_{air}$, $c_{p,air}$, $(T_{SP}\text{-}T_{s,air})$, and $U_{total}$ all remain approximately constant throughout the year. For a VAV system in Doha, Qatar, as $(T_{\infty}\text{-}T_{SP})$ drops from 25°C (45°F) in the summer to around 5°C (9°F) in the winter, $\dot{V}$, the volume of air required from the fan, should decrease proportionately. From the fan affinity laws, the decrease in power needed to run the fans at the decreased flow rate is

$$\frac{\dot{W}_2}{\dot{W}_1} = \left(\frac{S_2}{S_1}\right)^3 = \left(\frac{\dot{V}_2}{\dot{V}_1}\right)^3, \qquad (10)$$

where $\dot{W}$ is the fan power, $S$ is the fan speed, and the subscripts *2* and *1* denote the new and old operating conditions, respectively. From this simplified analysis, the contribution to the base load from the AHU fans in the winter should ideally be less than 1% of that observed in the summer. In reality, these mild-weather consumption decreases were capped by the operational limits of the fans, but they should still be significant for a full VAV system.

Because the TAMUQ air handlers were equipped with variable speed fans, there should be reduced cooling loads and electrical consumption in winter. However, the savings were not evident from Figure 15, suggesting the fans were operated at constant

speed throughout the year despite changes in demand. Observations of fan speed readouts also support this hypothesis.

In fact, the electrical consumption during the mild winter months of November through March was slightly *higher* than in the summer. Peak demand data confirm this phenomenon. Figure 21 shows the monthly peak electrical demand for the TAMUQ building during each bold month in Table 1, with the value for July again interpolated from June and August. Peak demand for the year is shown occurring in February and March.

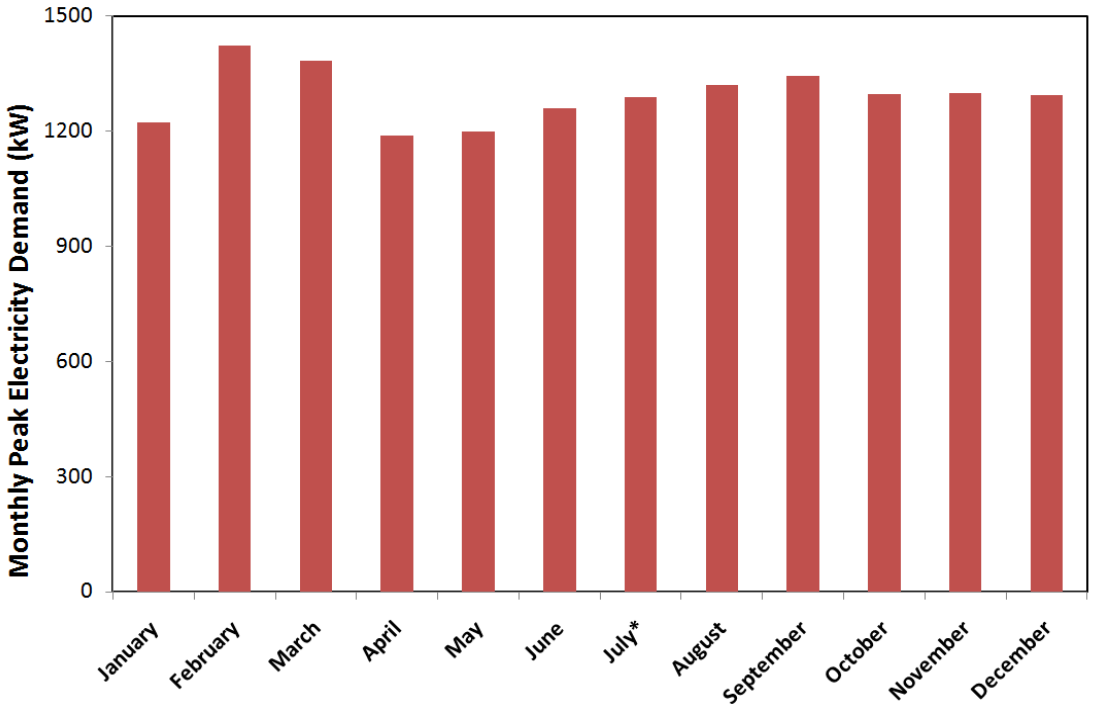


Figure 21. Monthly electricity peak demand. The value for July is interpolated.

Figure 19 provides further confirmation of higher winter electrical consumption. The average demand during high occupancy, mild weather periods was approximately 5% higher throughout the day than during high occupancy, hot weather periods. This apparent contradiction was actually more evidence that the fans were being operated at constant speed settings. When the external space loads given by Equation 8 were very small or even negative in the winter months, the only way to decrease $Q_{AHU}$ enough to maintain the set point when air volume was fixed was to increase the supply temperature $T_{s,air}$. The TAMUQ air handlers remained in cooling mode and provided approximately 14°C (57°F) supply air year-round. Therefore, $T_{s,air}$ must be increased using electric reheat coils in the VAV terminal units. The 300-plus VAV terminal units in use on the academic side had over 1500 kW of installed electric heating capacity. Even a small fraction of heaters in the VAV terminal units cycling on at one time could have caused the additional 50 kW increase in demand seen during an average winter day.

Figure 22 shows the total equivalent electricity consumption for each month including electricity consumed by central plant chillers to supply the metered chilled water energy. The chilled water consumption was converted into an equivalent electricity consumption based on

$$P_{CHW} = Q_{CHW} \times IPLV, \tag{11}$$

where $P_{CHW}$ was the electrical power consumed by the chiller to cool the chilled water and $IPLV$ was the integrated part load value, a measure of refrigeration cycle efficiency, adjusted for predicted part load performance throughout the year. The chillers in use at

the central plant that serve TAMUQ had an *IPLV* of 0.5 kW/ton, corresponding to a COP of 7.0 (McQuay 2010).

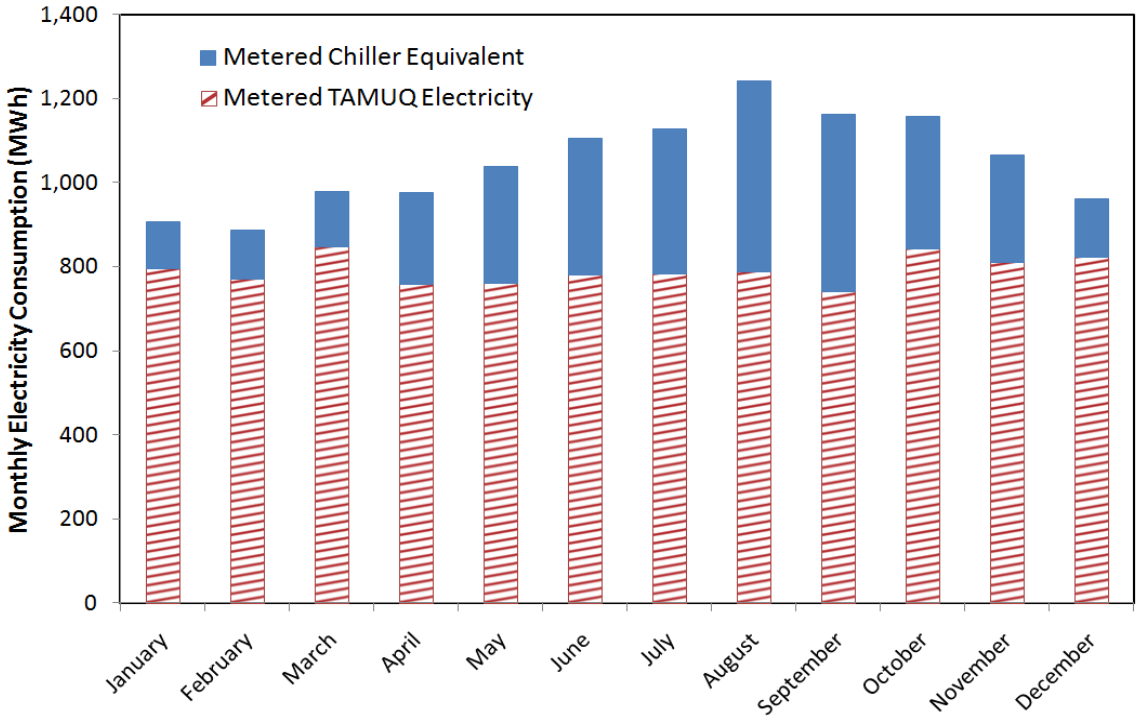


Figure 22. Monthly equivalent electricity use including calculated equivalent chiller consumption.

When the equivalent electrical consumption by the chillers was considered, it was calculated that the TAMUQ building had a baseline total annual energy consumption per area, known as an energy use index (EUI), of 418 kWh/m$^2$/yr (143 kBTU/ft$^2$/yr). In comparison, the average EUI among office buildings is 272 kWh/m$^2$/yr (93 kBTU/ft$^2$/yr), while the average among education facilities is 243 kWh/m$^2$/yr (83 kBTU/ft$^2$/yr) (DOE 2003). An average EUI for buildings 20,000-50,000 m$^2$ (200,000-500,000 ft$^2$) is 293 kWh/m$^2$/yr (100 kBTU/ft$^2$/yr).

# CHAPTER IV

# COMPUTER MODELING AND VERIFICATION

A building energy model was created using EnergyPlus version 6.0 to simulate improvements to the building's HVAC systems. The inputs to the model were based on the energy data gathered from the building, TAMUQ design drawings and equipment schedules, and direct observations around the building. The finished model was validated using the building energy data. This chapter summarizes the modeling process and presents the validation results.

## 4.1 Building the Model

Building energy models programmed with EnergyPlus are modular in nature. Basic building blocks known as objects describe the building parameters, which include physical building geometry, such as windows, walls, and doors; HVAC equipment such as fans, pumps, and heat exchangers; and information based objects such as control logic and building operation schedules. Weather information is also fed to EnergyPlus via a weather file that contains hourly temperature, humidity, wind, precipitation, and solar data. The following sections discuss these inputs as they applied to the TAMUQ model.

### *4.1.1 Building Geometry*

The geometry of the TAMUQ building was the starting point for the model. This included the dimensional and material makeup of the building, as well as how the various spaces were assigned to HVAC zones.

OpenStudio is a plug-in for Google© SketchUp (DOE 2011) that was used to graphically model the physical geometry of the building. Walls, floors, and roofs are modeled in EnergyPlus as two-dimensional planes with material properties and boundary conditions. X, Y, and Z coordinates define the surface vertices in the building space. Building materials are input as "constructions", another EnergyPlus object. Constructions are programmed as layers of user defined material objects, which contain information on thickness, conductivity, and emissivity. Boundary conditions are specified depending on whether the surface is internal or external, exposed or unexposed to the sun and wind. Finally, the HVAC zone to which the surface belongs is entered. Figure 23 shows a diagram of the programming structure for the building geometry. $\delta$ and $k$ in the diagram represent the wall thickness and thermal conductivity, respectively.

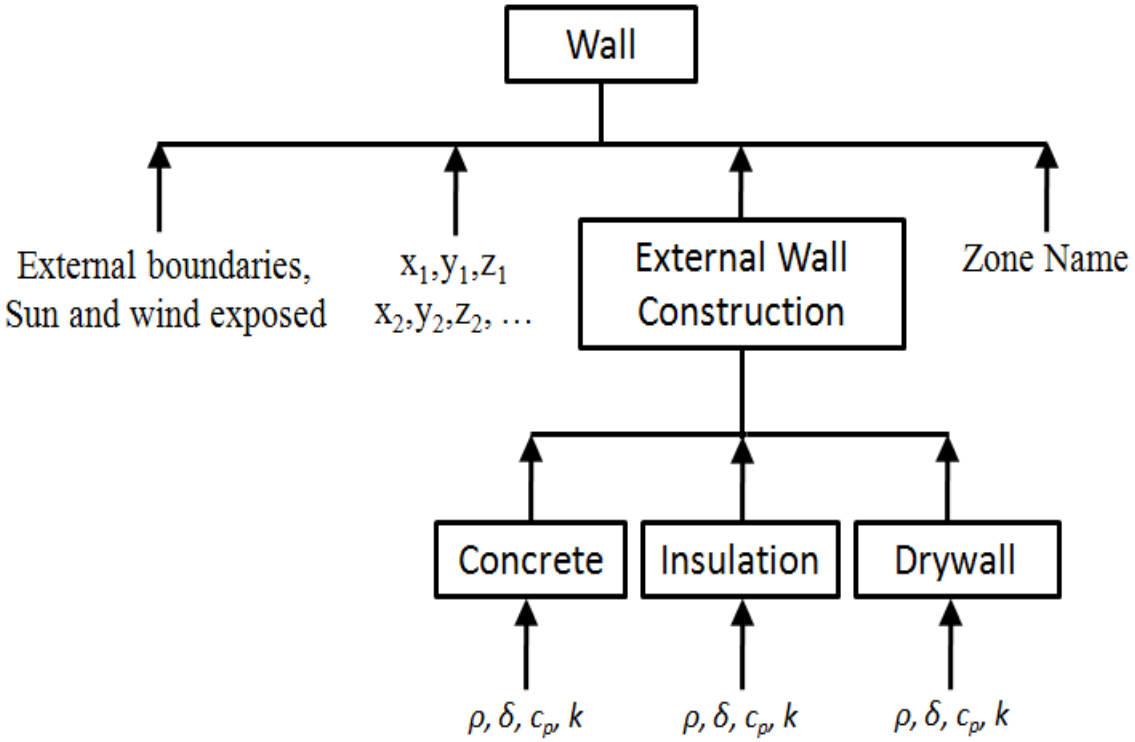


Figure 23. Diagram of building geometry programming structure.

Windows and doors are separate "fenestration" objects in EnergyPlus. In the case of windows, these objects contain additional information such as transmittance, shading and frame properties, and shading schedules. Fenestration objects require boundary condition inputs as well, but are hosted by a base surface such as a wall or roof, rather than being assigned directly to a zone.

For the TAMUQ building model, geometric inputs were based on architectural design drawings containing building dimensions. The precise constructions of the TAMUQ envelope were unknown. EnergyPlus default constructions were used with some alterations made to account for the exterior wall thickness, which was measured to

be 750 mm (29.5 in). Interior surfaces that contributed to the thermal mass of the building, but that had a negligible effect on its insulative properties, were modeled as "internal mass" objects. Internal masses have specified thermal capacitance properties, and are assigned to a zone, but lack specific surface coordinates within that zone. Table 4 summarizes the constructions used in the model. The "furniture surface" construction was applied to internal mass objects to approximate the presence of desks, cabinets, etc. around the building. It should be noted that adding internal masses to the model had a negligible effect on the energy use. Exact properties used for construction materials may be found in the appendix.

EnergyPlus zones were defined using HVAC design drawings, where the areas served by each individual VAV terminal unit was a separate zone. Figure 24 is a close-up of an HVAC drawing with VAV terminal unit symbols. Example zone assignments are shown for the area served by each unit.

Table 4. Constructions Used to Model Building Envelope.

| | Exterior Floor | Interior Floor | Exterior Wall | Interior Wall | Exterior Roof | Exterior Window | Exterior Door | Interior Door | Furniture Surface |
|---|---|---|---|---|---|---|---|---|---|
| **Zone Exterior** | 50mm insulation board | 19mm Acoustic tile | 200mm concrete block | 19mm gypsum board | 100mm lightweight concrete | Clear 3mm glass | 1mm Metal surface | 25mm wood | 1mm Metal surface |
| | 200mm heavyweight concrete | 5mm air gap | 200mm heavyweight concrete | 4mm air gap | 5mm air gap | 13mm air gap | 25mm insulation board | | 25mm wood |
| | | 100mm lightweight concrete | 50mm insulation board | 19mm gypsum board | Acoustic tile | Clear 3mm glass | | | 1mm Metal surface |
| | | | 4mm air gap | | | | | | |
| | | | 200mm concrete block | | | | | | |
| **Zone Interior** | | | 19mm gypsum board | | | | | | |

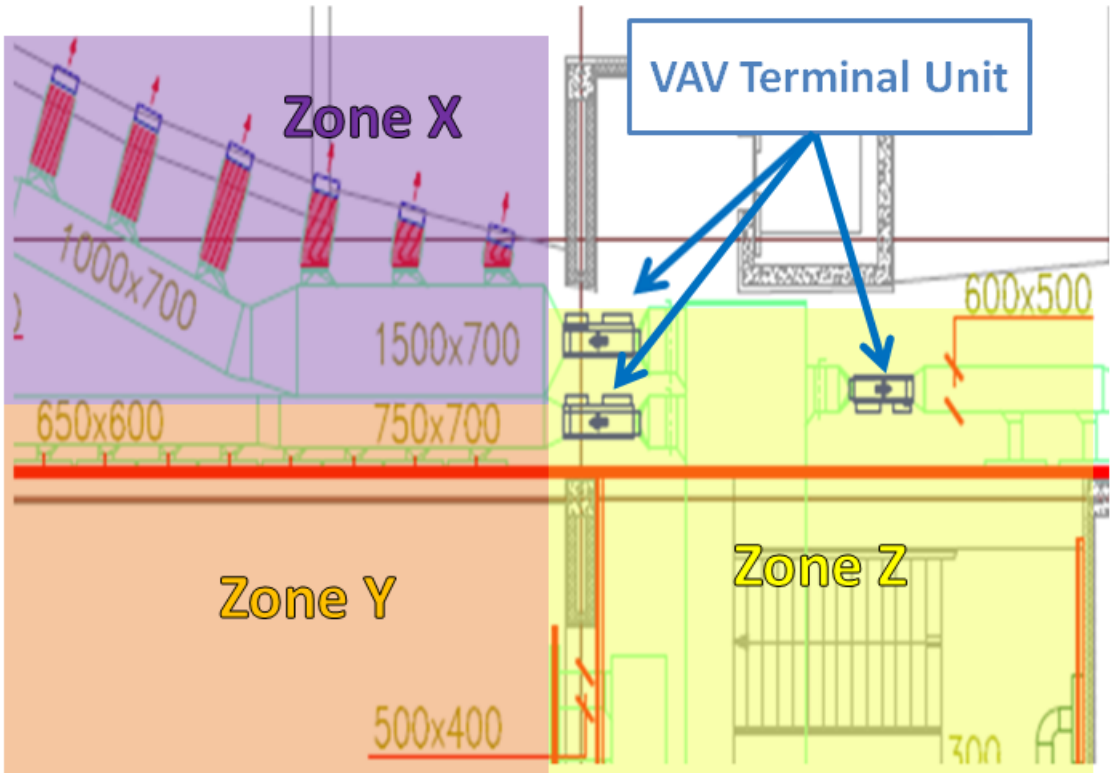


Figure 24. HVAC drawing sample showing VAV terminal units and zone assignments.

The TAMUQ building has both interior and exterior shading. Interior shades were modeled as low reflectance ($\rho_{solar} = \rho_{visible} = 0.2$), medium transmittance ($\tau_{solar} = \tau_{visible} = 0.4$) shades, as are found around the building. In EnergyPlus, interior shades are hosted by windows and given a schedule of operation. The schedule for the TAMUQ model assumed interior shading was active when the outdoor temperature was above 25°C (77°F) and inactive otherwise.

Exterior building shading is modeled much like walls, floors, etc., only without thermal properties. Coordinates are provided for structures such as overhangs and parapets that block incident solar radiation but do not contribute to building insulation.

EnergyPlus calculates the shadowing provided by these structures and adjusts heating and cooling loads accordingly. Figure 25 shows the completed building geometry as it appears in OpenStudio©. Surfaces representing exterior shading provided by the building structure are specified in the figure.

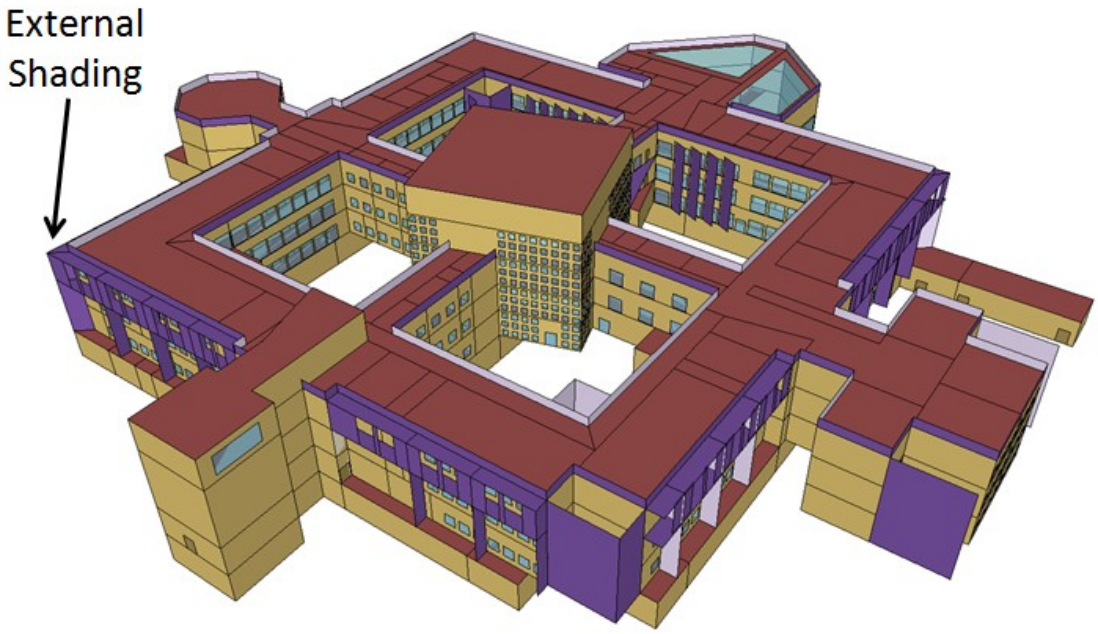


Figure 25. Completed TAMUQ building geometry in OpenStudio©.

### *4.1.2 HVAC Systems*

HVAC systems in EnergyPlus also have an object-oriented structure. Equipment components such as cooling coils, fans, and VAV terminal units are basic objects that, once given performance specifications, are fed as inputs to larger objects known as loops. Loops determine how the individual components are connected, and what areas

they serve. Figure 26 shows a diagram of an example air-side loop modeled in EnergyPlus. An air-to-air heat exchanger object is included in the loop to simulate the heat pipe and run-around coil pre-cooling installed in the TAMUQ air handlers.

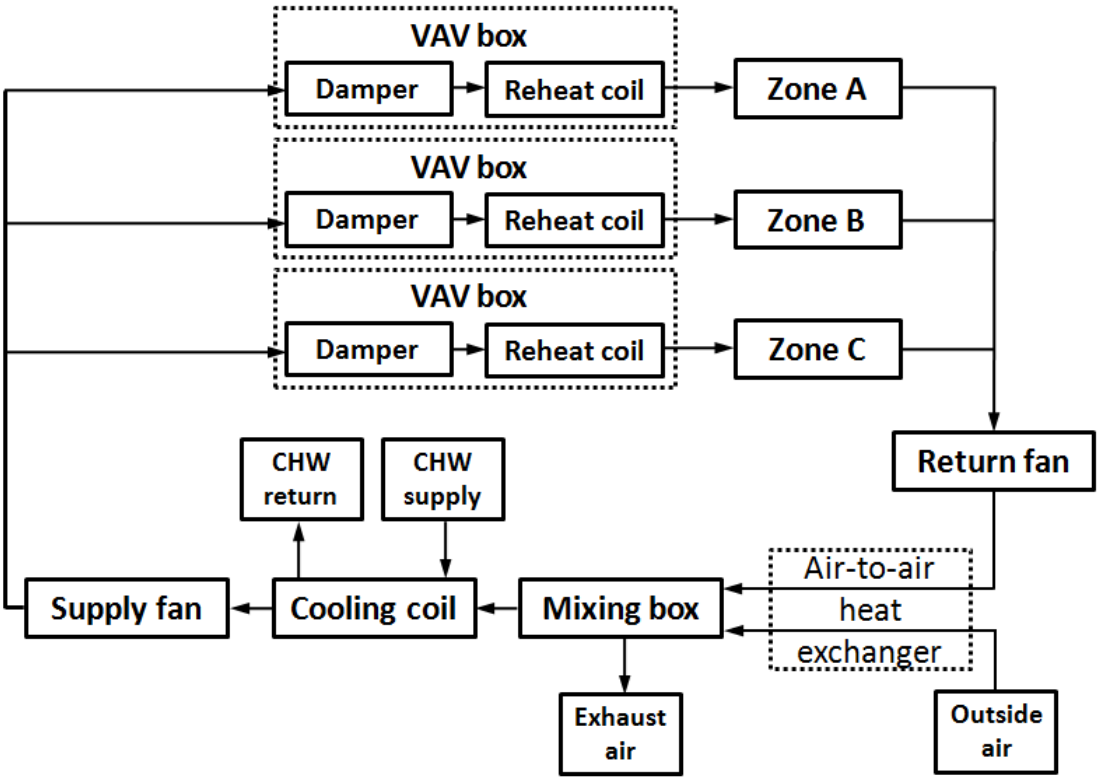


Figure 26. EnergyPlus air loop diagram.

The chilled water (CHW) supply and return inputs to the air-side loop in Figure 26 are part of their own water-side loop. This loop consists of a pumping arrangement like that of Figure 4, whose supply side splits into 46 branches to serve the AHU cooling coils. The cooling coil outlets combine into a single stream and return to the pump room inlet. The heat exchangers shown in Figure 4 were modeled as a district cooling source with unlimited capacity to simulate the off-site central chilled water plant.

All equipment data inputs were based on HVAC schedules provided by building operations staff. A complete list of the AHU specifications used can be found in the appendix.

### *4.1.3 Building Operation*

To accurately simulate the building, the model needed information on *how* the building and its systems operated throughout the year. Objects containing lighting and plug load information, hourly occupancy data, and equipment control logic were essential to the models validity.

#### *4.1.3.1 Modeling Lighting and Plug Loads*

The lighting load for the model was based on the occupancy load analysis of Section 3.3. The maximum observed occupancy load was 180 kW. The normally occupied building area, excluding plant and storage rooms, was 22,000 $m^2$ (220,000 $ft^2$), yielding a lighting power density of 8.2 $W/m^2$ (0.82 $W/ft^2$). Lighting power density was further delineated according to space function based on ASHRAE 90.1 (ASHRAE 2010c). Offices, bathrooms, and corridors were given an average lighting density of 8 $W/m^2$ (0.8 $W/ft^2$), while classrooms were given slightly more, at 9 $W/m^2$ (0.9 $W/ft^2$).

These values are 2-3 $W/m^2$ (0.2-0.3 $W/ft^2$) lower than what ASHRAE 90.1 actually specifies, and less than what is installed in the building. The modeled lighting

power densities represent an equivalent operational lighting power density that accounts for the actual peak fraction of lights on. By using this operational density, the multiplier schedule for electricity consumption due to lighting can come directly from the plot in Figure 20, showing the normalized occupancy load throughout a variety of day types. Electric power for lighting as a function of time for a given zone is then

$$P_{lights} = \varepsilon_{lights} A_Z \psi(t), \tag{12}$$

where $\varepsilon_{lights}$ is the peak lighting power density, $A_Z$ is the zone area, and $\psi(t)$ is the multiplier value as a function of the time of day and year. Since the peak lighting density was based on the total observed occupancy load, the model's lighting consumption also captures extraneous electrical users that have any non-random trend, recalling that the curves of Figure 20 were derived from average values over many days to suppress any random events. The remaining non-HVAC electricity use in the building can then be modeled as a constant plug load that is part of the base load described in Section 3.3.

The constant plug loads entered in the model were based on data gathered by undergraduate students. Teams of students conducted energy audits in different sectors of the building and categorized electrical equipment. Based on the categories and power density, it was estimated that approximately 20 W/m$^2$ (2 W/ft$^2$) of plug loads are constantly drawing power from the building.

*4.1.3.2 Modeling Building Occupants*

The peak occupancy of the academic side is around 600 people, with 450 being students. Building occupants were not expected to impact heavily on energy use, but reasonably accurate occupancy modeling was important for defining outside air requirements. The occupied spaces were divided into these five categories with regards to occupancy: plant and storage rooms, corridors, libraries, offices, and classrooms.

For plant and storage rooms, it was assumed that only one person, most likely maintenance personnel, would occupy the space when it was in use. Plant rooms averaged 100 $m^2$ (1000 $ft^2$) of space, thus the peak occupant density was set to 0.01 persons/$m^2$ (0.001 persons/$ft^2$) . Hourly zone occupancies were calculated analogous to lighting power, from

$$N_Z = \varepsilon_{people} A_Z \psi(t). \qquad (13)$$

$\varepsilon_{people}$ is the expected peak occupant density, and the multiplier schedule $\psi(t)$ is in this case defined as the probability of the peak occupancy occurring at a given moment. It was assumed that each plant room had 5% probability of being occupied at any time. Therefore, the plant occupancy schedule multiplied the estimated peak occupancy by a constant fraction of 0.05.

For corridors, the peak occupancy was assumed to be 10 people per 50 m (500 ft) length of hallway, or approximately 0.07 persons/$m^2$ (0.007 persons/$ft^2$) . This peak was expected to occur between one-hour class periods, and last five to ten minutes. The corridor occupancy schedule therefore multiplied the peak occupancy by 0.1-0.2 during

the heaviest class periods, between 8:00AM and 4:00PM, and tapered to 0.01 after-hours, to account for nightly security patrols.

Single-occupant offices averaged 17 $m^2$ (170 $ft^2$) of building space, thus the peak office occupant density was taken as 0.06 persons/$m^2$ (0.006 persons/$ft^2$) . Probabilities of office occupants being present in their offices were assumed to be tied to the lighting schedule, since all TAMUQ offices are equipped with motion-sensor lighting controls. The TAMUQ library was assumed to have similar occupant density and schedule to office space, and thus was included in the office occupancy definition.

Although the total number of students in the building was likely also related to the normalized occupancy loads, the real-time occupancy of the individual classroom spaces was more discrete in nature. Taking the total expected peak student occupancy, 400, divided by the total classroom area, 8000 $m^2$ (80,000 $ft^2$), would yield a peak occupant density of 0.05 persons/$m^2$ (0.005 persons/$ft^2$). But in a typical 150 $m^2$ (1500 $ft^2$) classroom, this would mean only eight occupants, whereas maximum TAMUQ class sizes average 20 students. Conversely, assuming 20 occupants per 150 $m^2$ (1500 $ft^2$) of classroom space would yield a peak student population of over 1000.

To solve this dilemma, the classroom zones were randomly split into three groups of equivalent total area. Peak occupant densities of 0.13 persons/$m^2$ (0.013 persons/$ft^2$) were assumed for each group, approximating the average class size of 20. The multiplier schedule for each group was staggered throughout the day such that only one group was at peak occupancy during a given hour, making the total student population in the building at any one time slightly less than the total enrollment of 450.

During the summer, the entire classroom schedule was multiplied by an addition fraction of 0.15 to account for reduced enrollment in the summer session. Table 5 summarizes the total floor area and peak occupant density for each zone category.

Table 5. Occupant Modeling Summary by Space Type.

| Space Category | Total Area ($m^2$) | Peak Occupant Density (persons/$m^2$) |
|---|---|---|
| Plant/Storage | 4500 | 0.01 |
| Corridors | 10600 | 0.07 |
| Library/Offices | 4900 | 0.04 |
| Classrooms A | 2400 | 0.13 |
| Classrooms B | 2400 | 0.13 |
| Classrooms C | 2600 | 0.13 |

*4.1.3.3 Modeling HVAC Control*

In addition to performance specifications of HVAC equipment in the building, operating conditions and controls were also entered into the model. This was the primary method of improving building energy efficiency once the baseline operating characteristics were modeled and validated.

The chilled water supply temperature to the AHU cooling coils was based on the metered chilled water data. Figure 27 shows weekly averaged chilled water supply temperatures as recorded during building energy metering. The red curve shows the scheduled supply temperature values that were modeled in EnergyPlus. The supply

temperature is higher, at 11.3°C (52.3°F), in the cool and dry early months of the year. It is reset to 10°C (50°F) in the hottest period from June through September, after which it is gradually stepped back to 11.3°C (52.3°C) as outside air temperatures become cooler again. The modeled supply temperature schedule is summarized in Table 6.

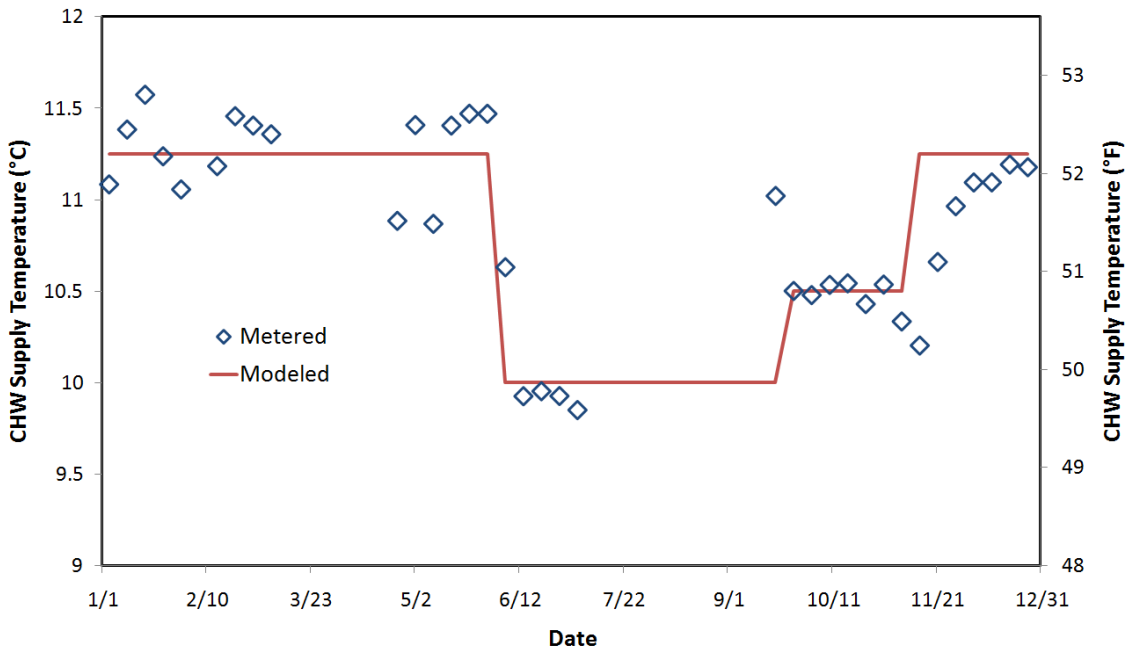


Figure 27. Metered chilled water supply temperature throughout year.

Table 6. Modeled Chilled Water Supply Temperature Schedule.

| Dates | CHW supply temperature (°C) |
|---|---|
| January 1 - May 31 | 11.3 |
| June 1 - September 26 | 10.0 |
| September 27 - November 8 | 10.5 |
| November 9 - December 31 | 11.3 |

The supply air temperature in the TAMUQ building was measured at an office diffuser with an infrared temperature sensor several times during the year. Each time the supply air temperature was 15°C (59°F). May of 2010 the supply air temperature was metered for a day from a diffuser in a third floor classroom, and was also found to hold constant at 15°C (59°F). In support of these findings, during a visit to the building control room, it was observed from the TAMUQ building management system (BMS) that all AHU's had a leaving-fan temperature set point of 14°C (57°F). The modeled AHU's were therefore also set to supply air at 14°C (57°F).

An audit of the building's thermostat settings showed most zones were set to a constant 23°C (73°F) cooling set point. The EnergyPlus zones were given these cooling set points as well. Figure 15 and Figure 19 showed evidence of electric heating due to overcooling during winter months. Some of this heating is from the reheat coils installed in the building's VAV terminal units, but much of it is from personal space heaters often found in TAMUQ offices. Therefore, heating was modeled using only VAV terminal

unit reheat, but was disabled during unoccupied hours to simulate occupants turning personal heaters off before going home. During occupied hours, a 20°C (68°F) heating set point was modeled to provide a sufficient dead band per ASHRAE 90.1 (AHSRAE 2010).

The essentially flat-line monthly electricity use shown in Figure 15 suggests the building's variable speed fans are being operated at constant speed. Results of auditing fan VFD readouts throughout the TAMUQ academic wing supported this hypothesis. Irrespective of time of year or ambient conditions, the supply and return fans remained on average at 45 Hz and 40 Hz, respectively. Fifty Hz would mean the fans were at maximum speed and, presumably, at the specified flow rates and pressure rises from the AHU schedule. Therefore, for the base case, all fans were modeled as constant speed fans with their flow rates and pressures adjusted down from the design values according to

$$\frac{\dot{V}_2}{\dot{V}_1} = \frac{f_{obs}}{50\ Hz}, \tag{14}$$

$$\frac{p_2}{p_1} = \left(\frac{f_{obs}}{50\ Hz}\right)^2, \tag{15}$$

where $p$ is the fan pressure and $f_{obs}$ is the observed VFD frequency, being 45 Hz for supply fans and 40 Hz for return fans.

Although the fans are operated at constant speed, the overall system is still VAV. The building's VAV terminal units still attempt to modulate the flow, and can still reduce the system volume to a degree. Figure 28 shows a fan performance curve for a fan running at constant speed. Typically the fan speed is set such that the unmodulated

system curve, System Curve 1 in Figure 28, intersects the given RPM line at the necessary design flow, which is determined from the maximum cooling load on the zone and Equation 9. When the VAV terminal units close their dampers, and the system curve moves from 1 to 2, the flow is modulated down, though not as much as if the RPM line were moved down with a VFD. This constant speed, quasi-VAV operation was modeled in EnergyPlus by still allowing VAV terminal unit objects to modulate flow, but within limitations.

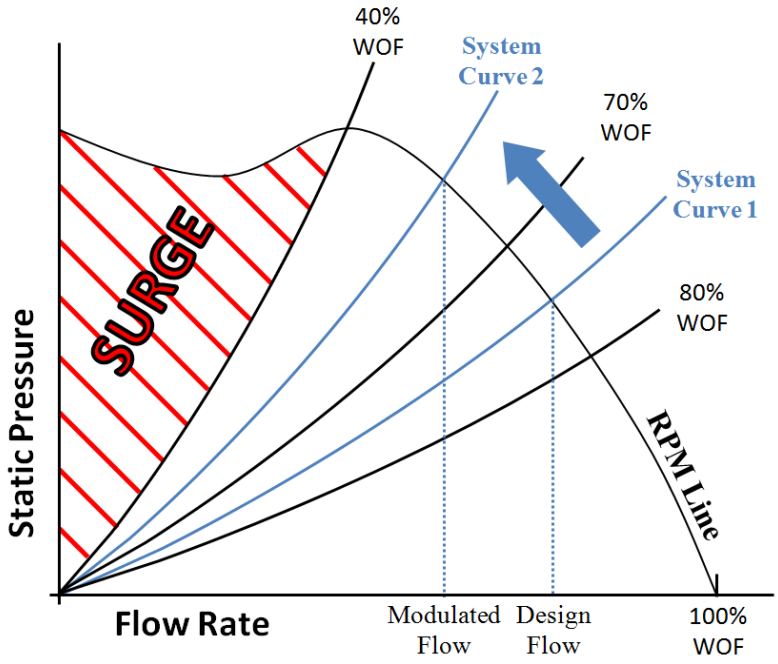


Figure 28. Fan curve at constant speed.

If the fan speed remains constant, the amount of modulation is limited by the surge region of the fan. Percent wide open flow (WOF) lines show equal percentages of maximum flow at any speed, and are also plotted on Figure 28. To maximize efficiency,

fans are selected to run between 60% and 80% WOF (Trane 2004). Unwanted fan noise and surging typically occurs below 40% WOF, meaning that the minimum safe flow rate at constant speed is approximately half of the design flow rate. This was reflected in the TAMUQ model, where VAV terminal units were given a minimum flow fraction of 50% of the cooling design flow.

The final HVAC operating characteristic modeled was AHU outside air control. Upon inspecting various AHU mixing boxes around the building, it was found that in all non-100% outside air AHU's, both the return inlet and outside air inlet dampers were 100% open. This was confirmed by observing the control settings in the BMS. It was therefore assumed that the baseline AHU's would intake their design percentage of outside air at all times. The design outside air percentages were taken from the AHU schedule.

### *4.1.4 TAMUQ Weather*

EnergyPlus uses hourly weather data to compute heating and cooling loads for the building. For the TAMUQ model, raw weather data came from the OTBD weather station at the Doha Airport over the year-long period from October of 2009 through September of 2010, as prescribed in Table 1 and Table 2. Hourly data fields included dry bulb temperature, relative humidity, atmospheric pressure, wind speed, wind direction, visibility, and condition observations. During periods with missing fields, which were

never more than five hours in duration, the data were linearly interpolated between the nearest times with available data.

Figure 29 shows the minimum, mean, and maximum daily temperatures in Doha for each month (OTBD Weather Station 2011). Solid curves represent data averaged over a five year period while data points represent data from the weather period simulated. Figure 30 shows a similar plot for the dew point temperature in Doha.

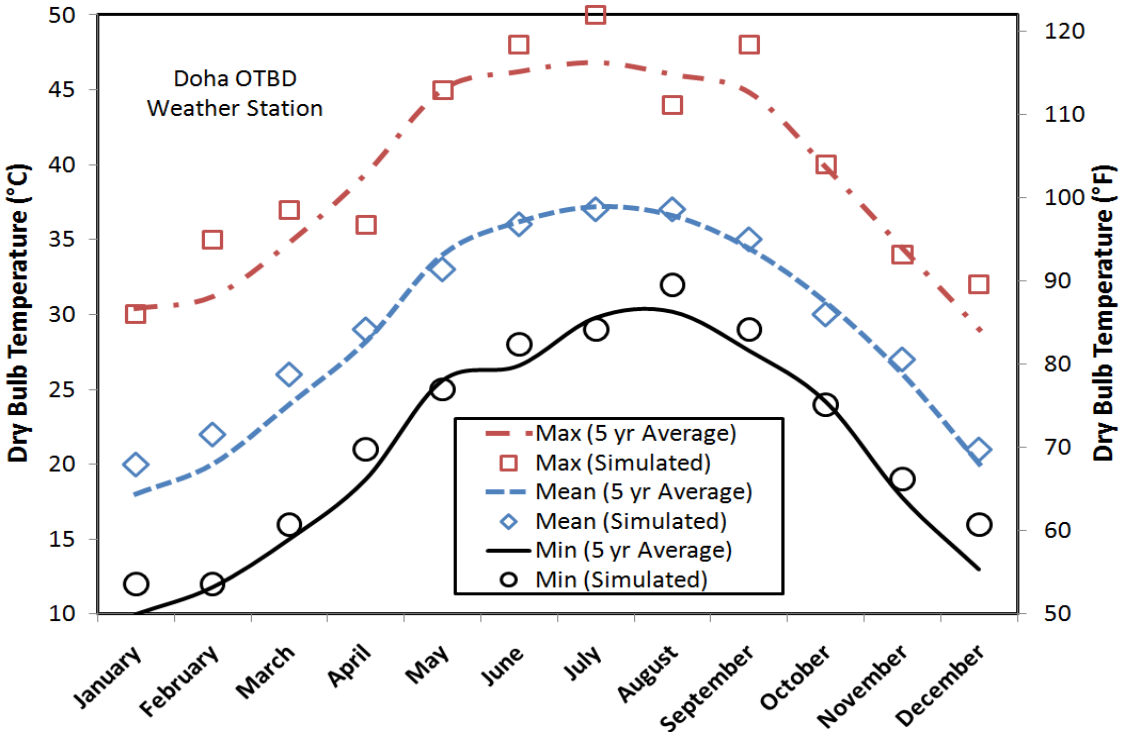


Figure 29. Daily minimum, mean, and maximum dry bulb temperatures by month.

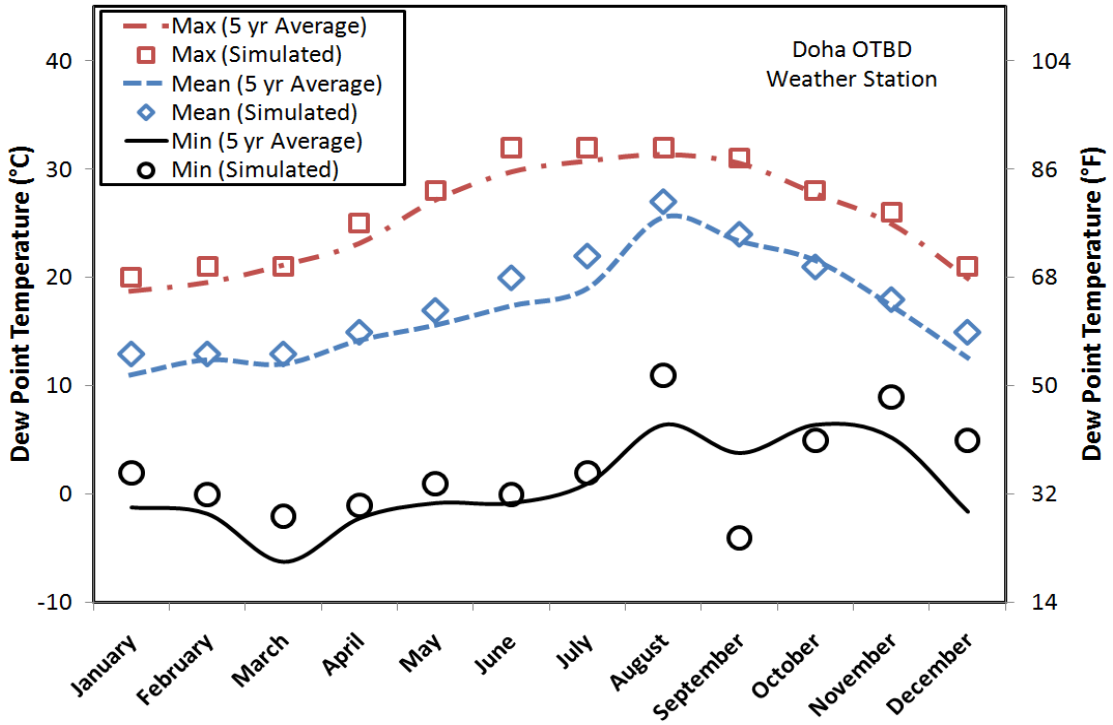


Figure 30. Daily minimum, mean, and maximum dew point temperatures by month.

The OTBD weather station data had to be translated to the EnergyPlus Weather (EPW) file format before it could be used in the simulation. EPW files use a quantitative rating for sky cover from one to ten, whereas weather station observations used word descriptions. Table 7 shows how the descriptive observations were converted into the EPW sky cover rating.

Table 7. Conversion from Condition Observations to EPW Sky Cover Rating.

| OTBD Observation | EPW Opaque Sky Cover |
|---|---|
| Clear | 0 |
| Haze | 2 |
| Scattered Clouds | 3 |
| Partly Cloudy | 4 |
| Mostly Cloudy | 5 |
| Light Rain | 7 |
| Light Thunderstorm | 8 |
| Rain | 9 |
| Thunderstorm | 10 |

EPW files also contain fields for incident solar radiation and diffuse solar radiation, which were unavailable from the OTBD data. Typical meteorological year (TMY) data for Abu Dhabi, United Arab Emirates was available (ASHRAE 2001), and solar data for Doha was assumed to be similar, as it is only 0.75° latitude further north.

### 4.2 Model Validation

After the TAMUQ model was completed, its HVAC operation and energy use were simulated for a complete year. Simulation results for electricity and chilled water consumption were then compared to the metered results presented in Section 3.3.

Figure 31 shows the simulated monthly electricity consumption, not including any chiller electricity usage, compared to metered consumption in the TAMUQ building. Recall that the July value for the metered data was interpolated from June to August. The total metered annual consumption was 9.51 GWh, while the total annual simulated consumption was 9.54 GWh. The simulated monthly consumption never varied more than ±5% from the corresponding metered monthly value. This is well within the EnergyPlus component uncertainties found by Shrestha (2006), and suggests the base case model is valid on a monthly basis. The simulation results also show the general constant-usage trend throughout the year, with slight increases in the winter months due to VAV reheating. This suggests the model is also capturing the dynamics of the building operation.

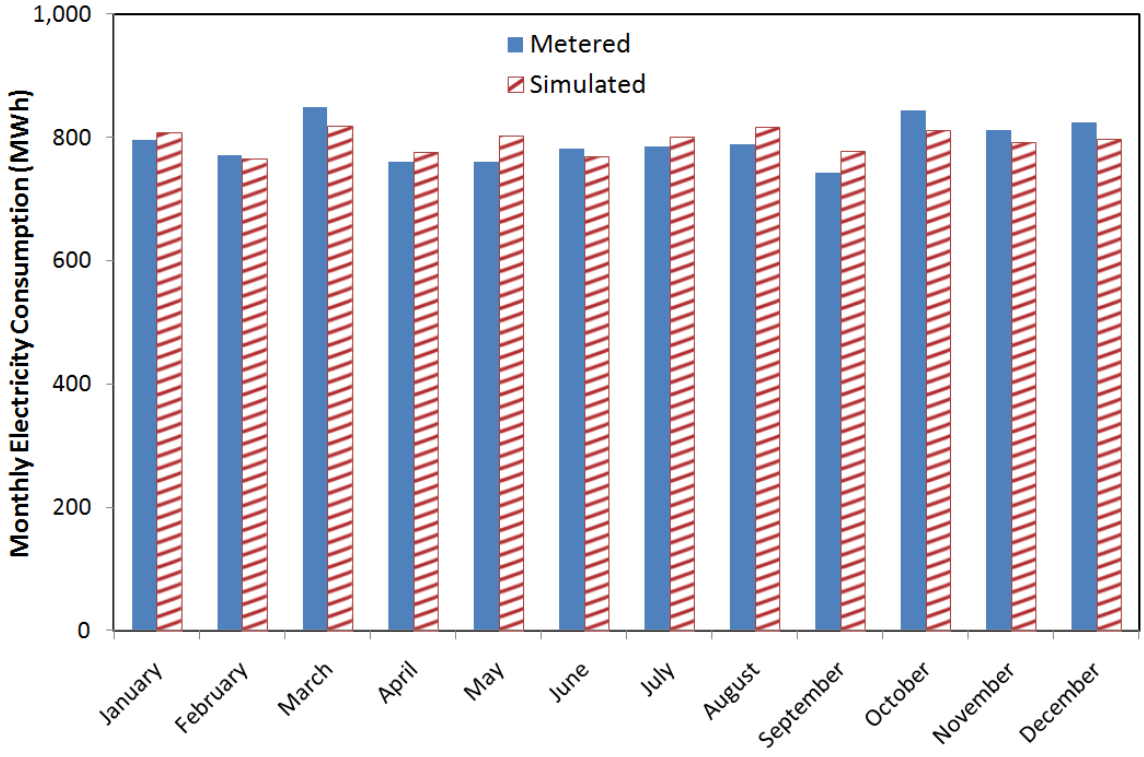


Figure 31. Comparison of monthly electricity consumption.

Figure 32 shows the simulated monthly peak demand compared to the metered monthly peak demand. Again, July metered values are estimated. The error in the simulated monthly peak demand was considerably higher than for the total consumption. The simulated peak was 44% over the measured peak in January, and over 15% in February, March, November, and December.

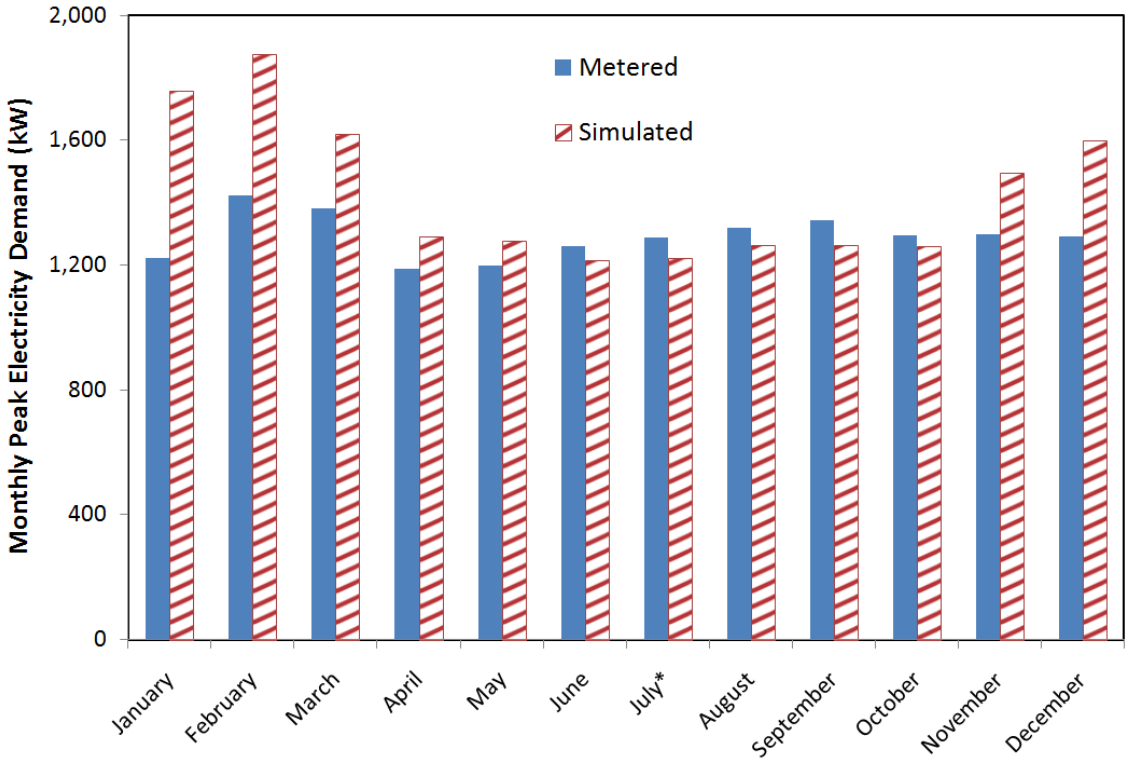


Figure 32. Comparison of monthly peak electricity demand.

Although monthly peak demand is an important measure for energy analysis and utility billing, it is difficult to predict accurately with a simulation. Peak demand depends on many variables and electrical users at once coming together. The complexity is increased with high energy users, such as electrical reheat. Reheat coils in VAV terminal units typically cycle on and off and have several energized stages to maintain a desired supply temperature (Trane 2011). When many reheat coils in a building are energized simultaneously, it can cause a large spike in demand, whereas if their on-cycles are more ordered, the demand is lower and more consistent. Many BMS's are equipped with peak load management routines that limit peak demand by disabling non-essential energy users until more demand capacity becomes available (Honeywell 2011, Peak Load

Management Alliance 2002). The EnergyPlus model lacked this capability, likely leading to the discrepancies in November through February when reheat was used the most.

Figure 33, Figure 34, and Figure 35 show the hourly electrical demand over an average day during high, medium, and low occupancy periods, respectively. Within each occupancy level, days were also separated into mild or hot weather seasons, as defined in Section 3.3. Data points represent the averaged metered demand, while solid curves represent simulated demand.

The hourly simulated electrical demand also agreed closely with the metered data. Hourly demand values had a maximum error of 20% over the metered values, occurring at 8:00AM during a mild weather, high occupancy day. Overall, 95% of the hourly values for the six day types were within ±10% of their metered counterparts. For both medium and high occupancy days in mild weather, sudden peaks occurred in the simulation at 8:00AM that caused the highest error from metered data. This is when the reheat was scheduled to come on in the model. During the night, when reheat was disabled, zone temperatures fell below their heating set points. When reheat was switched on at 8:00AM, more energy was needed to overcome the deficit from the night before, and the demand peaked. The real building likely had a more gradual reheat start-up.

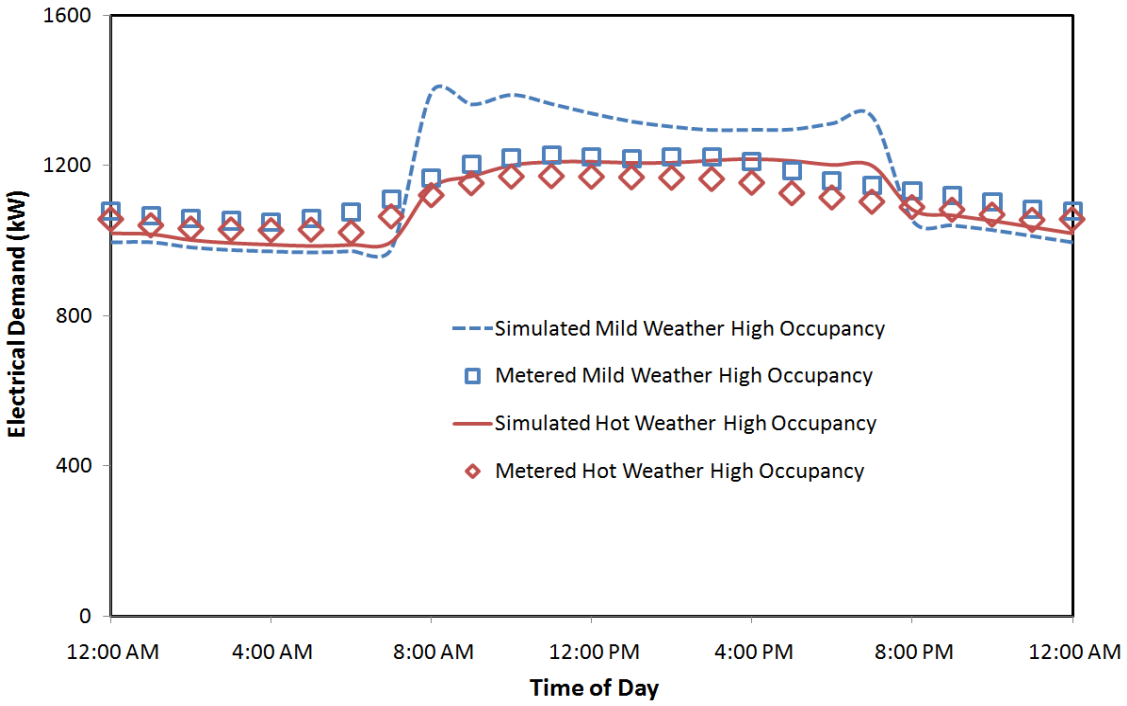


Figure 33. Comparison of hourly electrical demand during high occupancy periods.

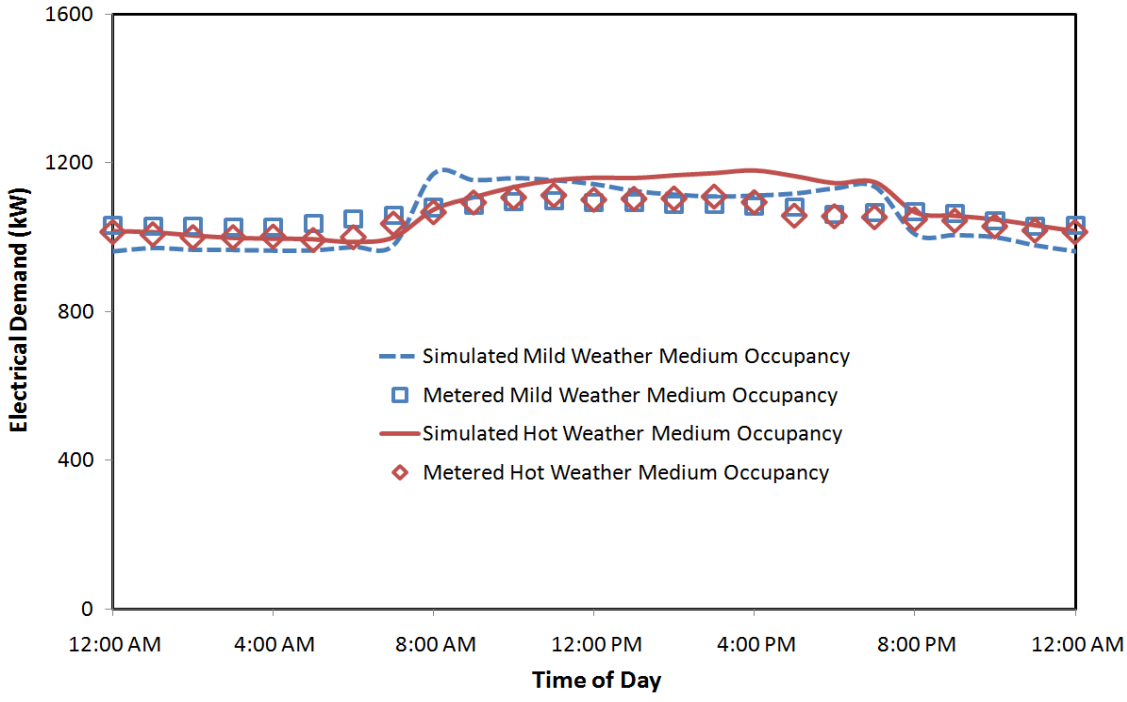


Figure 34. Comparison of hourly electrical demand during medium occupancy periods.

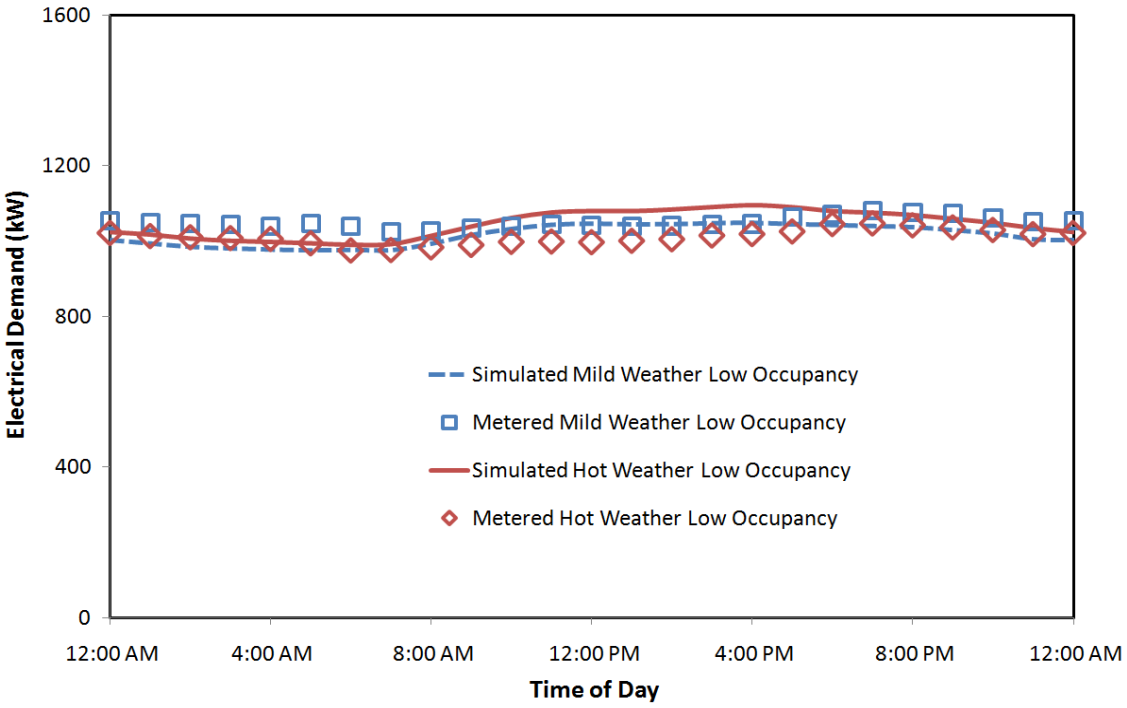


Figure 35. Comparison of hourly electrical demand during low occupancy periods.

Figure 36 shows the simulated monthly chilled water consumption versus metered. The total metered annual consumption was 78,400 GJ (74,300 $10^6$ BTU), while the total simulated annual consumption was 75,700 GJ (71,800 $10^6$ BTU). Due to the oscillating behavior of the research wing chilled water load that was estimated and subtracted from the whole-building data retroactively, significant error is introduced when time scales are shorter than a month. Therefore, the simulated and metered chilled water data were compared only on a monthly basis.

The maximum error in simulated monthly chilled water consumption occurred in April, at -18%. This is still within the 29% uncertainty possible in plant loop components, and specifically within the 18.5% uncertainty noted in EnergyPlus chiller

plant cooling loads (Shrestha 2006). For the combined annual load, the simulated error was only -3%. As can be seen in Figure 36, the simulation also closely predicted the seasonal dynamics of the chilled water consumption. When plotted as a function of month, the simulated and metered chilled water consumptions had an R-squared correlation coefficient of 0.95.

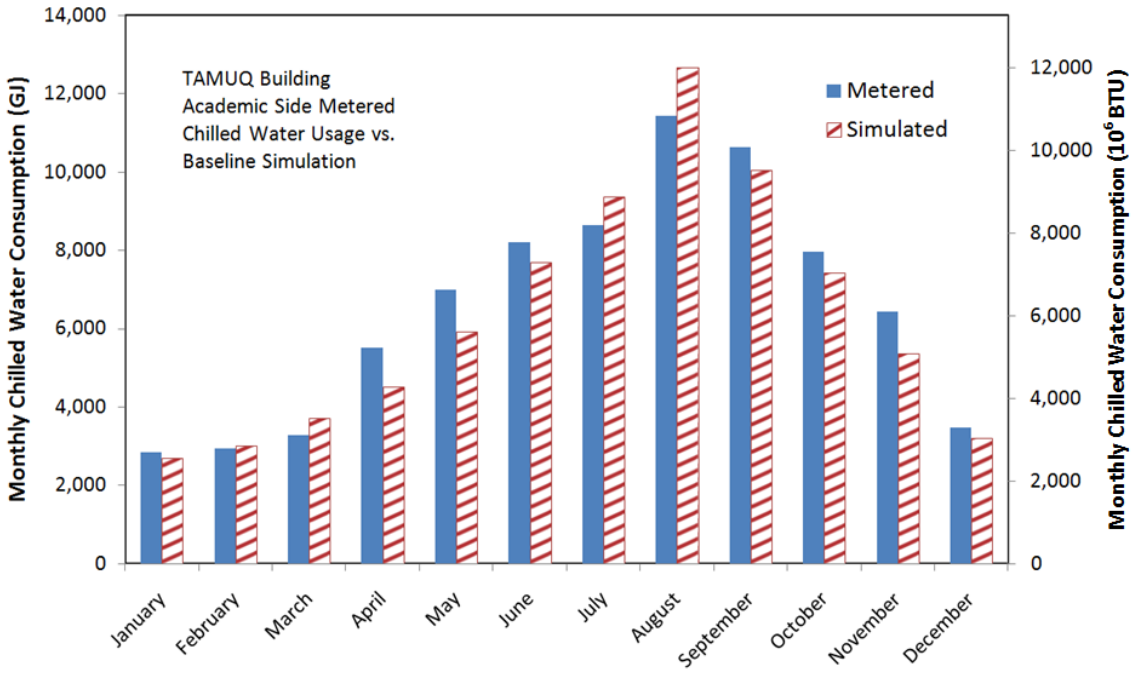


Figure 36. Comparison of monthly chilled water consumption.

# CHAPTER V

# ENERGY EFFICIENCY IMPROVEMENTS

After validating the base case model, adjustments were made to simulate energy efficiency improvements to the TAMUQ HVAC system. These adjustments included the following: operating primary AHU fans at variable speed, reducing outside air intake to IAQ minimums, and retrofitting VAV terminals with FPTU's. Efforts were also made to optimize the effects of these changes. The following sections discuss the improvement processes and their results.

## 5.1 Variable Speed Fan Operation

The primary AHU fans around the TAMUQ building were observed operating at constant speeds, despite being equipped with VFD's. This was verified by electrical metering data, and by simulation results when the fans were modeled as constant speed. Considerable savings can be realized by operating the fans at variable speeds.

### *5.1.1 Theory*

Figure 37 shows typical VAV system fan curves under constant and variable speed operation. For constant speed operation, VAV terminal units must close their dampers and move to System Curve 2C to attain the required modulated air flow to meet

the zone set points. The fan static pressure in this constant speed case increases as the flow decreases. The fan power, which is proportional to the product of flow and pressure, remains essentially the same. When the fan is operating at variable speeds, its speed is adjusted downward, from RPM line 1 to RPM line 2, so that the new operating point that yields the required flow falls on a pre-designed VAV modulation curve, shown in green. Note that both flow *and* pressure are decreased in the variable speed case. The power needed to run the fan is thus significantly lower as well.

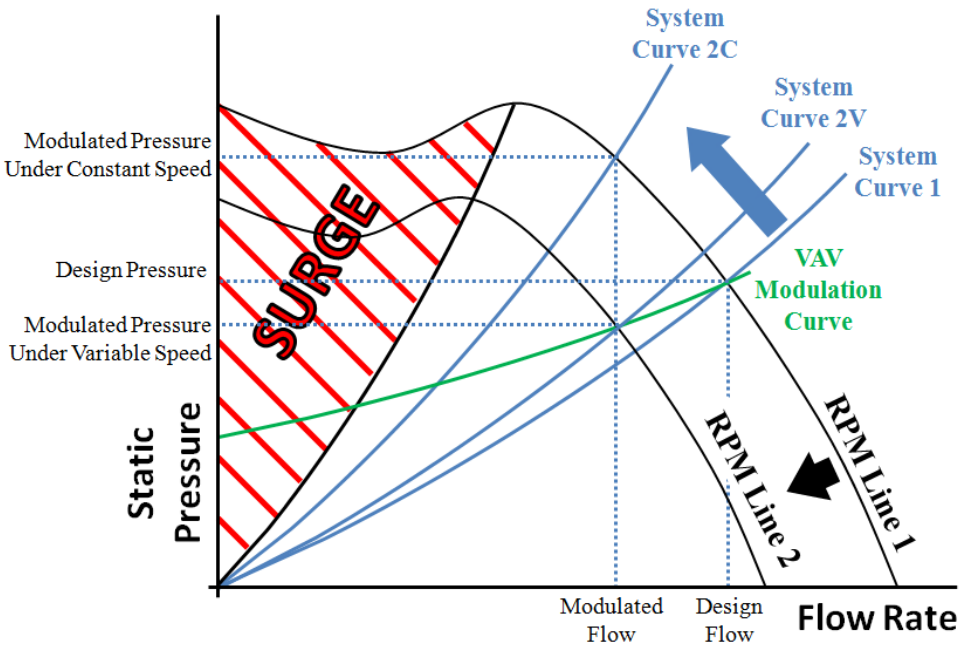


Figure 37. VAV system fan curves.

A variable speed system is also able to modulate air flow more than a constant speed system. Figure 38 shows a similar fan curve diagram demonstrating the minimum flow capabilities of constant vs. variable speed operation. In both cases the dampers are

closed their maximum amount without entering the surge region, shifting the system curve to System Curve 2. The flow at the intersection of this curve and the original RPM Curve 1 is the minimum possible safe flow under constant speed operation, as discussed in Section 4.1.3.3 and as modeled in the base case. When under variable speed operation, the RPM curve can again shift down the VAV modulation curve to RPM line 2. This is the minimum safe flow rate under variable speed operation, and it is lower than that at constant speed. With variable speed fans, the power required at part load operating points is lower *and* the minimum part load operating point is lower. Because the cool air flow can be reduced further to meet small cooling loads without overcooling, the latter benefit not only saves further on fan energy, but also reduces reheat energy use.

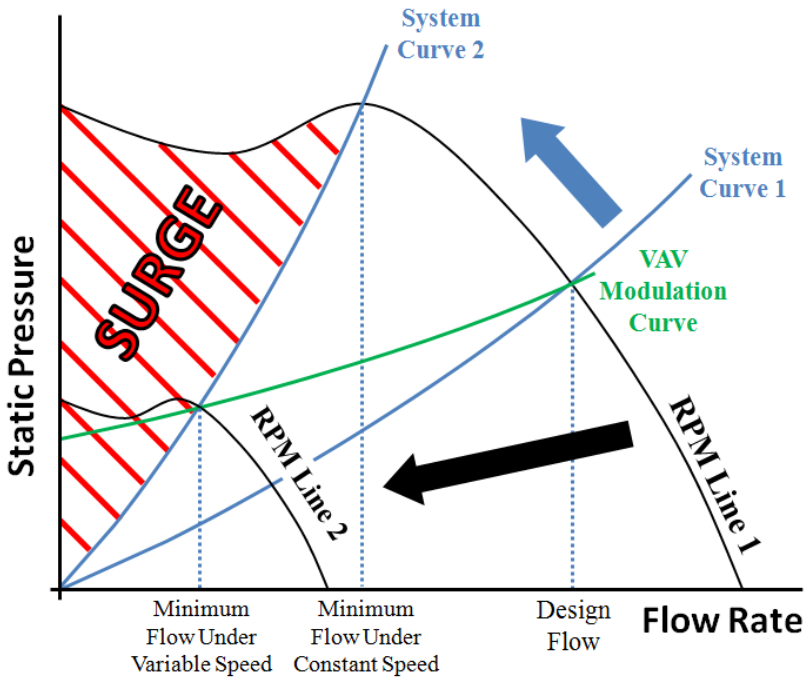


Figure 38. Constant and variable speed fan minimum flows.

EnergyPlus calculates the part load power consumption of fans based on the fraction of the design volume flow rate. The equation that relates fan power fraction to fan flow fraction was taken from ASHRAE 90.1 and is shown along with its plotted curve in Figure 39 (ASHRAE 2010c).

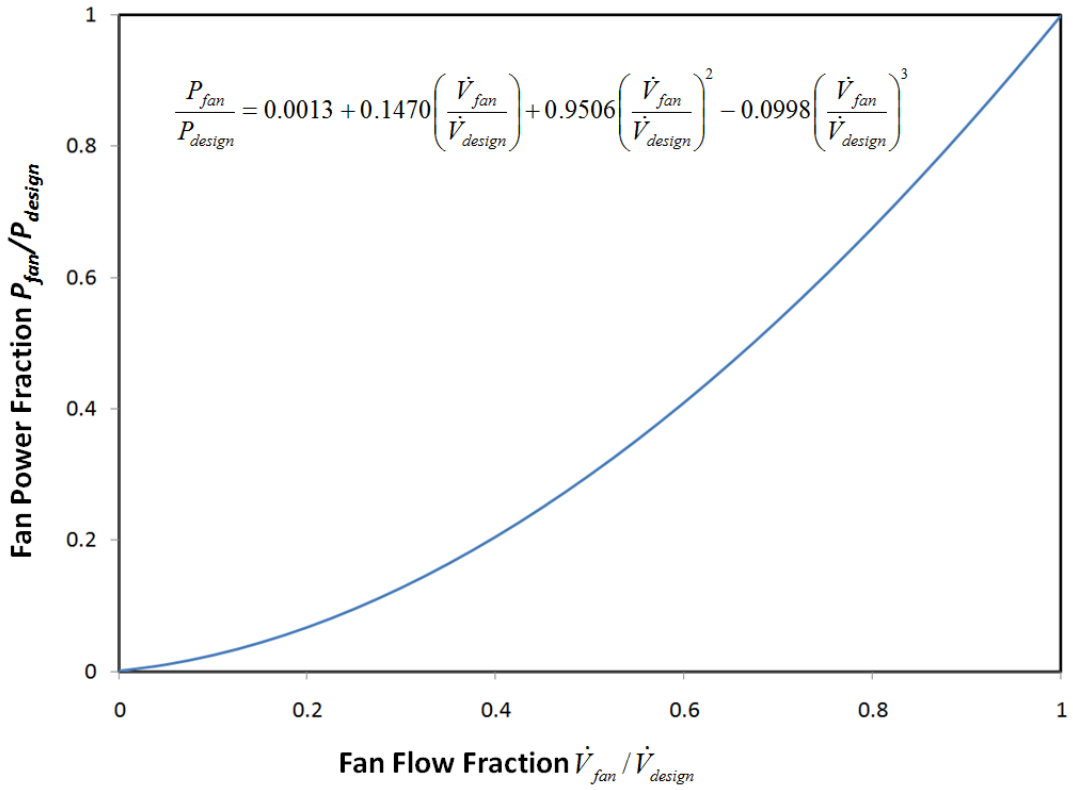


Figure 39. Fan power fraction as a function of fan flow fraction (ASHRAE 2010c).

Variable speed fan operation can also yield chilled water savings. The cooling load on an AHU cooling coil can be calculated from

$$Q_{CC} = \dot{V}_{air}\left[\rho_{air} c_{p,air}\left(T_{mixed} - T_{s,air}\right) + h_{fg}\rho_{air}(\omega_{mixed} - \omega_{s,air})\right], \qquad (16)$$

where $\omega$ is the moisture content of air and the subscripts *mixed* and *s* denote the mixed outside and return air streams and the off-coil supply air, respectively. $h_{fg}$ is the latent heat of vaporization for water. Because part load air flows are reduced for a variable speed system, the energy used by AHU cooling coils to cool the air at part loads are reduced proportionately as shown in Equation 16, given a constant off-coil set point.

### *5.1.2 Simulation Results*

Figure 40 shows the effects on monthly electrical usage of utilizing the existing fan VFD's at TAMUQ, with a minimum flow setting of 30% of design flow, as recommended by ASHRAE 90.1 (ASHRAE 2010c). The variable speed monthly values exhibit the summer peak shape one would expect from true VAV operation. The simulation showed that variable speed fan operation at this minimum flow setting could potentially save 16% over annual baseline electricity usage.

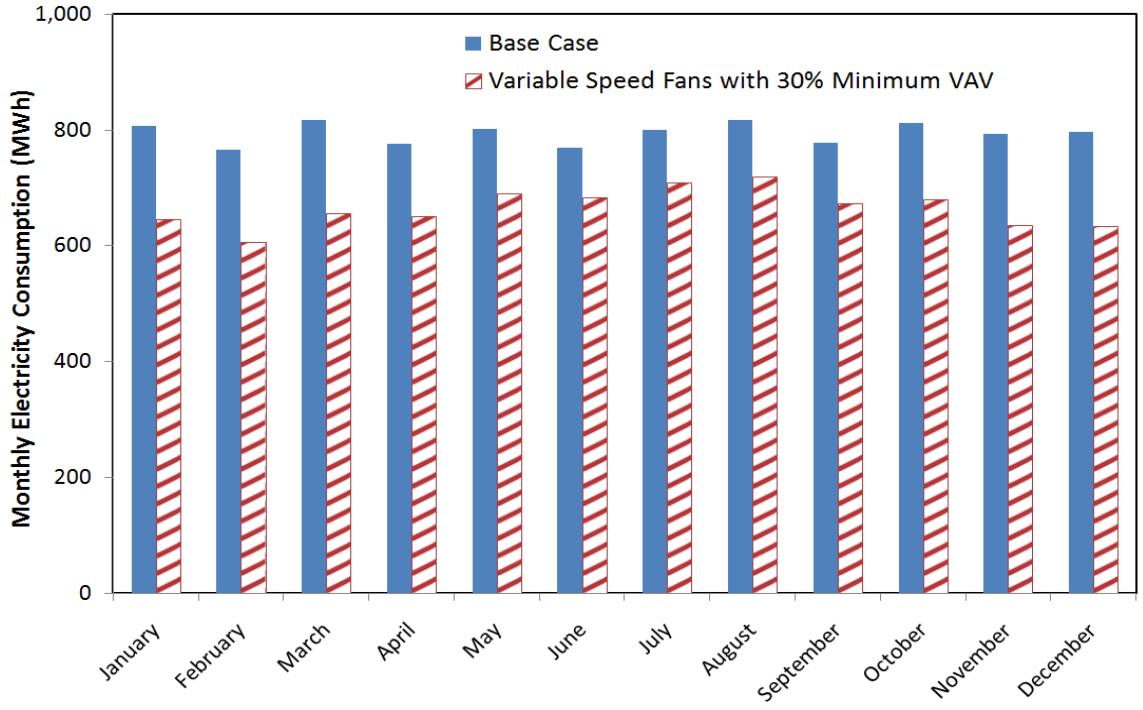


Figure 40. Effect on electrical consumption of variable speed fan operation with 30% minimum VAV flow rate.

Figure 41 shows the effect on monthly chilled water usage of operating the AHU fans at variable speed. Chilled water consumption is decreased because of reduced air flow rates during part load periods. Simulation results showed potential annual chilled water savings of 22%.

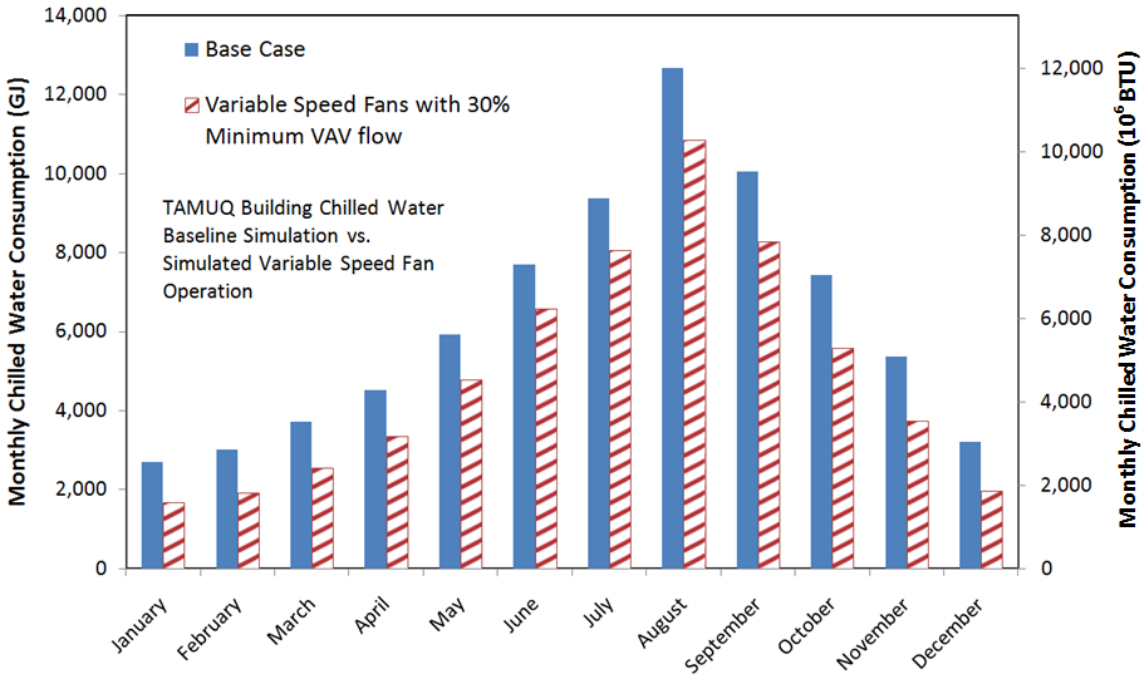


Figure 41. Effect on chilled water consumption of variable speed fan operation with 30% minimum VAV flow rate.

Figure 42 shows the contribution of all major electricity users to the annual electricity usage. The simulated chilled water consumption was converted to an equivalent electricity consumption by the central plant chillers using Equation 11. Switching to variable speed fans had the most dramatic effect on fan consumption, as was expected. The equivalent chilled water electricity had the next largest decrease, followed by reheat. Note that reheat was not a significant portion of the total consumption. This made sense, recalling that the increases in metered electricity seen in winter months were noticeable, but small in magnitude. Simulated base case reheat accounted for 4% of the total electricity consumption, not counting chiller equivalent, while in the variable speed case it accounted for 2%.

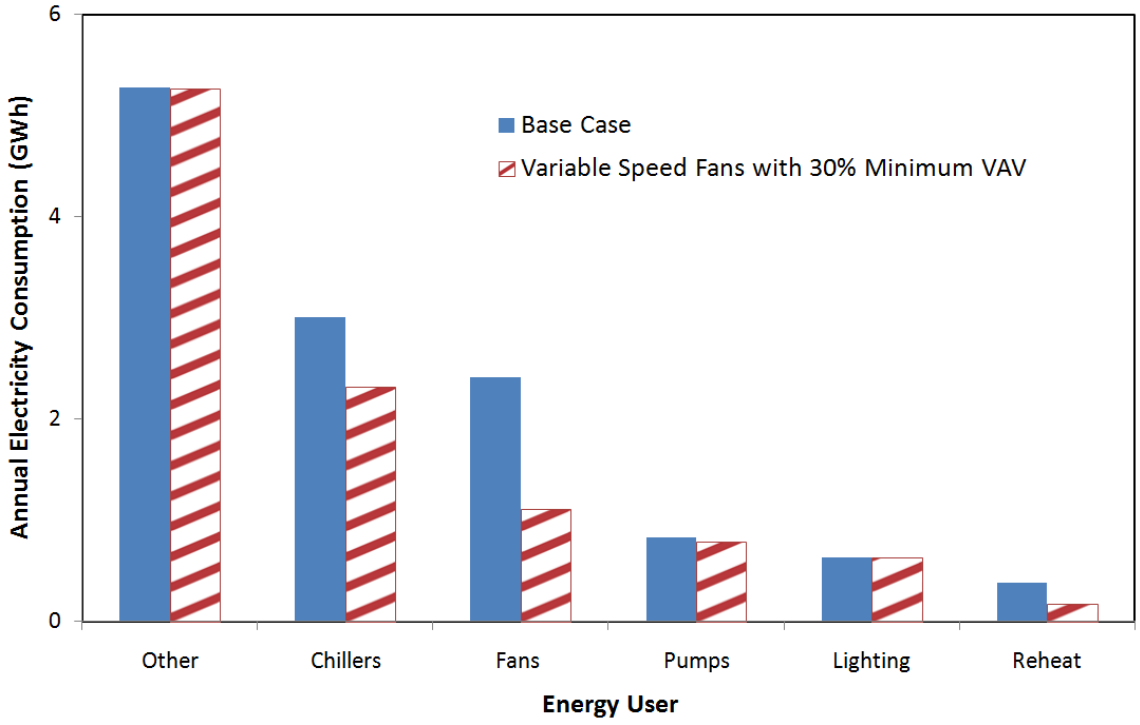


Figure 42. Annual electricity use constituents.

When the equivalent chiller electricity from chilled water savings was considered, true VAV operation could potentially save 18% over the base case for total equivalent electricity consumption. Given that the utility rate for government buildings in Qatar was $0.0412/kWh (Kahramaa 2011), this is equivalent to annual energy cost savings of $90,000.

Restrictions on minimum flow for variable speed fans are typically governed by IAQ standards rather than actual fan limitations (Cho and Liu 2009). Settings for minimum VAV flow rate can vary from 20% to 50% of cooling design flow, and depend on the required outside air flows of the zones, the designed outside air intake of the AHU, and the design heating loads (Davis et al. 2009, Cho and Liu 2009). Figure 43

shows the potential percentage savings over the TAMUQ base case for electricity and chilled water as a function of the minimum VAV flow setting. For electricity, there were additional savings for reducing minimum flow until around 20% of the design cooling flow, after which savings begin to level out. For chilled water, the general trend was the same, but savings level closer to 10% of cooling design flow. Figure 43 shows graphically that once the TAMUQ system was operated in a true VAV mode, reducing minimum flow rates much below 20%, the lower range found in the literature, was not only ill-advised from an IAQ standpoint but also held little promise for additional significant energy savings.

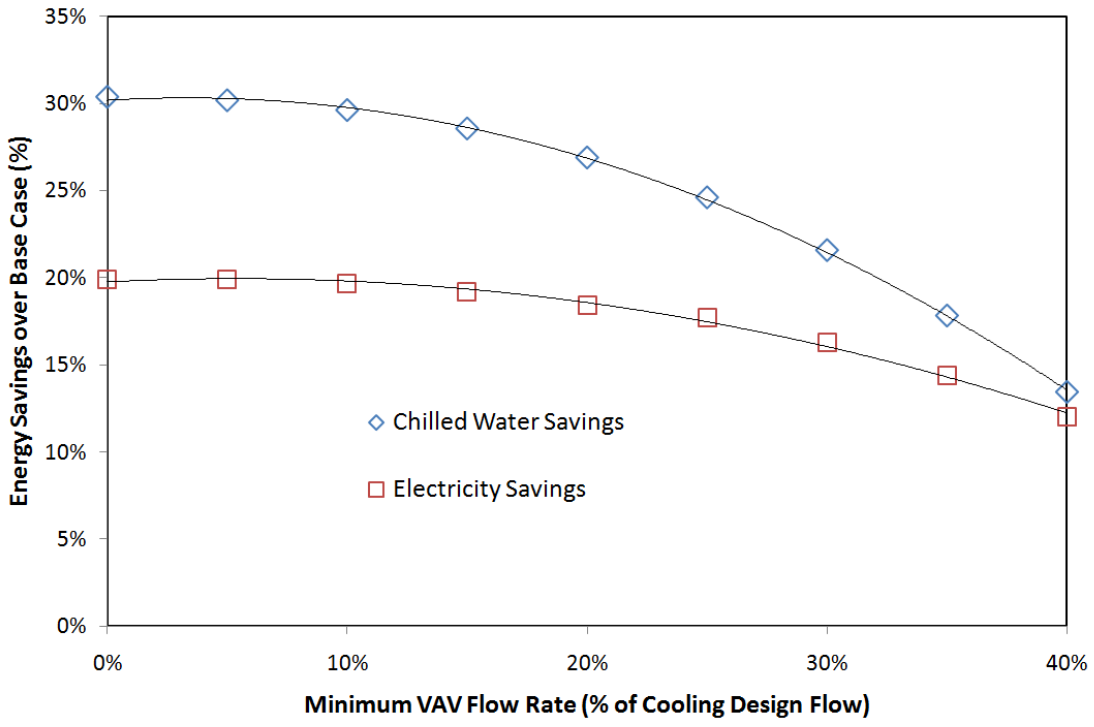


Figure 43. Energy savings as a function of minimum VAV flow.

## 5.2 Reducing Outside Air Intake

The TAMUQ AHU's were observed with their outside air dampers 100% open. As such, it was assumed in the baseline model that they used their design percentages of outside air at all times, which ranged from 20% to 100% of total flow. Controlling this amount of outside air, particularly at low occupancy periods, to just meet IAQ standards can yield potential chilled water savings from AHU cooling coils.

### *5.2.1 Theory*

The cooling load on an AHU cooling coil was given by Equation 16. The moisture content and temperature of the mixed return and outside air stream can be calculated from

$$\omega_{mixed} = x\omega_{\infty} + (1-x)\omega_{r,air} \qquad (17a)$$

$$T_{mixed} = xT_{\infty} + (1-x)T_{r,air}, \qquad (17b)$$

where $x$ is the fraction of outside air and the subscript $r$ represents the return air stream. Substituting Equations 17a and 17b into Equation 16, it can be seen that chilled water cooling load has a direct relationship with the fraction of outside air. On August nights in Doha, outside conditions can reach 33°C (91°F) and 90% RH, giving $\omega_{\infty}$ as 0.03 $kg_w/kg_a$. Assuming return conditions similar to the space set points, 23°C (73°F) and 50% RH, and off coil set points of 14°C (57°F) and 95% RH, the supply and return moisture contents are less than one third this at 0.009 $kg_w/kg_a$. At these conditions, the

load on the cooling coil using 100% outside air can be up to eight times more than using no outside air, and over three times that using 20% outside air. Adding the fact that zone cooling loads and thus air flow rates are also highest during these summer periods, reducing outside air flow can save significant amounts of chilled water energy.

The amount of outside air needed to maintain IAQ is found in ASHRAE standard 62.1 (ASHRAE 2010b). ASHRAE defines the required outside air volume delivered to a zone as a function of the area and occupancy of that zone, according to

$$\dot{V}_{OA,z} = R_p N_z + R_a A_z. \tag{18}$$

$N_z$ and $A_z$ are the occupancy and floor area of a given zone, respectively, and $R_p$ and $R_a$ are multipliers dependent on the function of the zone. Classrooms and laboratories require more fresh air than a supply closet, for example.

For systems serving multiple zones, the volume of outside air is determined from

$$\dot{V}_{OA,AHU} = \frac{D \sum_{all\ zones} R_p N_z + \sum_{all\ zones} R_a A_z}{E_v}. \tag{19}$$

$D$ is an occupant diversity modifier calculated from

$$D = \frac{N_s}{\sum_{all\ zones} N_z}, \tag{20}$$

where $N_s$ is the system design population, defined as the maximum number of occupants expected to be in all zones combined at once. $E_v$ is a ventilation efficiency calculated from the minimum value of

$$E_{vz} = 1 + X_s - Z_{pz} \tag{21}$$

across all zones, where $X_s$ is the average outside air fraction given by

$$X_s = \frac{D \sum_{all\ zones} R_p N_z + \sum_{all\ zones} R_a A_z}{\dot{V}_{total,AHU}}, \tag{22}$$

and $Z_{pz}$ is the primary outdoor air fraction for a zone given by

$$Z_{pz} = \frac{\dot{V}_{OA,z}}{\dot{V}_{total,z}}. \quad (23)$$

Since zone occupancy fluctuates over time, the value of $N_z$ in Equation 18 is determined from the average occupancy over a time duration in minutes determined from

$$t_{avg} = \frac{50V_z}{\dot{V}_{OA,z}}, \quad (24)$$

where $V_z$ is the volume of the zone space in $m^3$ and the zone outdoor air flow is in L/s. For most zones, this time period is an hour or more.

In EnergyPlus, the hourly zone occupancy schedules and floor areas were used to control the outside air flow rate of the TAMUQ air-handlers according to the above procedure. This simulates using occupancy sensors in a building to calculate a real-time outside air requirement. The TAMUQ building is already equipped with motion sensors in most areas to control lighting. Together with other sensors such as sound and $CO_2$, these could easily be extended through the BMS to precisely control AHU outside air use as well (Dong and Andrews 2009).

### *5.2.2 Simulation Results*

Figure 1 shows the effect of outside air control on TAMUQ monthly electricity consumption. The effect is negligible, likely only resulting from slight differences in chilled water pump rates.

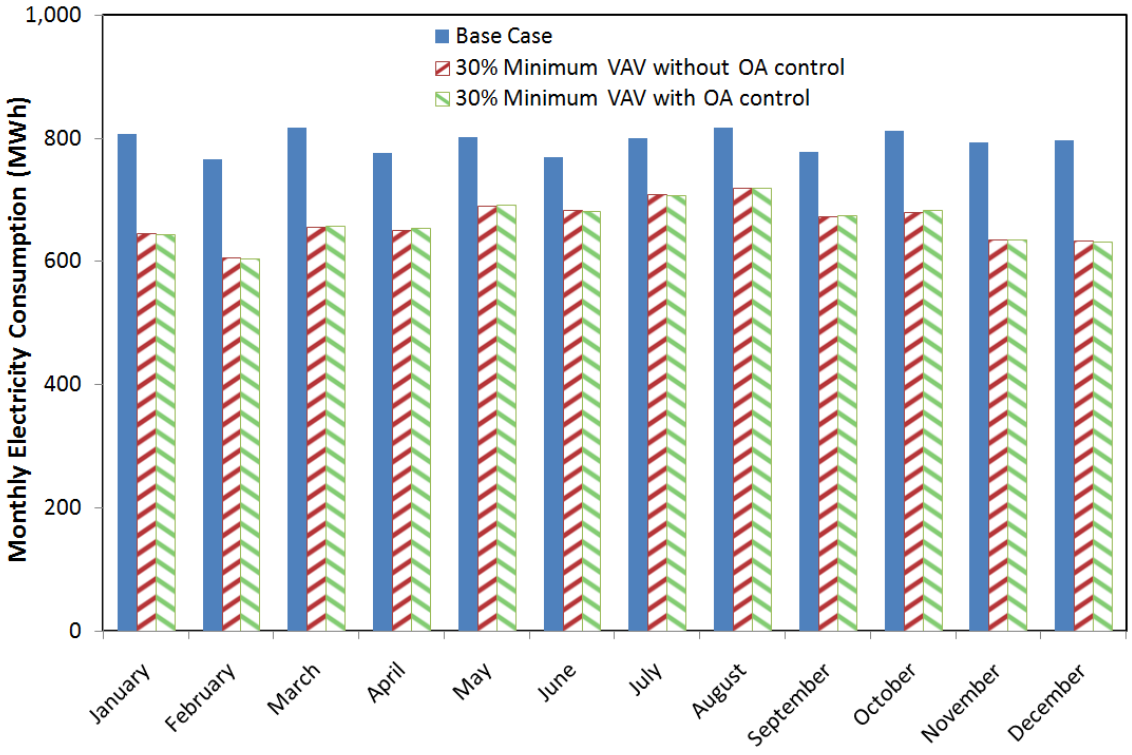


Figure 44. Effect of outside air control on electricity consumption.

Figure 45 shows the effect of outside air control on monthly chilled water consumption. Controlling the outside air to just meet IAQ standards yields significant chilled water savings, as expected. Note in particular the increased savings in summer months. Results showed the addition of outside air control to the variable speed fan operation could potentially save 23% more annual chilled water energy over variable speed fans alone. Both variable speed fan operation and outdoor air control together show potential chilled water savings of 39% from the base case. Using Equation 11 to compute equivalent chiller electricity savings, outside air control could save the TAMUQ building an additional $20,000 per year in utility costs over variable speed operation alone, bringing total monetary savings to $110,000 per year.

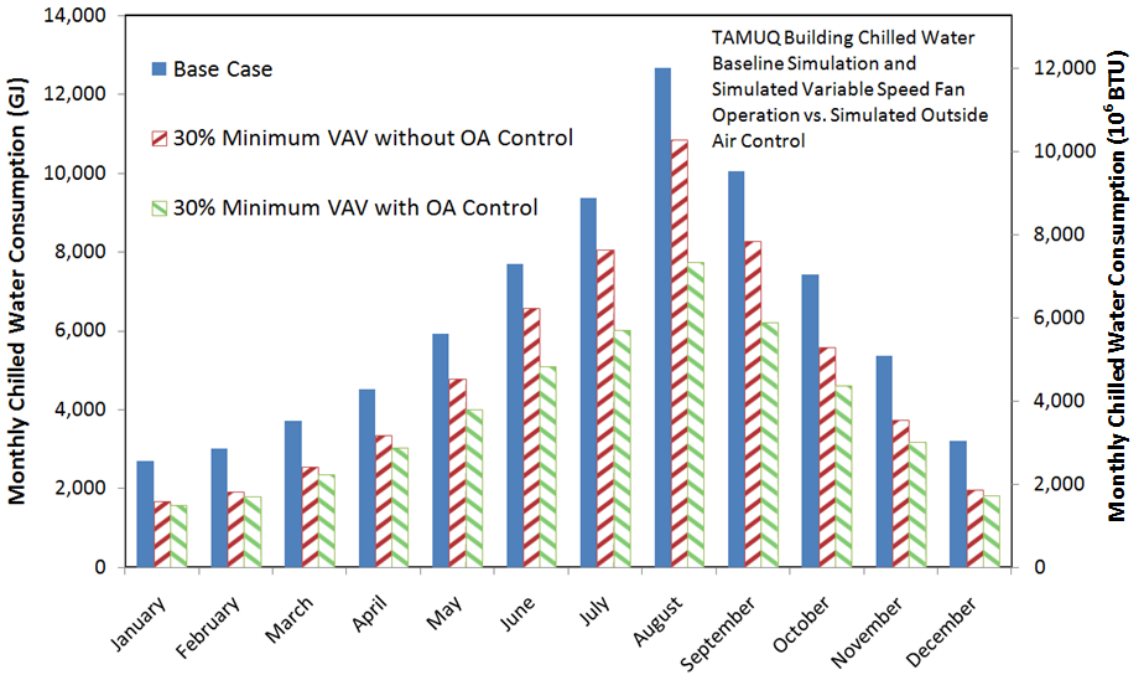


Figure 45. Effect of outside air control on chilled water consumption.

Figure 46 gives an idea of the excess outdoor air use in the base case, and its improvement with outside air control. Zone outside air flow is plotted on the X-axis, normalized to the required outside air flow at the time according to the procedure of ASHRAE 62.1:

$$\dot{V}_{norm} = \frac{\dot{V}_{OA,actual}}{\dot{V}_{OA,required}}. \qquad (25)$$

Values greater than unity represent excessive outside air flows, while those less than unity represent inadequate ventilation during a given hour. On the Y-axis is the percentage of zone-hours throughout the year when outside air flow was at above the specified normalized flow rate. Ideal outside air control appears as a vertical line at a normalized flow of one, where 100% of the time all zones were supplied just enough

fresh air without any waste. The base case curve in Figure 46 is far from ideal, with more than half of the zone-hours at five or more times the required outside air flow. Enabling true VAV operation helps slightly. By reducing total flows during part load periods, outside air flows are reduced as well. Adding outside air control brings the curve much closer to the ideal case. Some zones still remain above requirements due to cases where multiple zones having different outside air needs are served by the same air handlers

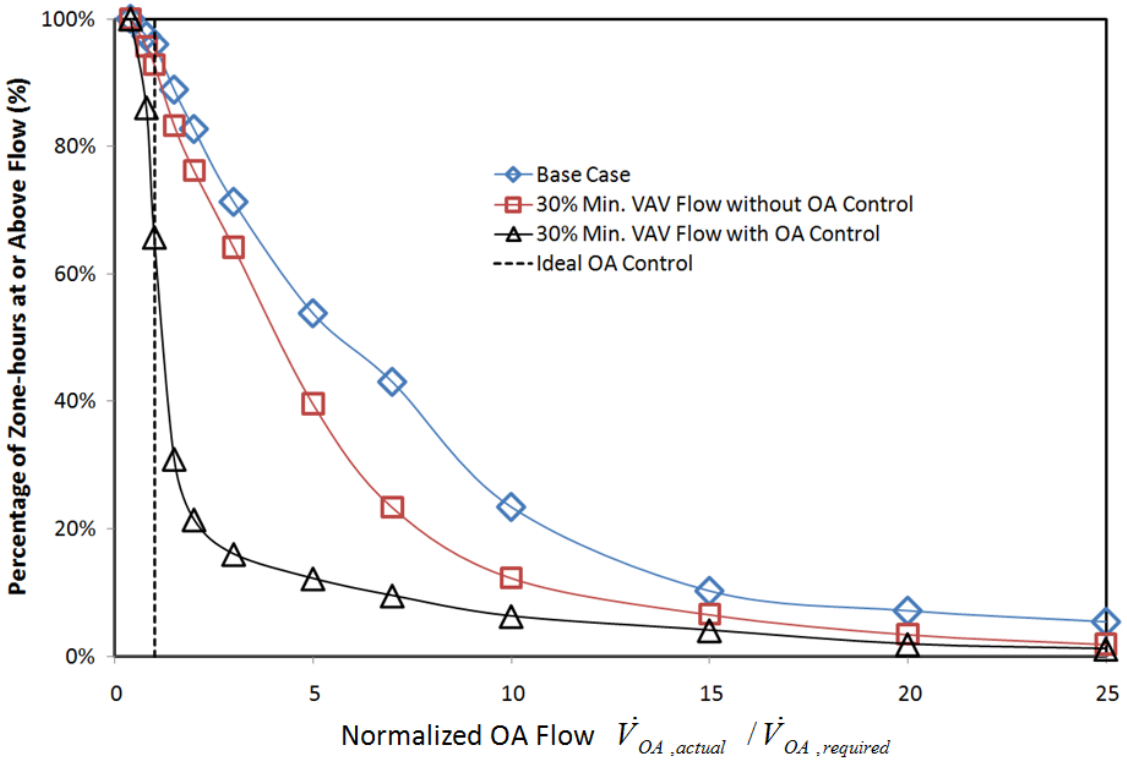


Figure 46. Fraction of zone-hours exceeding outside air requirements.

As seen in Figure 46, even with outside air controllers, some zones still remained above requirements and more were brought below requirements than in the base case. Part of the overuse was due to more outside air being intentionally used during times

when ambient conditions were cooler than the return air temperature and offer "free cooling". The remainder was due to cases where multiple zones having different outside air needs were served by the same air handlers. The ASHRAE 62.1 multi-zone system outside air procedure, Equations 19-23, attempt to account for this. Figure 47 shows a similar plot comparing the ASHRAE 62.1 multi-zone system procedure to a simple sum of the individual zone requirements given by Equation 18. The overuse instances were reduced when using the zone sum method, but at the expense of more out-of-compliance zone-hours.

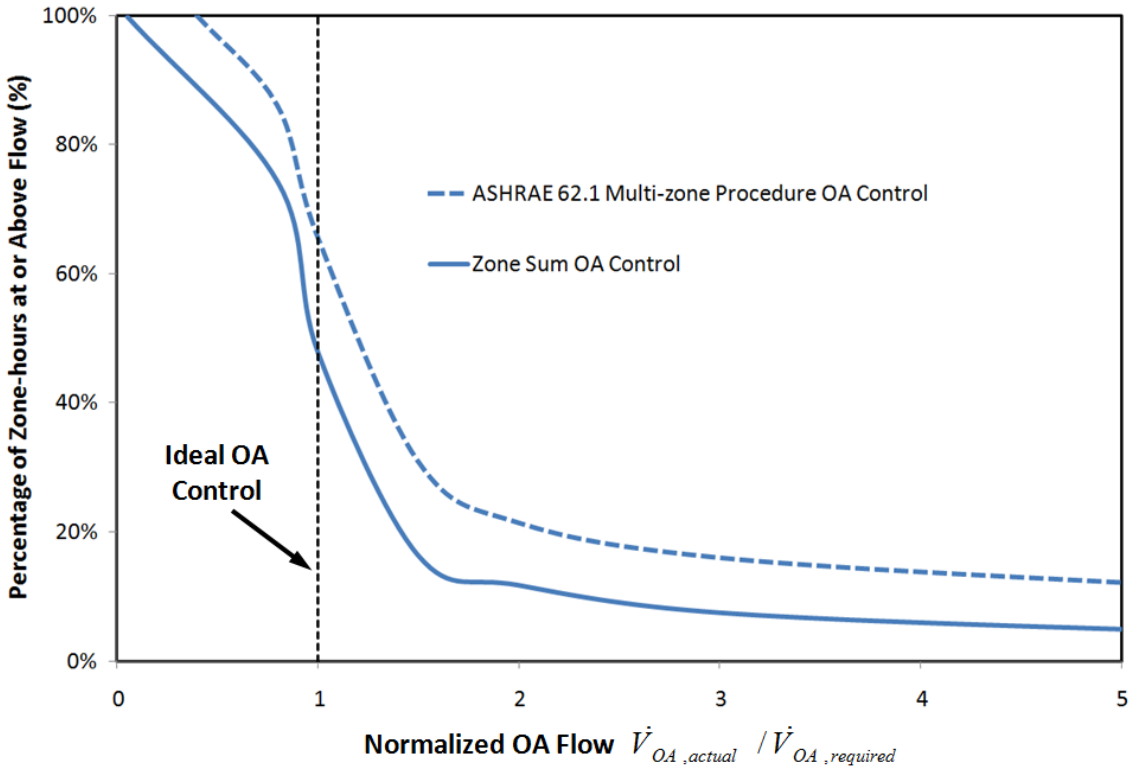


Figure 47. Comparison of ASHRAE 90.1 multi-zone procedure to zone outside air requirement sum.

Compromising IAQ, even by the small amount resulting from using a sum of individual zone requirements rather than the multi-zone procedure, can have significant consequences for occupant productivity (Sterling et al. 1994; Mathews et al. 2001). Hedge and Gayden (2009), and Lan et al. (2011) showed that uncomfortable indoor environments, including poor IAQ, can reduce office productivity by up to 10%. Shaughnessy et al. (2006) showed that increased $CO_2$ levels in classrooms stemming from inadequate ventilation can lead to significantly worse student performance on standardized tests, again by up to approximately 10%.

One way to quantify the costs of reduced IAQ was monetarily. A productivity-due-to-IAQ cost analysis was conducted on the TAMUQ building. The cost of one semester's tuition at TAMUQ was $9,900 per student for 12 credit hours (TAMUQ 2010). A survey at the University of New Hampshire found that students there study out of the classroom for 4.7 hours, on average, per three-hour-course per week (Finkel 2005). Assuming a similar number for TAMUQ, and that 80% of these study hours were spent in the TAMUQ building, a standard 15-week semester costs the average student approximately $24 per hour spent in the building. The average hourly wage of the non-student work force in the building was assumed to be close to this. Therefore, $24/hr can be considered a rough monetary value of productivity at TAMUQ.

For the analysis, any zone out of ASHRAE 62.1 ventilation compliance incurred a five percent penalty on productivity value during that hour for *each* occupant of the zone during that hour. All zone costs were summed at each time step. The sum of the

cost at each time step represented the approximate annual cost to building productivity due to lack of IAQ, according to

$$C_{IAQ} = \sum_{all\ hrs} \sum_{all\ zones} \begin{cases} \$1.20 N_z, & \dot{V}_{norm} < 1 \\ 0, & \dot{V}_{norm} \geq 1 \end{cases}, \qquad (26)$$

where \$1.20 is five percent of the hourly productivity value calculated above. Five percent was chosen as a mid-range value from the findings of Shaughnessy et al. (2006), Hedge and Gayden (2009), and Lan et al. (2011). Figure 48 shows the IAQ productivity costs of the different control scenarios. All but the base case also employed VAV operation with 30% minimum flow rate. Note that controlling outside airflow to ASHRAE 62.1 minimums results in productivity costs significantly greater than energy cost savings. Note also the additional high cost of simply summing the individual zone requirements to control AHU outside air intake.

As a disclaimer, Figure 48 is not intended to directly suggest that simply maximizing the amounts of outside air, as was essentially done in the base case, is the best practice from a cost perspective. In reality, other environmental factors also have a pronounced effect on productivity such as humidity and thermal comfort. Excess outside air can lead to overly humid, undercooled, or overcooled indoor conditions which could actually detriment productivity even more. Figure 48 is only meant to show the incremental productivity costs associated with varying degrees of outside air intake *alone*.

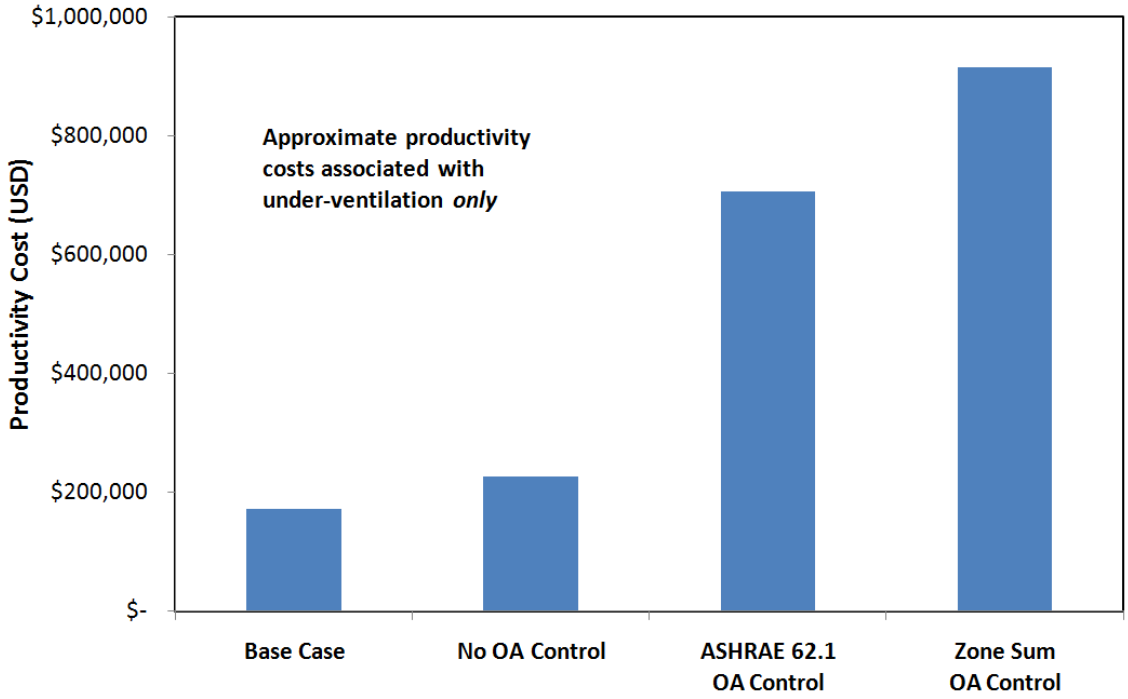


Figure 48. Productivity cost of compromising IAQ.

Figure 49 shows the IAQ costs for the different control scenarios when mitigated by energy cost savings. True VAV operation without outside air control saves a small amount in total from the base case, but clearly the additional chilled water savings from adding outside air control do not outweigh the costs incurred by under-ventilating some zones. It should again be stressed that the IAQ cost analysis was approximate and mostly qualitative in nature. The exact cost figures in Figure 48 and Figure 49 were intended to demonstrate the relative effects of different outside air control methods.

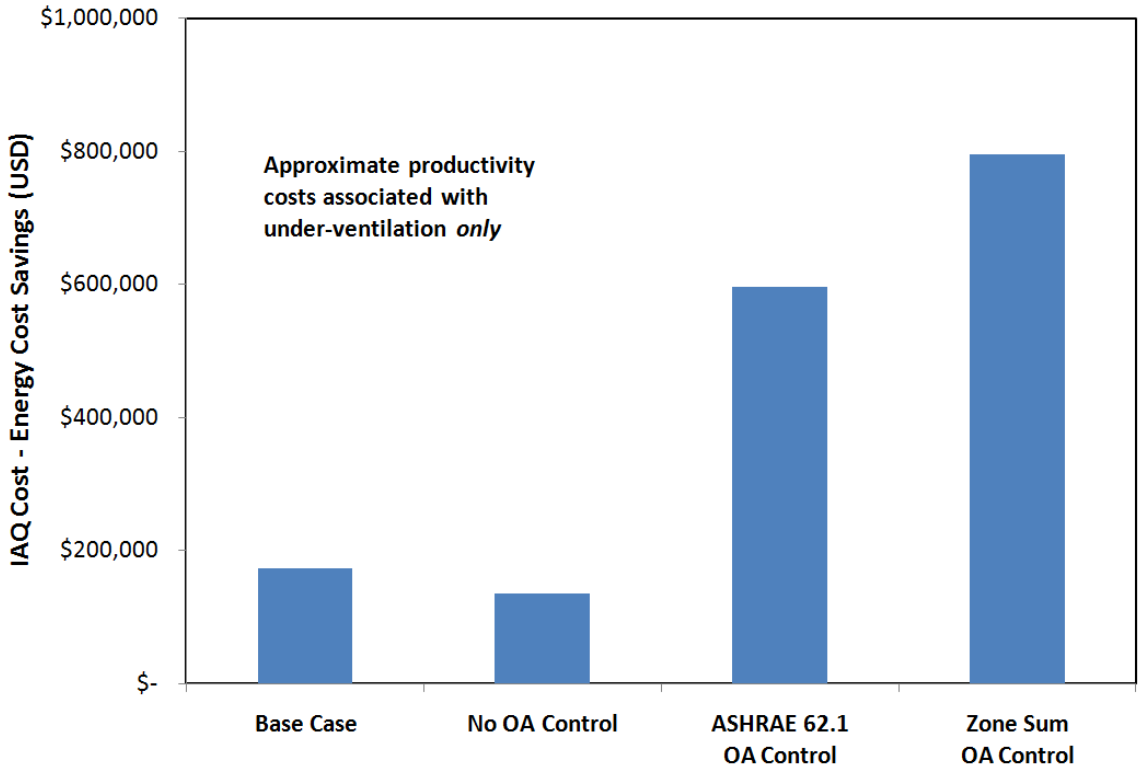


Figure 49. Productivity cost minus energy cost savings.

One way to more closely approach ideal outside air control without reducing ventilation too much and affecting productivity is through a dedicated outside air system (DOAS) (Mumma 2001). In a DOAS, the outdoor latent and sensible loads are decoupled from the indoor mostly sensible-only loads. Certain AHU's in the system cool outside air only, and can deliver precise amounts of ventilation air as necessary to the zones. The remainder of the cooling load is satisfied by less energy intensive re-cooled return air. This is done through separate air-handlers with a dual-duct system, fan coil units, or radiant cooling ceiling panels (Mumma 2001). In this way, a DOAS can closely

approach the ideal outside air control curves of Figure 46 and Figure 47, maximizing cooling savings while maintaining IAQ.

To model a DOAS at TAMUQ, EnergyPlus hourly occupancy and zone floor area data were used to calculate the required outside air flow to each zone at each hour from Equation 18. The excess flow of outside air was then calculated from

$$\dot{V}_{OA,z,X} = \dot{V}_{OA,z,actual} - \dot{V}_{OA,z,required}. \qquad (27)$$

Finally, the potential cooling energy savings from cooling this excess flow at return conditions rather than current ambient conditions was calculated similar to Equation 16, from

$$Q_{CC,X} = \dot{V}_{OA,z,X}\rho_{air} max\{[c_{p,air}(T_\infty - T_{r,air}) + h_{fg}(\omega_\infty - \omega_{r,air})], 0\}. \qquad (28)$$

The potential savings were considered zero if the per-mass total energy term in square brackets was negative, representing a period of free cooling. The excess outside air flow, $\dot{V}_{OA,z,X}$, was allowed to be negative, representing periods of underventilation that would need more outside air in an ideal DOAS, subtracting slightly from total potential savings.

Figure 50 shows the predicted monthly chilled water consumption of all three outside air control methods – ASHRAE 62.1, zone requirement sum, and DOAS – as compared to the base case. Employing a DOAS reduced chilled water consumption further than ventilation control using both the ASHRAE multi-zone system procedure and a simple zone requirement sum. A DOAS could save 30% on annual chilled water consumption over an ASHRAE 62.1 outside air control system, and 49% over the base case. In monetary terms, a DOAS could potentially save $124,000 annually in equivalent total electricity costs.

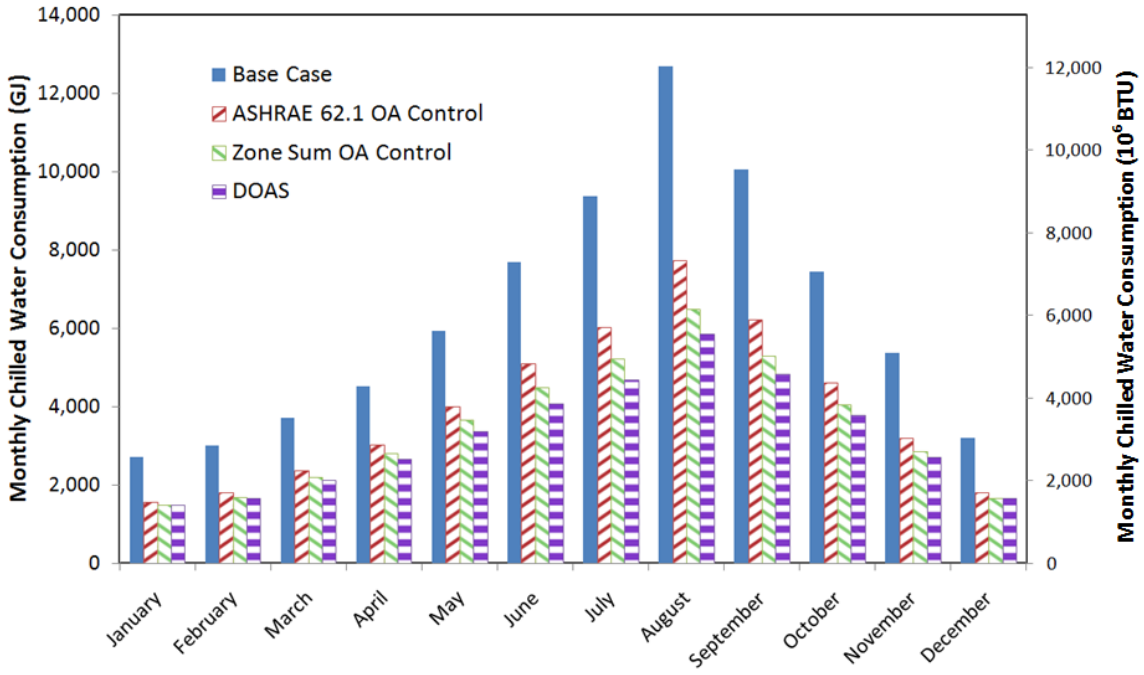


Figure 50. Effect of a DOAS on monthly chilled water consumption.

In addition to being more energy efficient, a variable volume DOAS using 100% outside air could also precisely ventilate zones according to their individual requirements. Under-ventilation would therefore not be an issue, and the productivity cost associated with IAQ would be near zero. A DOAS would be the optimum outdoor air control system in terms of energy use and total energy/productivity costs. With both variable speed fan operation and optimal control of outside air using a DOAS, the simulated EUI for the improved building was calculated to be 318 kWh/m$^2$/yr (108 kBTU/ft$^2$/yr).

## 5.3 FPTU Retrofits

FPTU retrofits were considered as an energy saving method. FPTU's induce warmer return air into the supply air stream during part load periods. Widespread overcooling was observed in the building, along with electric reheat usage noted in the metered and baseline simulation results. In the right conditions, FPTU's can mitigate these issues, increasing building comfort and decreasing building energy consumption.

### *5.3.1 Theory*

FPTU's can have two configurations: series or parallel. In a series configuration, shown in Figure 51a, the terminal fan is in line with the primary air stream. A series fan must run at all times, and supplies a constant total flow rate comprising primary and return air (Cramlet 2008). At part cooling loads when dampers modulate the cooled primary flow, more warm return air is induced to make up the constant supply flow. In a parallel configuration, shown in Figure 51b, the terminal fan is outside the air stream, and cycles on to induce return air only when heating becomes necessary for the zone.

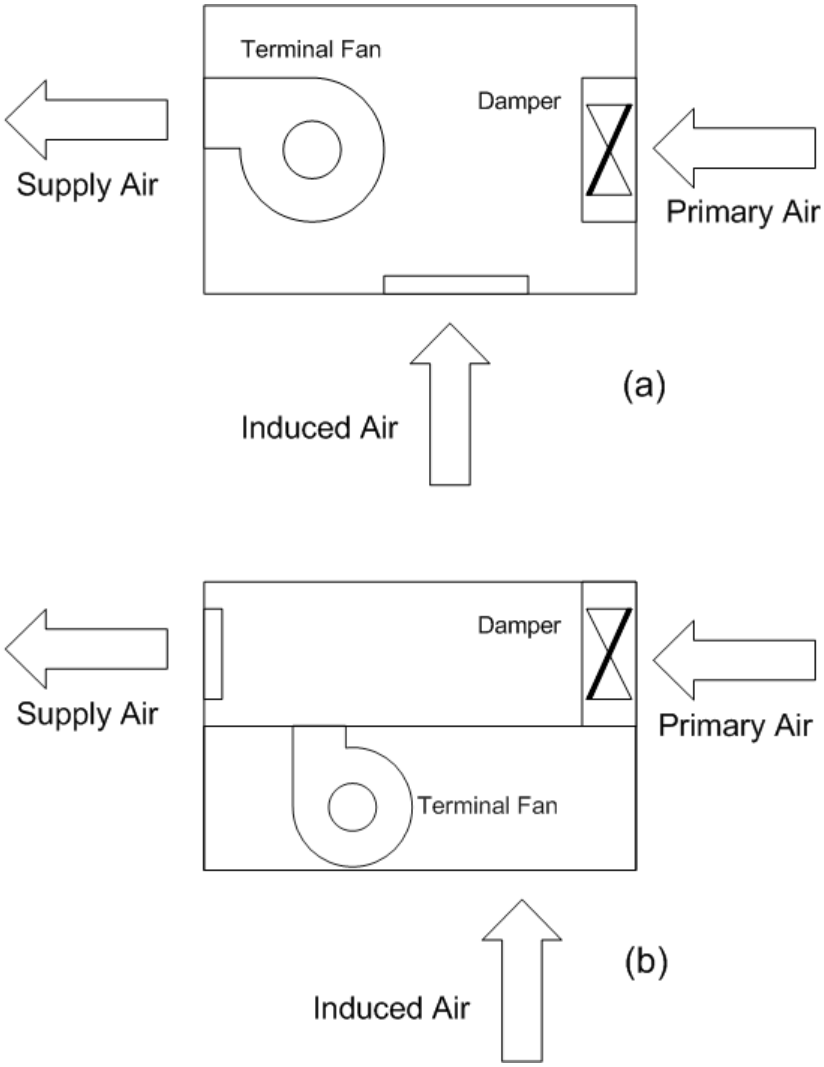


Figure 51. Series (a) and Parallel (b) FPTU configurations (Cramlet 2008).

In addition to the two fan configurations, FPTU fan motors also have two types. The first is an alternating current (AC) induction motor controlled by a silicon controlled rectifier (SCR), and the second is a direct current (DC) electronically commutated motor (ECM). SCR controlled units typically have control voltage set at time of installation, after which they are run at constant speed. ECM controlled units allow for more dynamic

operation, where the input voltage and resultant speed and flow rates are adjustable in the field (Cramlet 2008). ECM motors have also been shown to be more efficient than similar sized SCR units (Edmondson et. al. 2011). The energy consumption when using either motor type in either fan configuration was simulated for a representative section of the TAMUQ building.

To analyze FPTU performance at TAMUQ, a model was constructed based on work by Davis et al. (2009). The model simulated using different FPTU types in the zones of a single TAMUQ air-handler for one year. A fully VAV system was considered in the model, and hourly heating and cooling loads from EnergyPlus were used to calculate the air flows required from the primary and terminal fans.

The maximum sensible cooling load for each zone on the system, times an oversize factor of 1.15 (ASHRAE 2010c), defined the design cooling load for each zone, $Q_{cl,design,z}$. The zone design air flow rates were then calculated using the design load, according to

$$\dot{V}_{design,z} = \frac{Q_{cl,design,z}}{\rho_{air} c_{p,air} (T_{SP,c} - T_{s,air})}. \quad (29)$$

$T_{SP,c}$ represents the thermostat set point when in cooling. The system design air flow rate was then given by the sum of the zone design flows:

$$\dot{V}_{design,AHU} = \sum_{all\ zones} \dot{V}_{design,z}. \quad (30)$$

Since series FPTU's operate at a constant flow rate, the design flow rates for all series units were identical to $\dot{V}_{design,z}$ for each zone. The design flow rates for parallel units were taken as 50% of the design cooling flow for their respective zones, as prescribed in ASHRAE 90.1 (ASHRAE 2010c).

The air flow rate from an FPTU fan was found to depend primarily on the control voltage input to the ECM or SCR, and a representative system pressure (Furr et al. 2007, Cramlet 2008). This pressure was the static pressure downstream from the FPTU, $p_{down}$, in the case of parallel units, and the inlet air velocity pressure to the FPTU, $p_{iav}$, in the case of series units. The equation correlating these variables to the flow rate was found to be

$$\dot{V}_{FPTU} = \alpha_1 + \alpha_2 v_{in} + \alpha_3 {v_{in}}^2 + \alpha_4 p, \qquad (31)$$

where $v_{in}$ is the input voltage, $p$ is $p_{down}$ for parallel units and $p_{iav}$ for series units, and $\alpha_{1\text{-}4}$ are regression coefficients taken from Cramlet (2008). For SCR motors, $v_{in}$ ranged from 160-277 VAC, while for ECM motors $v_{in}$ ranged from 0-10 VDC.

For the AHU analyzed, the total system static pressure at design was taken from the TAMUQ AHU schedule. Of the total pressure, 62 Pa (0.25 in. w.g.) was assumed to be downstream of each FPTU at the design flow rate due to downstream ductwork and diffusers (Thermal Products Corporation 2011, Davis et al. 2009). A downstream pressure factor was given by

$$K_{down} = \frac{62\ Pa}{\dot{V}_{design,z}{}^2}. \qquad (32)$$

The remainder of the design static pressure was assumed to be upstream from the terminal units and due to ductwork, cooling coils, filters, etc. An upstream pressure factor was then calculated from

$$K_{up} = \frac{p_{design,AHU} - 62\ Pa}{\dot{V}_{design,AHU}{}^2}, \qquad (33)$$

where $p_{design,AHU}$ and $\dot{V}_{design,AHU}$ are the total static pressure and air-handler flow rate from the AHU schedule.

Knowing the design static pressures, and the design flow rate for each FPTU, Equation 31 was solved for the control voltage required. Although FPTU's with ECM control have the ability to adjust input voltage to meet the demand, for this analysis ECM voltages were assumed constant at the design value throughout the simulation.

The minimum flow of primary air was a critical input to the model. Based on its value, the minimum attainable cooling supply to each zone was calculated from

$$Q_{min,z} = \rho_{air} c_{p,air} m\dot{V}_{design,z}(T_{SP,h} - T_{s,air}), \quad (34)$$

where $T_{SP,h}$ represents the temperature set point when in heating mode, and $m$ is the minimum VAV flow fraction. If the minimum cooling supply was greater than the cooling load for a zone during a given time step, heating was assumed. The FPTU fan power was added to the zone cooling loads to model heat added from the fan motors. When in heating mode, the amount of additional reheat necessary to maintain the zone heating set points was

$$Q_{rh,z} = Q_{min,z} - Q_{cl}(t) - \dot{W}_{FPTU}, \quad (35)$$

where $Q_{cl}(t)$ is the cooling load at the time step, negative if a heating load. $\dot{W}_{FPTU}$ is the FPTU power, given by

$$\dot{W}_{FPTU} = \alpha_I + \alpha_{II} v_{in} + \alpha_{III} {v_{in}}^2 + \alpha_{IV} {v_{in}}^3 + \alpha_V p. \quad (36)$$

$\alpha_{I\text{-}V}$ again represent regression coefficients from Cramlet (2008). The regression coefficients used in the model were derived experimentally only for series and parallel boxes with eight inch inlet sizes.

For the FPTU cases, the primary flow required for each zone was determined from

$$\dot{V}_{p,z} = \begin{cases} \frac{Q_{cl}(t)}{\rho_{air} c_{p,air} (T_{SP,c} - T_{s,air})}, & cooling\ mode \\ m\dot{V}_{design,z}, & heating\ mode \end{cases}. \quad (37)$$

For the non-FPTU case, when a certain amount of heating becomes necessary, the reheated supply air temperature needs to be quite hot to maintain the heating set point at the minimum VAV flow rate. A discharge temperature greater than 8.3°C (15°F) above the room temperature is known to cause uncomfortable zone air stratification and short circuiting of warm supply air to the return grilles (ASHRAE 2005). Therefore, for these high heating periods, the primary supply volume had to be increased again to meet the heating load while not exceeding the discharge air temperature limit, according to

$$\dot{V}_{p,z} = \frac{-Q_{cl}}{\rho_{air} c_{p,air} \Delta T_{rh,max}}, \quad (38)$$

where $\Delta T_{rh,max}$ is the maximum allowable temperature difference between discharge temperature and space temperature, 8.3°C (15°F). Since FPTU's have higher flow rates from induced return air, they need no extra primary air to satisfy heating requirements.

At each time step, the primary flows to each zone determined from Equations 37 and 38 were summed to find the total flow required from the primary fan:

$$\dot{V}_{p,AHU} = \sum_{all\ zones} \dot{V}_{p,z}. \quad (39)$$

Given this primary flow, the upstream static pressure drop in the system was

$$p_{up} = K_{up} \dot{V}_{p,AHU}^{\ 2}. \quad (40)$$

The downstream static pressure drop for each zone depended on the individual zone flows, according to

$$p_{down,z} = K_{down}\dot{V}_{p,z}{}^{2}. \quad (41)$$

The pressure drops due to the VAV terminal units were calculated from

$$p_{par,z} = \frac{\dot{V}_{p,z}{}^{2}}{\alpha_{par}} \quad (42a)$$

$$p_{ser,z} = \frac{\dot{V}_{p,z}{}^{2}}{\alpha_{ser}} - 67\ Pa \quad (42b)$$

$$p_{non,z} = \alpha_{non1} + \alpha_{non2}\dot{V}_{p,z} + \alpha_{non3}\dot{V}_{p,z}{}^{2}. \quad (42c)$$

The subscripts *par*, *ser*, and *non* represent parameters for the parallel, series, and non-FPTU cases, respectively. The $\alpha$ constants for parallel and series units were taken from Cramlet (2008). The $\alpha$ constants for non-FPTU pressure drop were derived from curve fitting to manufacturers specifications for VAV terminal units of the same size as the FPTU's studied (Trane 2011).

A common VAV system control strategy is to modulate fan speed and flow such that at least one VAV terminal unit damper in the system remains 100% open (Hartman 1989). Equations 42a-42c were derived assuming 100% open dampers. Therefore, adding the full-open VAV-terminal-unit pressure drops to the downstream pressure drops for the respective zones gives the minimum possible pressure drop for each zone at the given required flow. The primary fan will modulate to the maximum of these, giving the total static pressure for the primary fan as

$$p_{p,AHU} = p_{up} + (p_{down,z} + p_{box,z})_{\max}, \quad (43)$$

where $p_{box,z}$ is $p_{par,z}$, $p_{ser,z}$, or $p_{non,z}$, depending on the VAV terminal unit type.

A regression analysis of AHU fan manufacturer data for a fan in the size range of the TAMUQ AHU (Trane 2004) gave the fan flow in terms of fan speed and total static pressure:

$$\dot{V}_{p,AHU} = a_1 + a_2 p + a_3 p^2 + a_4 S + a_5 S^2 + a_6 pS + a_7 p^2 S^2. \quad (44)$$

$p$ is the total static pressure on the fan from Equation 43, and $a_{1\text{-}7}$ are regression coefficients. $\dot{V}_{p,AHU}$ and $p$ were known, and Equation 44 was solved for the fan speed, $S$. The primary fan power could then be calculated from

$$\dot{W}_p = \frac{bS^3}{\eta_p}, \quad (45)$$

where $\eta_p$ is the fan efficiency and $b$ is a constant relating fan speed to power, again curve fitted from manufacturer data (Trane 2004).

The moisture content of the return air for each zone was

$$\omega_{r,z} = \omega_{s,air} + \frac{Q_{lat}(t)}{h_{fg}\rho_{air}\dot{V}_s}, \quad (46)$$

where $Q_{lat}(t)$ is the latent load on the zone for the time step and $\dot{V}_s$ is the total supply flow to the zone including primary and induced return flow. The return air temperature for each zone was assumed to be the zone set point, $T_{SP,c}$ or $T_{SP,h}$, depending on whether the zone was in cooling or heating mode. The total moisture content and temperature of the return air stream back to the AHU mixing box was the average of all zone moisture contents and temperatures weighted for individual zone flows. The mixed moisture content and temperature were then calculated from Equations 17a and 17b. The outside air fraction, $x$, was a constant input to the model. Finally, the load on the AHU cooling coil was calculated from Equation 16, where $\dot{V}_{air}$ was replaced with $\dot{V}_{p,AHU}$ at the given

time step. In the case of series FPTU's, the terminal fan operates even during cooling periods. The FPTU power must be added to the cooling coil load because the cooling coil must overcome the temperature rise due to the series fan.

### *5.3.2 Simulation Results*

An AHU representative of the TAMUQ building as a whole was chosen for the FPTU analysis. The AHU chosen serves 11 zones with a design flow rate of 6000 L/s (12,700 CFM) and a cooling capacity of 100 kW (28 tons). The individual zone flow rates range from 200-600 L/s (420-1270 CFM). As a caveat, these flow rates represented the high end of the acceptable ranges for the eight inch series FPTUs. Therefore, the performance of the ECM controlled terminal fans in comparison to SCR control was not typical of the two control types. ECM is typically more efficient at lower flows, and in reality box sizes would be selected accordingly (Cramlet 2008). This preliminary analysis was intended primarily to show the principles at work in FPTU's and how they affect building energy efficiency. As a future study, the model should incorporate relations for a variety of inlet and fan sizes, making it a more robust research and design tool.

A primary factor affecting terminal unit energy performance was the minimum VAV fraction. Figure 52 shows the annual primary fan energy for both FPTU configurations with both motor control types, along with that for non-FPTU's, as a function of minimum flow fraction. The motor control type had no effect on the primary

fan energy at any flow fraction for the parallel FPTU's, and only a marginal effect for the series units. At lower minimum flow fractions, parallel units used less primary fan energy, but after 40% cooling design flow, series units used less. At primary flows closer to the design cooling flow, the series fans offered a pressure drop advantage over the other units, and the primary fan power was lower. A higher minimum flow rate meant more total time during the year operating near the cooling design flow, so the total series primary fan energy was lower. VAV terminal units without fans drew the least energy from the primary fan at all minimum flow rates plotted, but it should be noted that at 70% minimum flow, series units become the overall lowest user. However, at this setting, total primary fan energy for all units were nearly three times those at the 50% setting. Minimum flow settings beyond 50% of cooling design flow were ignored for this reason.

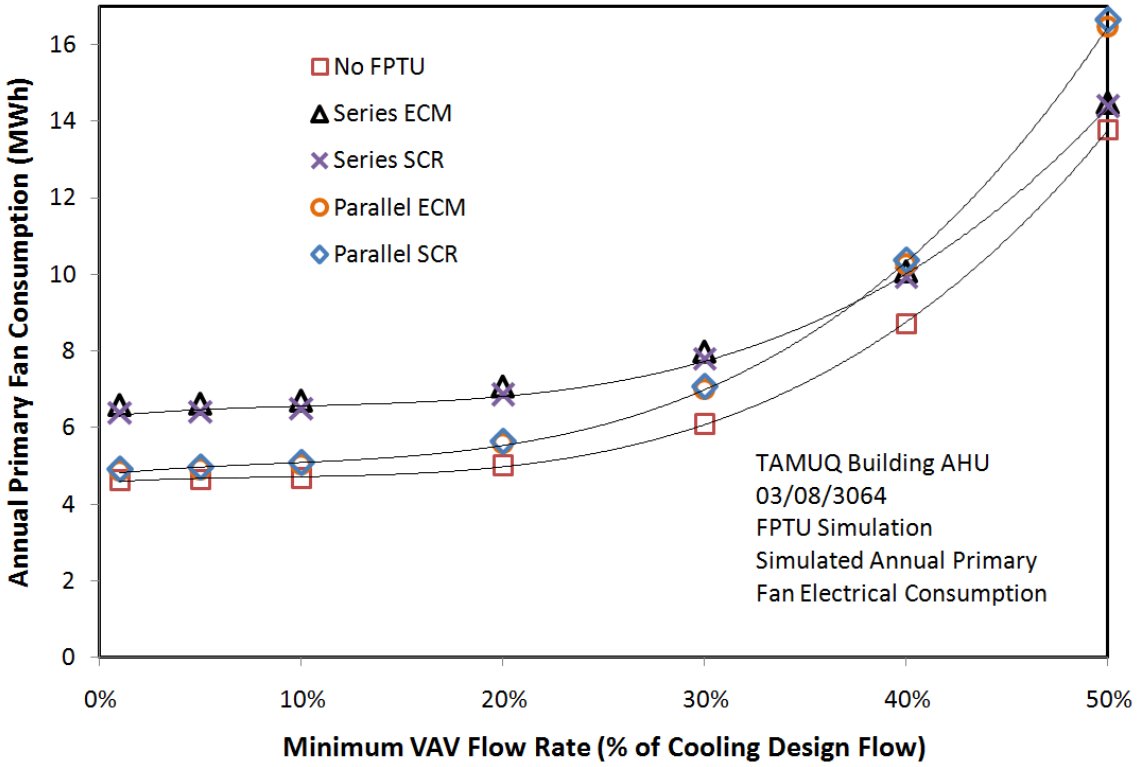


Figure 52. Annual primary fan energy vs. minimum VAV flow.

Figure 53 shows the yearly terminal fan energy for each unit type as a function of minimum flow. A series FPTU's supplies a constant air volume to its target zone, so the control voltage is set to provide the design cooling air volume at all times, regardless of the primary flow settings. The series fan consumption in Figure 52 was therefore also independent of this setting. In contrast, parallel fan consumption was small at low minimum primary flow rates, but increased with the minimum primary flow rate. Parallel units operate only when in heating mode. When the minimum primary flow rate is higher, more time is spent in heating mode, and more parallel fan energy is consumed. Note the differences in consumption for ECM and SCR motors. For the parallel units, given the loads on the zones, the terminal fans operated near the bottom of the flow

range, where ECM provided more efficient control. Conversely, the series fans operated at the top of their flow range, where SCR was more efficient. This is also the reason for the slight difference in primary fan energy usage for the series units in Figure 52. Since the ECM series fans used more energy, they added more heat to the supply air. The off-coil primary air temperature was assumed constant, so to provide the required cooling energy to the zones, primary flow had to be increased. The difference in Figure 53 is less than 10%, and the difference in Figure 52 is even smaller, around 2%.

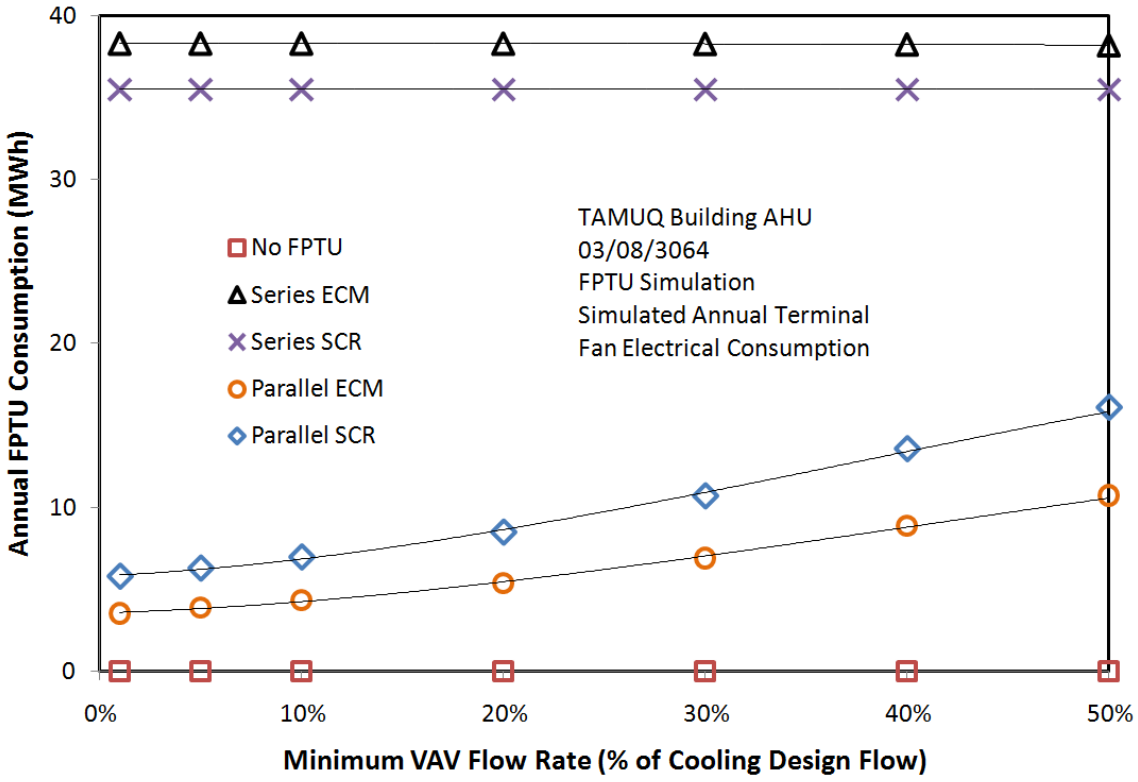


Figure 53. Annual FPTU fan energy vs. minimum VAV flow.

Figure 54 shows the total reheat energy for the different terminal units as a function of minimum primary flow rate. The non-FPTU case used the most reheat energy, followed by the parallel units and finally the series units. For the most part, Figure 54 is a direct reflection of the FPTU fan consumption, because terminal fan energy went toward heating the air stream. The parallel ECM and SCR curves have a larger offset in comparison to their series counterparts, which are essentially coincident. The difference in ECM and SCR terminal fan energy from Figure 53 was spread over the entire year for series units due to their constant operation. Since parallel units operate only in heating mode, the parallel fan energy difference was only spread over periods when reheat was also active, causing a larger overall difference in Figure 54. All terminal unit curves in Figure 54 behave nearly linearly with minimum primary flow rate, with the exception of the non-FPTU case. Recall that in modeling the non-FPTU system, the zone to discharge air temperature difference was maintained below 8.3°C (15°F) to prevent short circuiting and zone stratification (ASHRAE 2005). At low minimum flow rates and high heating loads, the system requires above-minimum primary flow to keep the discharge temperature within the limit. This additional primary air is at the cold off-coil temperature, and requires additional reheat energy to heat it to the maximum discharge temperature. FPTU's deliver this extra air at the warm return temperature, so there is no net gain in reheat requirement.

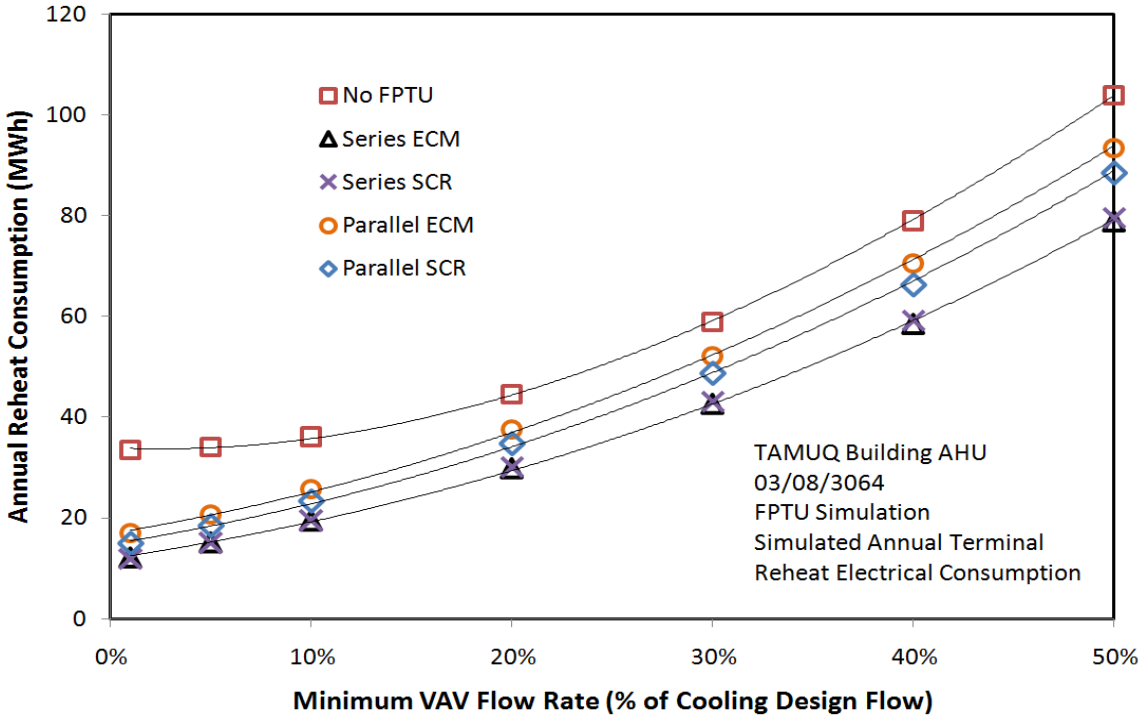


Figure 54. Annual reheat energy vs. minimum VAV flow.

Figure 55 demonstrates the extra reheat flow phenomenon for the non-FPTU case. The fraction of zone-hours in the simulation that would have exceeded the maximum discharge temperature at the minimum flow is plotted against minimum flow fraction. The number is quite high at near-zero minimum flow. Over one fourth of the simulation requires more primary air, reheat, and cooling coil energy than is necessary. The fraction drops quickly however, and reaches under 5% when minimum flow is 30% of design flow. Thirty percent of design flow is the ASHRAE 90.1 limit on volume of cooled and reheated air (ASHRAE 2010c).

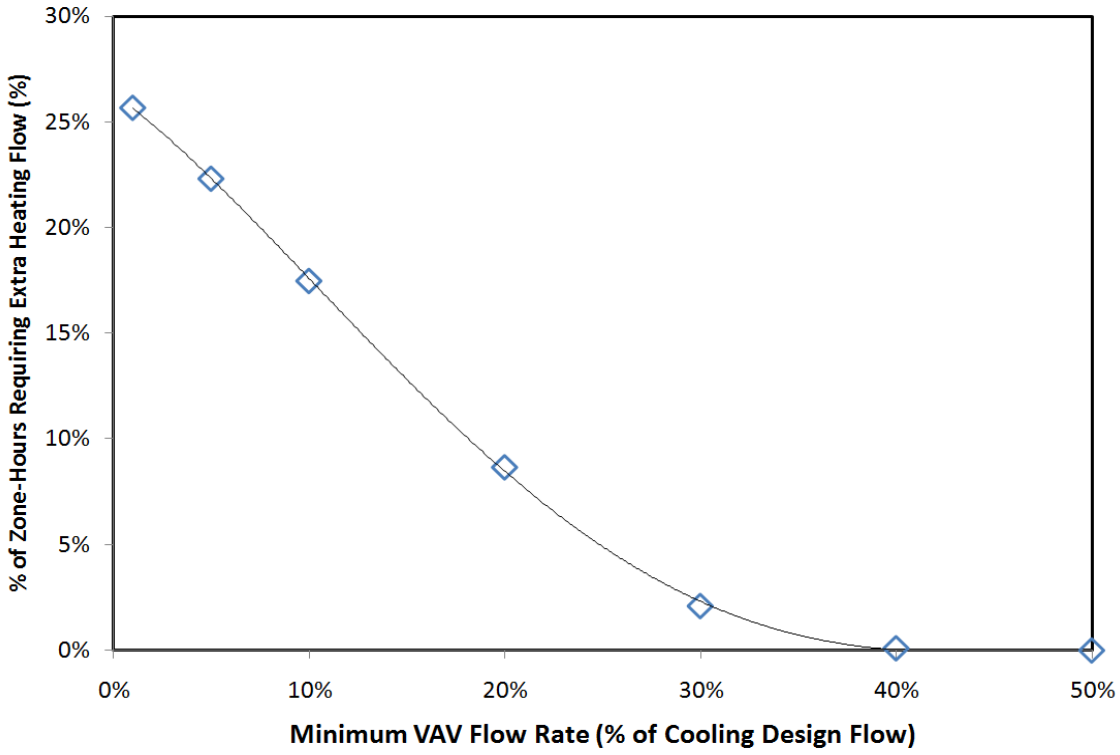


Figure 55. Zones exceeding discharge temperature limit at minimum flow.

Figure 56 shows the chilled water consumption from the cooling coil of each VAV terminal unit type as a function of minimum primary flow. The series units required the most cooling coil energy, followed by the non-FPTU's and parallel FPTU's. To overcome the constant added heat from the series fans, more primary air was required, and more energy was consumed from the cooling coil. Again, because of the discharge air temperature limit, extra cooled air was required from the non-FPTU's at low minimum flows and high heating loads, causing the total cooling coil energy to be slightly higher.

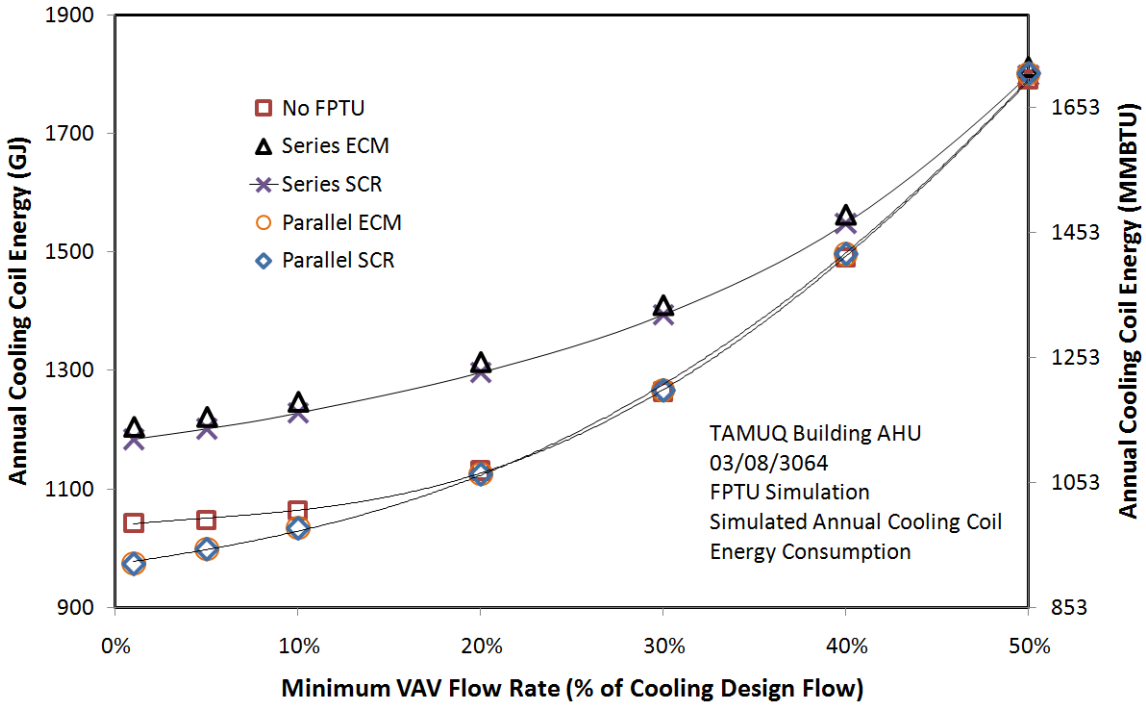


Figure 56. Annual cooling coil energy vs. minimum VAV flow.

Figure 57 shows the total equivalent electricity use for the year when cooling coil energy is converted to chiller electricity from Equation 11. It can be seen that parallel FPTU's did show some savings potential at very low minimum VAV flows, mostly due to the heating limits of non-FPTU systems shown in Figure 55. Series fans showed no potential savings until reaching unreasonably high minimum flow rates. The potential savings for parallel units drop to zero at a minimum flow of around 20% of cooling design flow, and are slightly negative thereafter. Unfortunately, minimum flow rates much below 20% are not feasible due to ventilation restrictions discussed in Section 5.2.

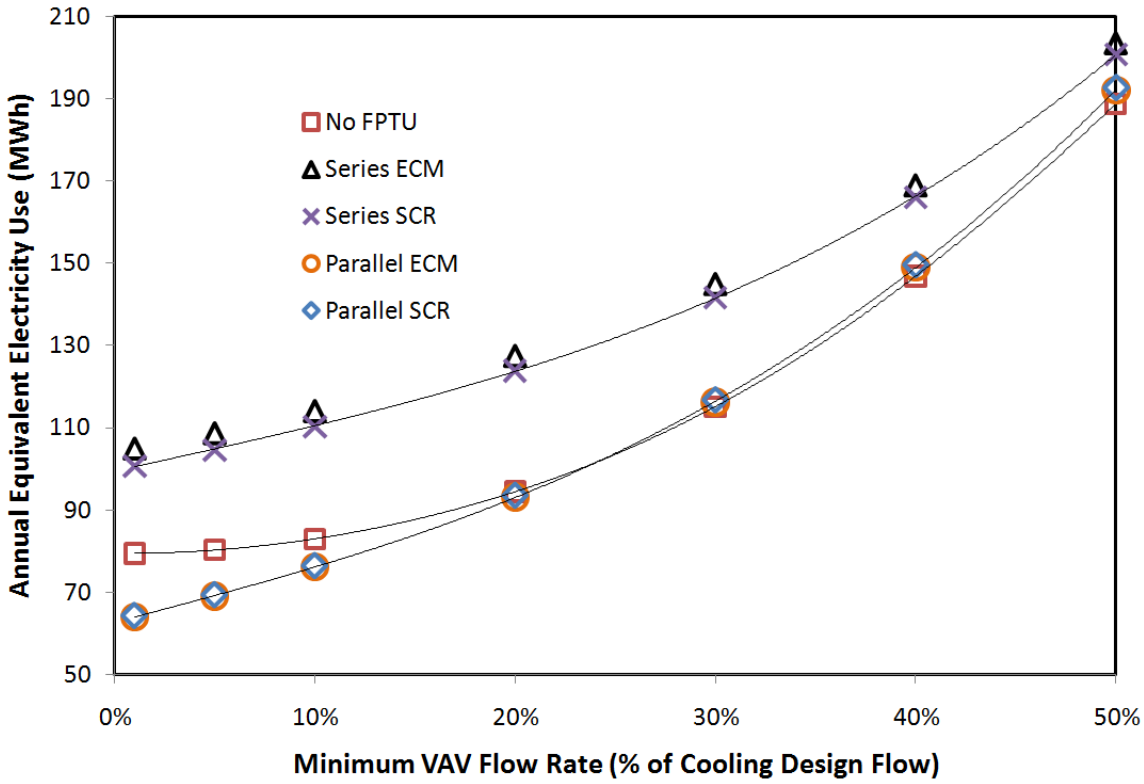


Figure 57. Equivalent annual electricity consumption vs. minimum VAV flow.

No significant overall difference was found between using SCR or ECM controlled terminal fans in either FPTU configuration. Any advantage posed by one in power draw per volume flow is mitigated by the other in less need for electric reheat. This is not strictly true for series units, which operate even when reheat is not in use. Indeed, a slight difference is seen in Figure 57 between the series controllers for this reason.

The real advantage of using ECM over SCR lies in its flexibility. In this analysis, the FPTU voltages and flow rates were assumed constant at their design values throughout the simulation. Future testing of FPTU energy saving potential should

account for variability of series and parallel ECM speed to track the heating or cooling load. This aspect was neglected here due to the voltage range limitations of the FPTU equations used.

This simulation also assumed the return air being induced by the FPTU's was at the zone temperature. Manufacturers' FPTU endorsements often cite the use of "warm" plenum air for "free" reheating (Trane 2010). If a warmer return air stream were assumed, additional savings from FPTU's could be realized.

Even with the assumptions used in this simulation, it was shown that while not necessarily *more* efficient than a traditional no-fan VAV system, FPTU's, specifically of parallel configuration, were just as or nearly as efficient. A comfort advantage could then conceivably be claimed for FPTU's, given that they maintain higher total flow rates, even at medium to low cooling loads. A study of office environmental quality found that smell and freshness were two factors voted least favorable by the occupants, while air movement was voted one of the most important factors to the occupants (Kamaruzzaman 2011). Constant flow rates offered by FPTU's could help promote all three of these factors, possibly increasing productivity.

# CHAPTER VI

# CLIMATE COMPARISONS

A secondary objective of the TAMUQ study was to investigate the effect of climate on each proposed efficiency improvement. Measures having more marked improvement in the extreme hot and humid conditions like Doha's could then be recommended more highly for promoting sustainable building in such areas.

Phoenix, Arizona and Houston, TX were chosen as locations to compare to the results found for TAMUQ in Doha. Phoenix sees similar extreme temperatures – and thus sensible cooling loads – to Doha's during the summer, but without as much humidity. Figure 58 shows typical daily minimum, maximum, and mean daily dry bulb temperatures for each month in Doha compared to those in Phoenix (OTBD Weather Station 2011, NREL 2008b). The daily highs and means are very similar, although the lows are lower in Phoenix because it gets colder at night. Figure 59 is a similar plot with minimum, maximum, and mean dew point temperatures shown for the two locations. Phoenix is considerably drier, with its peak dew points only just approaching the daily average in Doha.

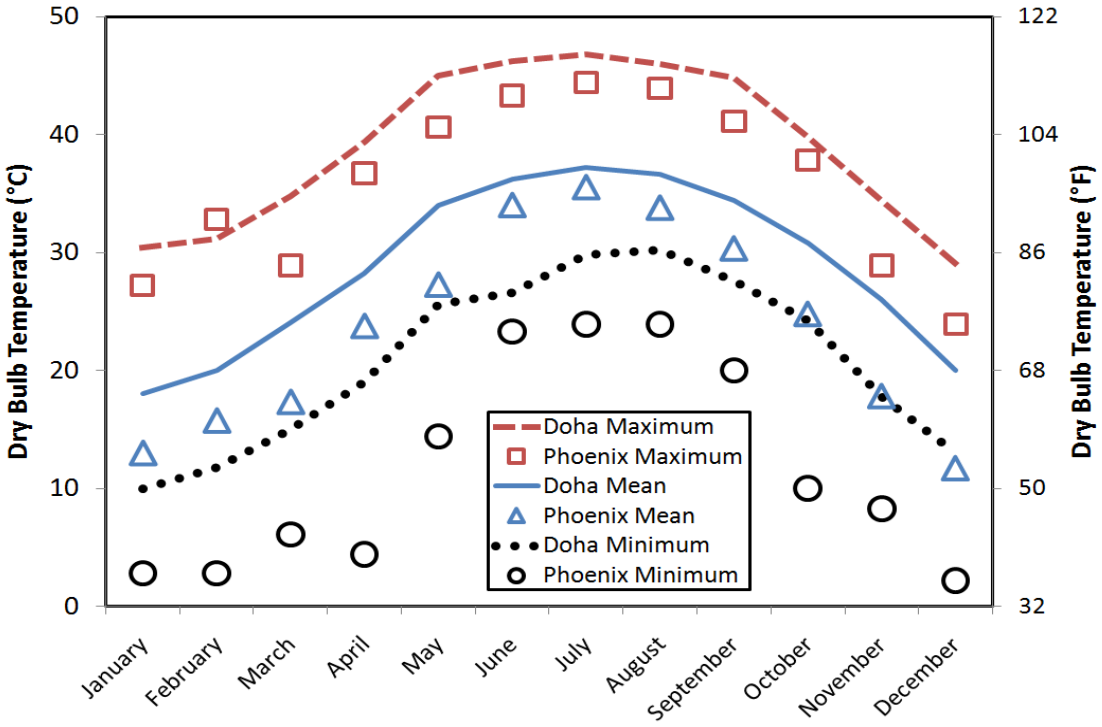


Figure 58. Doha vs. Phoenix daily high, low, and mean dry bulb by month.

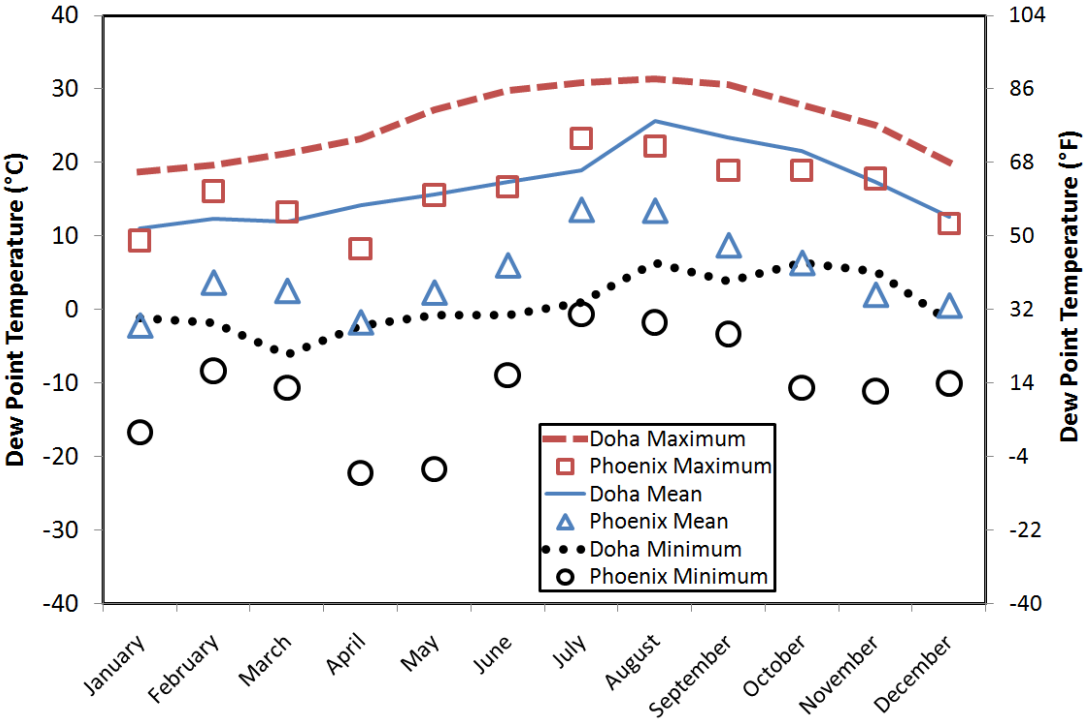


Figure 59. Doha vs. Phoenix daily high, low, and mean dew point by month.

Houston, like Doha is quite humid in the summer, but typically with lower dry bulb temperatures, as seen in Figure 60 (NRELa 2008). Like the dew point in Phoenix, the high dry bulb in Houston is nearer the average in Doha, and the average in Houston nearer the low in Doha. Houston also sees much lower lows in the winter. Figure 61 shows the dew point in Houston compared to Doha's. The dew points of the two locations are much more similar, with the average and low in Houston even exceeding that in Doha during early summer, when Doha's weather is drier.

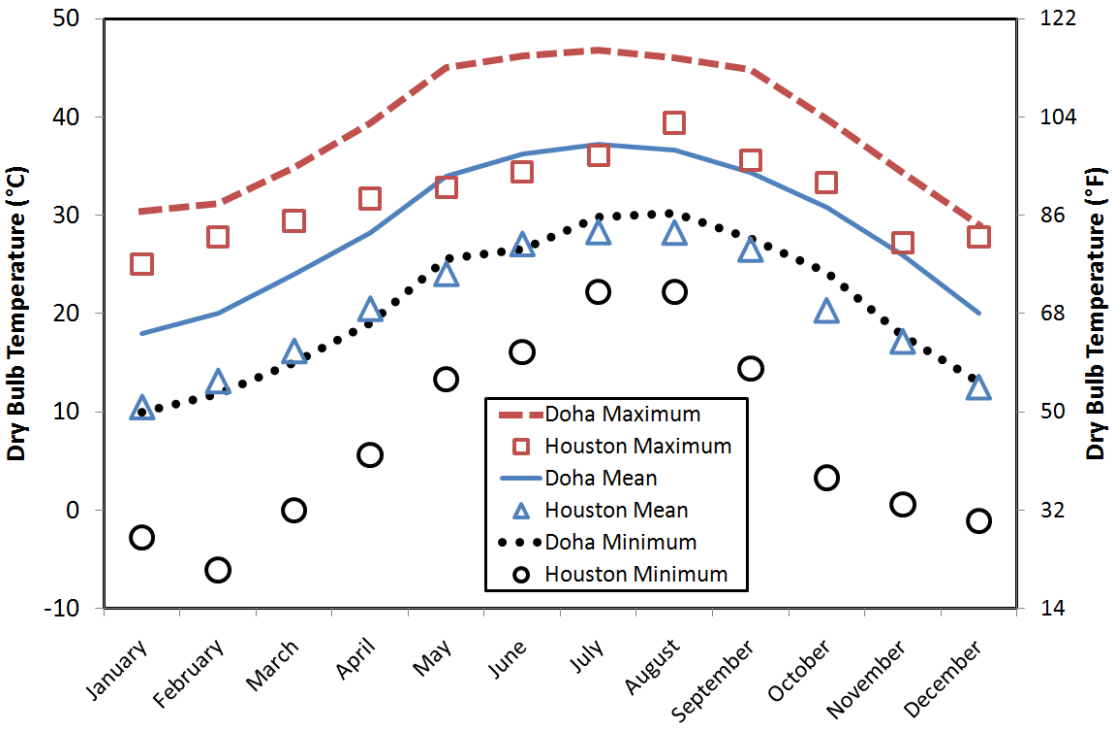


Figure 60. Doha vs. Houston daily high, low, and mean dry bulb by month.

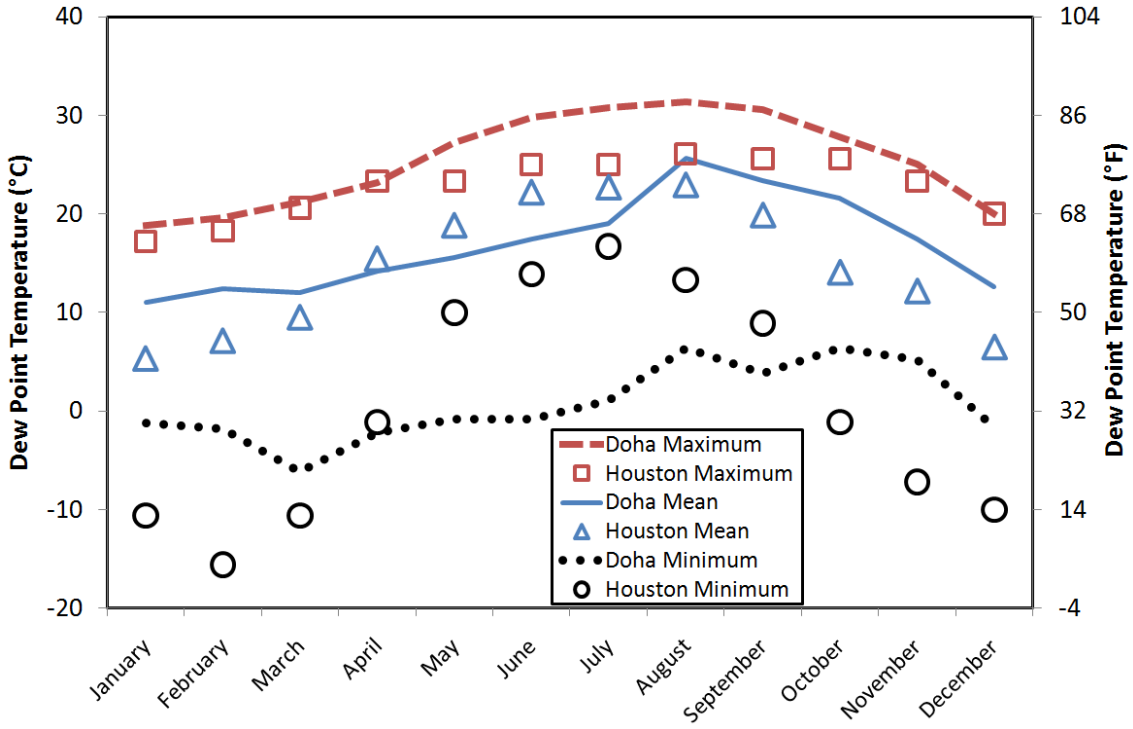


Figure 61. Doha vs. Houston daily high, low, and mean dew point by month.

Baseline and improved simulations were run for the TAMUQ building with the same operation schedules, only with different weather inputs for Phoenix and Houston. The difference in altitude for Phoenix was neglected. Equipment capacities were also resized to fit the respective climates. The results are presented and discussed in the following sections.

### 6.1 Variable Speed Fan Operation

Changing from constant speed fan operation to variable speed fan operation at TAMUQ with a 30% of design flow minimum flow rate was simulated for Phoenix and

Houston. The results were compared to those found in Section 5.1.2 for Doha. Figure 62 shows the monthly electrical consumption for the TAMUQ building when located in the three locations. Electricity use for each location is shown for the base case and for true VAV operation.

VAV operation yielded savings for all three location, but to different degrees. Savings potential also depended on the time of year. For the base case, Houston was the highest electricity user, followed by Phoenix, and then Doha. The differences were mostly due to heating requirements in the winter for Houston and Phoenix, where winter temperatures are lower. In the summer, the three were approximately the same. This is because the peak sensible cooling loads to which the AHU's are designed are similar, and for constant speed operation, the AHU fans remain closer to the design flow, and use nearly constant power.

For the variable speed simulations, winter reheat and overcooling energy were reduced for all three locations, although overall heating trends remained. Differences in summer energy use were more apparent. Because of Houston's lower dry bulb temperatures in the summer, allowing full VAV operation saved enough to make it the lowest summer consumer. Phoenix and Doha also realized summer savings from VAV operations, but more so for Doha. Dry bulb temperatures and outside convective cooling loads are similar in the two, as was shown in Figure 58. However, the average solar load in Phoenix during the summer is around 30% more than in Abu Dhabi, from which the solar loads for nearby Doha were taken (ASHRAE 2001, NRELb 2008). The total

sensible cooling load was therefore greater in Phoenix, requiring more fan power, and more electricity overall.

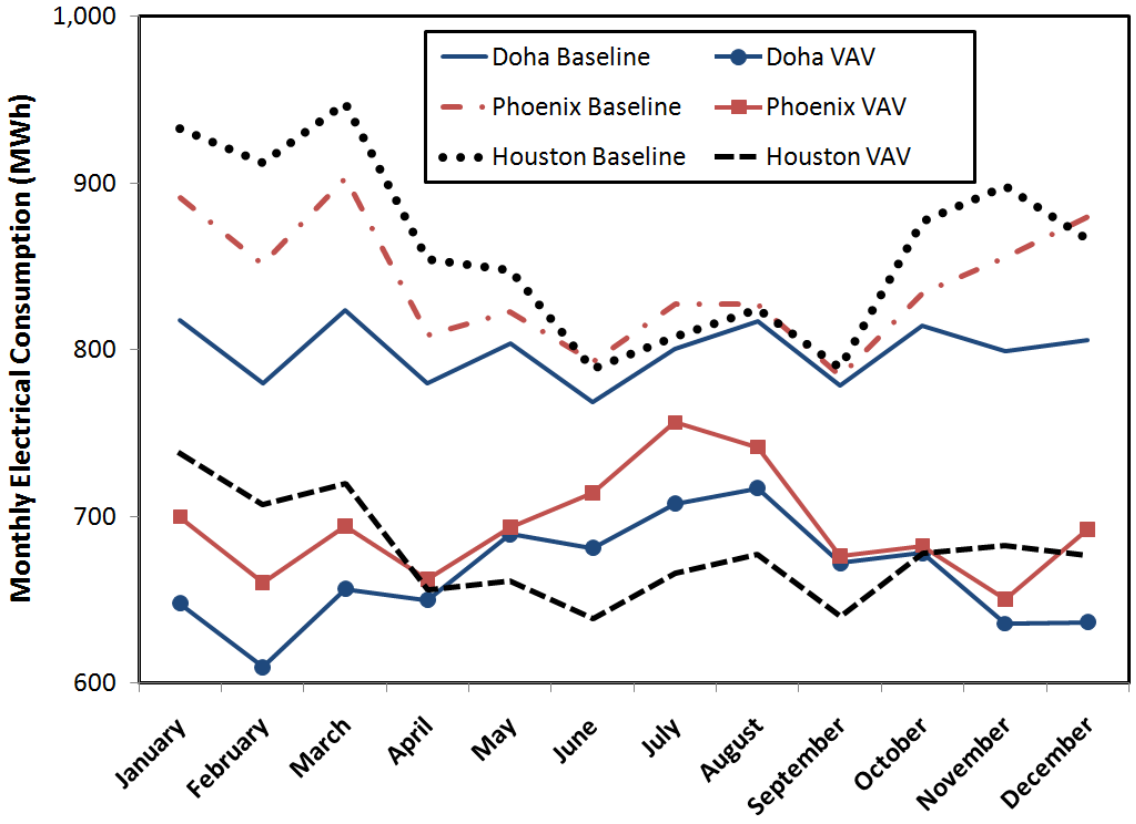


Figure 62. Monthly electricity use for Doha, Phoenix, and Houston.

Figure 63 shows the monthly chilled water consumption for the three different locations, using both constant and variable speed operation. As expected, the chilled water load in Doha was significantly higher due to the combination of sensible and latent loads on the cooling coils. Converting to full VAV operation had the most dramatic effect for Houston, just as it did for electricity consumption. This is again because

Houston's lower summer temperatures allowed for more flow modulation once in a variable mode, and thus lighter loads on the AHU's.

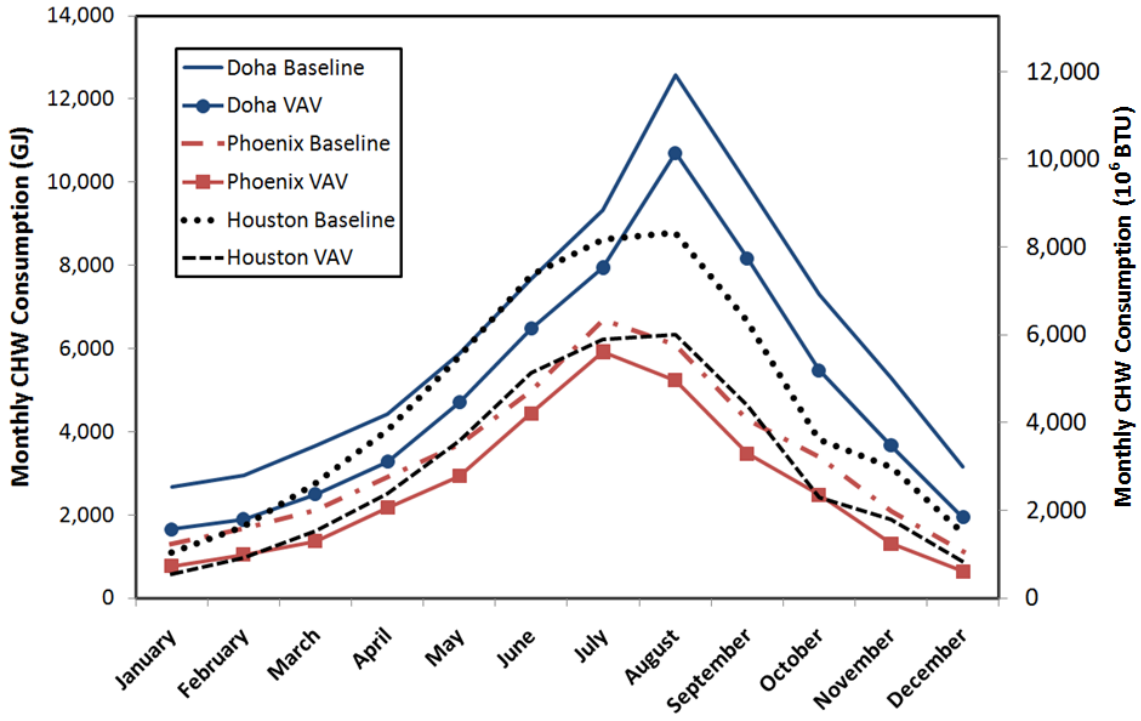


Figure 63. Monthly chilled water consumption for Doha, Phoenix, and Houston.

Figure 64 shows the effect of VAV operation on the equivalent electricity use of HVAC components for the three locations. Chilled water consumption was converted to an equivalent electricity used by the central plant chillers using Equation 11. Note that reheat made up a much larger portion of the electricity usage in Houston, whereas in Doha, chiller consumption was much higher. In Phoenix, fan consumption was dominant, while chiller consumption was low. Consumption from pumps had negligible differences across both location and fan operation. Again, because dry bulb temperatures

and sensible cooling loads are lower overall and reach lower lows in Houston, full VAV operation yielded significant savings, nearly 70%, from AHU fans.

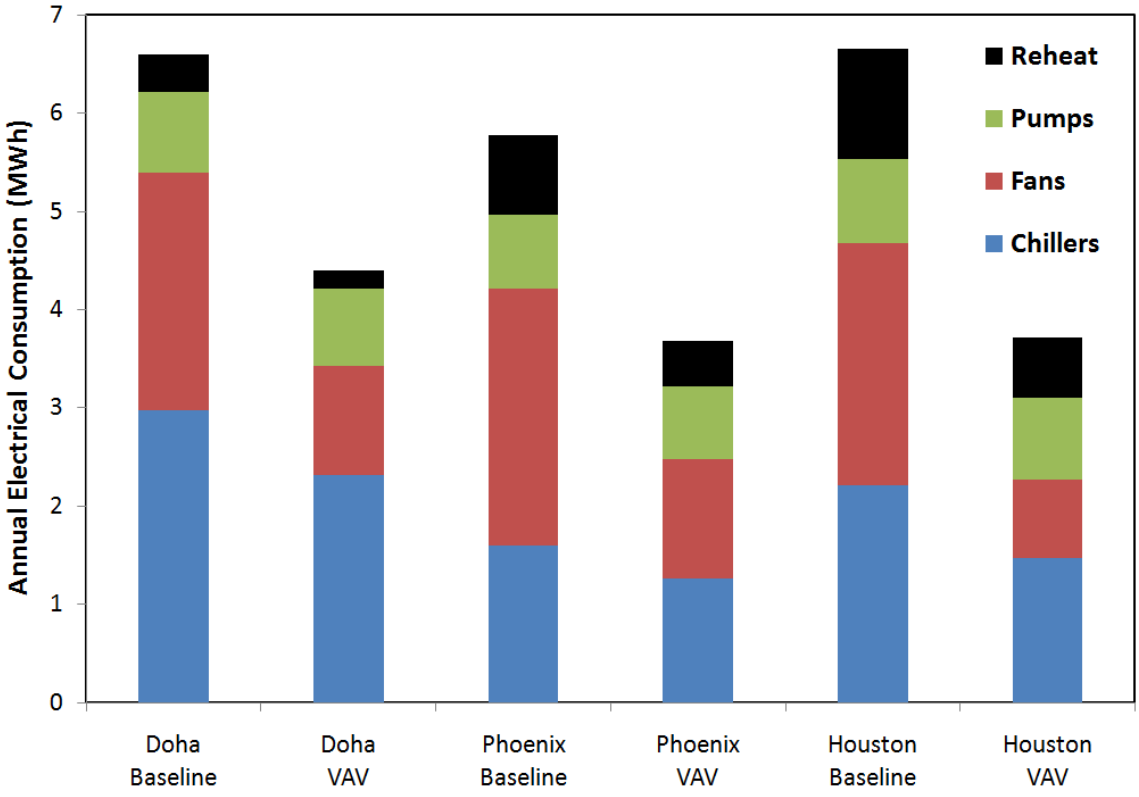


Figure 64. VAV effect on equivalent electricity use for three locations.

Figure 65 shows the total yearly electrical cost and percentage HVAC savings resulting from VAV operation. Cost savings in Phoenix were slightly lower than in Doha, but a higher fraction of the HVAC consumption was saved because Phoenix used less energy in the base case. The highest potential savings from converting to VAV operation were seen in Houston, at nearly 45% and $121,000. The base case in Houston and Doha used approximately the same equivalent electricity, but switching to variable speed operation saved over 30% more in utility costs when performed in Houston. This

again was due to Houston's more variable and lower dry bulb temperatures during the summer, which allowed more fan modulation and resulted in significant fan savings.

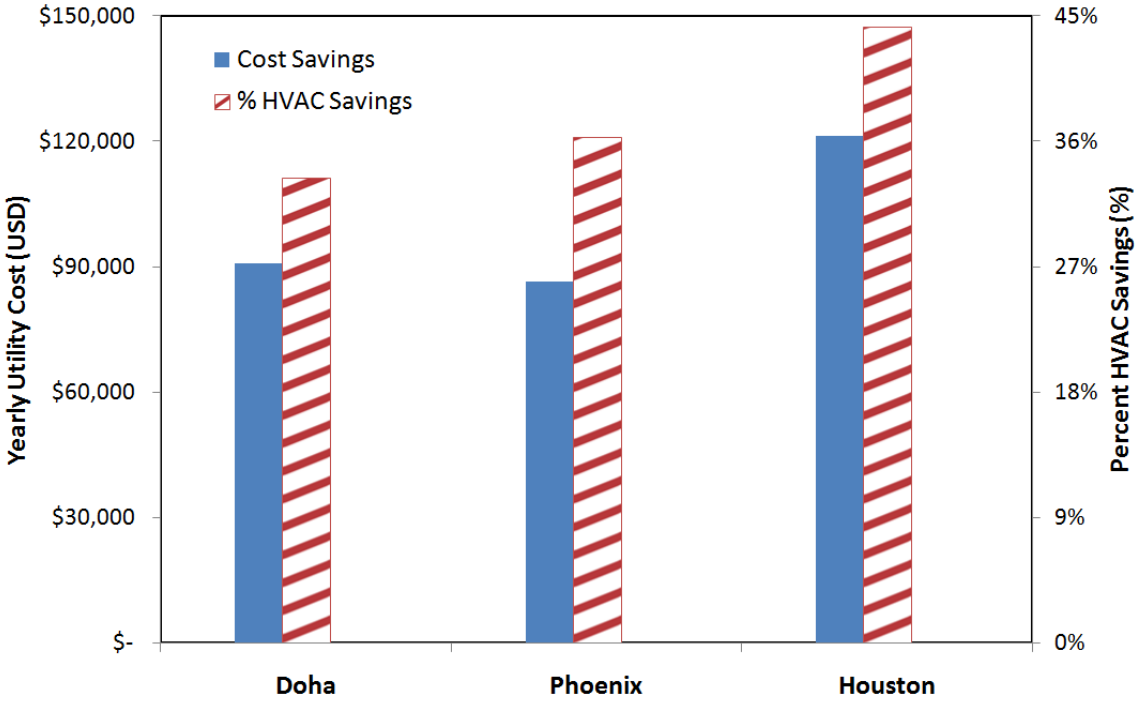


Figure 65. Potential cost and percent HVAC energy savings for three locations.

## 6.2 Outside Air Control

The effect of outside air control in the different locations was also studied. Figure 66 shows the monthly chilled water consumption at the three locations for the base case, and for cases using a DOAS. As expected, outside air control yielded large savings for Doha and Houston, where high sensible and latent loads were saved by reducing outside

air flows, while savings for Phoenix were smaller because outside air was considerably drier.

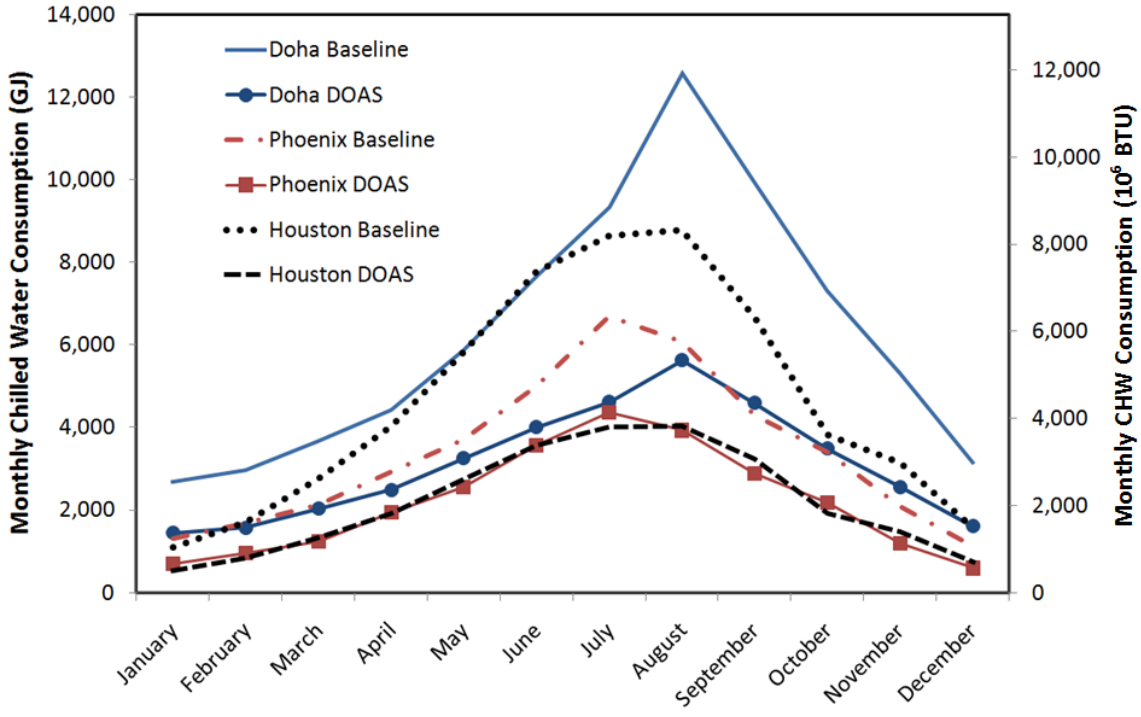


Figure 66. Chilled water use for base case vs. a DOAS in the three locations.

The chilled water load for the outside air controlled simulation in Phoenix and Houston seem to be nearly identical. This is coincidence however, as Figure 67 shows when the load is split into its latent and sensible components. The sensible load in Phoenix is extreme while the latent load is almost nonexistent for much of the year. Houston's latent and sensible loads are both in the middle, making the total loads for the two look similar. Integrated over the whole year, both the latent and sensible loads in Doha are the highest of the three locations, which explains the higher savings resulting

from DOAS operation there. These total potential savings from a DOAS over 30% minimum VAV operation without outside air control are shown in Figure 68 in monetary terms. Converting a standard VAV system using constant design fractions of outside air to a DOAS in Doha could save nearly twice as much annual chiller electricity costs than in Houston, and almost four times the potential in Phoenix. Addition of a DOAS would be a more profitable investment in extreme climates such as Doha's, where both latent and sensible savings from the coil would be high, as shown in Figure 68.

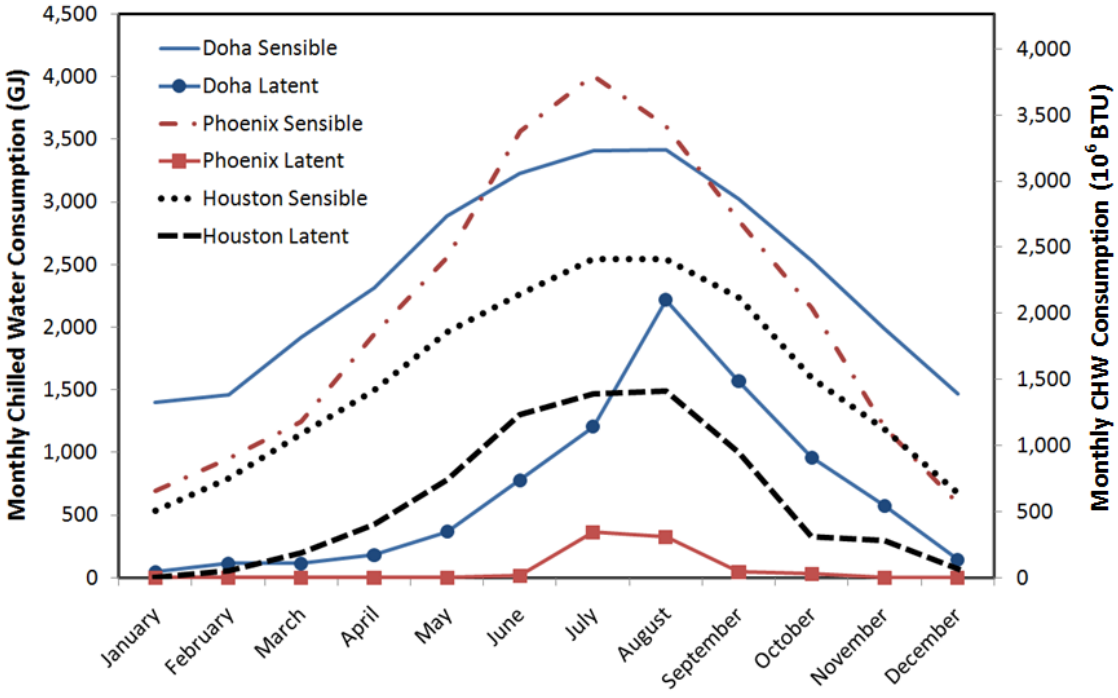


Figure 67. Latent and sensible components of DOAS chilled water consumption.

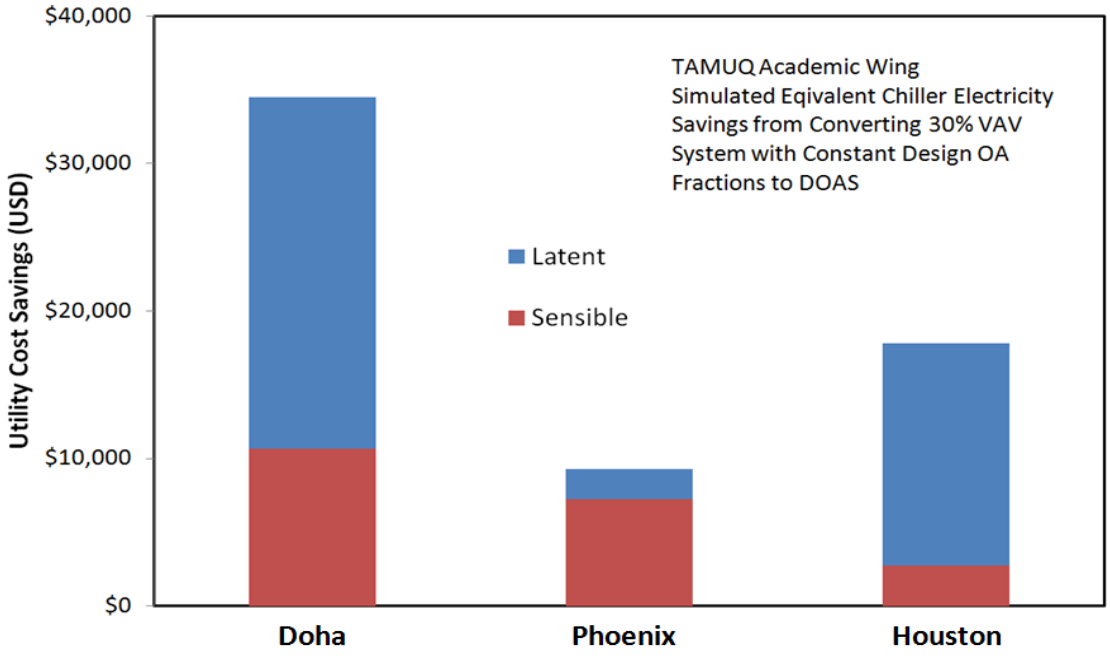


Figure 68. Equivalent utility cost and chilled water energy savings.

### 6.3 Fan Powered Terminal Units

The FPTU model developed as part of this project had some limitations. Only eight inch inlet FPTU's were considered, which limited the airflow to individual zones that could be reliably used in the empirical relations. The zones and associated design flows used for the FPTU study in Doha were already at either end of this valid range. Changing these inputs based on the different heating and cooling loads experienced in other climates gave invalid results from the model as it was built. It is recommended as a future study that the FPTU model be expanded for multiple box sizes and wider flow ranges so it may be more robust in predicting FPTU performance in many situations.

# CHAPTER VII

# SUMMARY AND CONCLUSIONS

Building energy use makes up nearly a third of total energy consumption. Of this third used in buildings, as much as 45% is used to heat, ventilate, and air condition them. In the Middle East, new building construction is steadily increasing. In addition, the extreme hot and humid conditions there put even further strain on HVAC systems.

The purpose of this research was to quantify the potential energy savings from improving HVAC operation in a building in Doha, Qatar. The TAMUQ engineering building in particular was studied as an example of a building in an extreme hot and humid environment. To test HVAC efficiency improvement measures, a computer model of the building was constructed using EnergyPlus. The model was validated using building chilled water and electricity data that were metered prior to building the model.

Building power usage on the academic side was metered from four switchgear in the academic substation, using three-phase power meters. Chilled water flow rates were metered using ultra-sonic flow meters while supply and return temperatures were metered with RTD's. Metering took place over a 16 month period, and 12 months of data were chosen between October, 2009 and September, 2010 for direct comparison with the baseline computer model.

Analysis of the metered energy data, as well observations of equipment and BMS readouts, revealed two major operational flaws in the building's HVAC system. Although all 46 AHU's were equipped with variable speed fans, the fans were operated

at constant speed year-round. Furthermore, AHU outside air dampers were kept 100% open at all times, inducing and cooling excess hot and humid air, even during low occupancy periods. These issues were addressed in simulations beyond the base case. A third HVAC alteration, retrofitting the building with FPTU's, was also studied.

The base case simulation matched the monthly metered electricity usage to within ±5%. When comparing average hourly electricity usage during high, medium, or low occupancy, and hot or mild days, 95% of the simulated data were within ±10% of the metered data. All simulated monthly chilled water consumption data were within ±18% of the metered data, with an R-squared correlation coefficient of 0.95. The correlation coefficient suggested the seasonal change in chilled water consumption was well captured in the model.

Operating the AHU fans at variable speed to track part loads showed potential for saving 16% on annual electricity usage over the base case, when the minimum VAV flow setting was set to 30% of cooling design flow. Potential chilled water savings at this setting were 22% over the base case. Total equivalent electricity savings were calculated by converting chilled water savings to chiller electrical consumption savings. This equated to $90,000 of potential utility cost savings annually at local utility rates. Changing minimum flow settings to allow for further air modulation during part load periods was found to have negligible additional energy savings beyond 20% of cooling design flow.

In addition to variable speed fan operation, outside air control was added to the model to control outside air intake to IAQ minimums according to ASHRAE 62.1. No

electricity savings were realized, but chilled water consumption was reduced by 39% from the base case. Monetary savings from reduced chiller electrical consumption were $20,000 more than variable speed fan operation alone, bringing total potential yearly utility savings to $110,000. A simple analysis of productivity costs due to reduced IAQ was conducted for the base case and the controlled case. Increased under-compliance with IAQ standards when controlling outside air was shown to potentially cost more to productivity than it might save in utilities. To remedy this, a DOAS was proposed and modeled to precisely control outside air to IAQ minimums without under-ventilating certain zones. A DOAS was shown to save an additional $4,000 per year in equivalent electrical utility costs over controlling mixed air fractions to ASHRAE 62.1 multi-zone standards. Presumably, a DOAS would also eliminate productivity costs from under-ventilation.

A computer model was built outside of EnergyPlus, but using EnergyPlus-generated heating and cooling loads as inputs, to simulate the performance of FPTU's on a representative TAMUQ AHU. Both parallel and series fan configurations were studied, each with both ECM and SCR motor control. FPTU's were compared to a base case with standard no-fan VAV terminal units. Due to restrictions on discharge air temperature aimed at avoiding zone stratification, parallel FPTU's showed marginal savings over the base case at minimum VAV flow settings below approximately 20% of cooling design flow. Series FPTU's used more energy than parallel FPTU's and non-FPTU's for all flow settings. No significant difference was found between control types, but further study is needed to investigate the benefits of ECM control when the terminal fan flow is

allowed to modulate to track loads. The model showed that parallel FPTU's consume only slightly more energy than a non-FPTU system even when minimum flow setting is high. Energy used to run the terminal fan during part load periods is not wasted by any means, and secondary benefits to FPTU's such as increased air movement at all times can therefore be considered an advantage to a traditional no-fan system.

A secondary purpose of this research was to study the benefits of HVAC improvements in the extreme heat and humidity of Doha, Qatar, compared to slightly milder climates. Houston and Phoenix were chosen as comparison locations, being humid but not as hot, and hot but not as humid, respectively.

It was found that conversion to variable speed fan operation was more beneficial in Houston and Phoenix than in Doha. This was because of the lower low temperatures in these locations. VAV operation saves the most over constant volume during part load periods and milder climates provide more. Moving from the constant speed base case to variable speed fan operation resulted in potential monetary savings 30% higher in Houston than those found for Doha. TAMUQ air-handlers are already equipped with VFD's, so this finding is less applicable there. TAMUQ fans should be switched to variable speed operation immediately regardless. However, as a general guide to sustainable building in extreme hot and humid climates, VAV operation is a better investment where winters are colder and nightly summer lows are lower.

In contrast, a DOAS was shown to be an excellent investment in climates such as Doha's, where reducing outside air intake reduces both latent and sensible cooling coil loads substantially. Over variable speed fan operation alone, adding a DOAS had

additional potential utility cost savings of $35,000 in Doha, compared to $18,000 in Houston and just $9,000 in Phoenix.

The empirical regression equations used to model FPTU performance were limited to a single box size, and thus a finite flow range. Inputs different from those specific to TAMUQ in Doha were outside this valid range. As a future study, the FPTU model should be expanded to multiple box sizes to make it more robust as a research and design tool.

# REFERENCES

ASHRAE. 2001. *Abu Dhabi IWEC Weather Data WMO#412170.* Atlanta, GA: American Society of Heating, Refrigerating and Air-conditioning Engineers.

ASHRAE. 2004. *ASHRAE Standard 55: Thermal Environmental Conditions for Human Occupancy.* Atlanta, GA: American Society of Heating, Refrigerating and Air-conditioning Engineers.

ASHRAE. 2005. *ASHRAE Fundamentals Handbook*. Atlanta, GA: American Society of Heating, Refrigerating and Air-conditioning Engineers.

ASHRAE. 2010a. *ASHRAE Research Strategic Plan 2010-2015*. Atlanta, GA: American Society of Heating, Refrigerating and Air-conditioning Engineers.

ASHRAE. 2010b. *ASHRAE Standard 62.1-2010: Ventilation for Acceptable Indoor Air Quality.* Atlanta, GA: American Society of Heating, Refrigerating and Air-conditioning Engineers.

ASHRAE. 2010c. *ASHRAE Standard 90.1-2010: Energy Standard for Buildings Except Low-Rise Residential Buildings.* Atlanta, GA: American Society of Heating, Refrigerating and Air-conditioning Engineers.

Bryant, J., M. Davis, D. O'Neal, and A. Cramlet. 2009. Experimental verification of a three zone VAV system model operating with fan powered terminal units (RP-1292). *ASHRAE Transactions* 115(1):314-321.

Cho, S., J. Mukhopadhyay, C. Culp, J. Haberl, and B. Yazdani. 2007. Recommendations for 15% above-code energy-efficiency measures for commercial office buildings. *Proceedings of the Fifteen and a Half Symposium on Improving Building Systems in Hot and Humid Climates,* San Antonio, TX:1-12.

Cho, Y., and M. Liu. 2009. Minimum airflow reset of single duct VAV terminal boxes. *Building Environments* 44(9):1876-1885.

Cho, Y., M. Liu, G. Wang, J. Wang, and T. Rauscher. 2009. VFD applications for constant volume air-handling units. *ASHRAE Transactions* 155(2):824-830.

Cramlet, A. 2008. Performance of ECM controlled VAV fan powered terminal units. M. S. Thesis, Mechanical Engineering, Texas A&M University, College Station, TX.

Crawford-Brown, D. 2009. A'Samaliah Island, UAE: A case study in sustainability. *Proceedings of Institution of Civil Engineering* 162:60-64.

Crawley, D.B., J.W. Hand, M. Kummert, and B.T. Griffith. 2005. Contrasting the capabilities of building energy performance simulation programs. *Proceedings of the Ninth International IBPSA Conference*, Montreal, Canada:231-238.

Davis, M., D. O'Neal, J. Bryant, and A. Cramlet. 2009. Modeling the performance of single-duct VAV systems that use fan powered terminal units. *ASHRAE Transactions* 115(1):307-313.

DOE. 2003. *2003 CBECS Detailed Tables*. Accessed at http://www.eia.gov/emeu/cbecs/cbecs2003/detailed_tables_2003/2003set14/2003pdf/c3a.pdf on June 5, 2011. Washington, DC: US Department of Energy.

DOE. 2011. *OpenStudio Plug-in for Google SketchUp.* Accessed at http://apps1.eere.energy.gov/buildings/energyplus/openstudio.cfm#about on April 28, 2011. Washington, DC: US Department of Energy.

Dong, B., and B. Andrews. 2009. Sensor-based occupancy behavioral pattern recognition for energy and comfort management in intelligent buildings. *Proceedings of the Eleventh International IBPSA Conference,* Glasgow, Scotland:1444-1451.

Fanger, P.O. 1972. *Thermal Comfort: Analysis and Applications in Environmental Engineering*. New York: McGraw-Hill.

Finkel, L. 2005. Student study hours per credit hour. *UNH Faculty Senate Motion #IX-M21.* University of New Hampshire, Durham, NH.

Fischer, J.C. 2000. A new ventilation system integrates total energy recovery, conventional cooling and a novel "passive" dehumidification wheel to mitigate the energy, humidity control and first cost concerns often raised when designing for ASHRAE Standard 62-1999 compliance. *Proceedings of the Twelfth Symposium on Improving Building Systems in Hot and Humid Climates,* San Antonio, TX:24-33.

Furr, J., D. O'Neal, M.A. Davis, J.A. Bryant, and A. Cramlet. 2008. Performance of VAV parallel fan powered terminal units: Experimental results and models. *ASHRAE Transactions* 114(1):83-90.

Gidwani, B.N. 1984. Optimization of chilled water systems. *Proceedings of the First Symposium on Improving Building Systems in Hot and Humid Climates,* College Station, TX:83-91.

Hartman, T. 1989. TRAV – A new HVAC concept. *Journal of Heating/Piping/Air Conditioning* July 1989:69-73.

Hedge, A. and D.E. Gayden. 2010. Indoor environment conditions and computer work in an office. *HVAC&R Research* 16(2):123-138.

Honeywell. *Demand Response Services*. Accessed at https://buildingsolutions.honeywell.com/Cultures/en-US/Markets/Utilities/DemandResponse/ on May 2, 2011. Dallas, TX: Honeywell.

Hunn, B. 2010. 35 years of standard 90.1: Early and mid-1970s. *ASHRAE Journal* 52(3):36-38.

Joo, I., M. Liu, and G. Liu. 2007. Application of fan airflow stations in air-handling units. *Energy Engineering* 104(2):66-67,69-80.

Kahramaa. 2011. *Tariff*. Accessed at http://www.km.com.qa/en/customer/Pages/RateInformation.aspx on May 1, 2011.

Kamaruzzaman, S.N., C.O. Egbu, E. Zawawi, A. Ali, and A. Che-Ani. 2011. The effect of indoor environmental quality on occupants' perception of performance: A case study of refurbished historic buildings in Malaysia. *Energy and Buildings* 43:407-413.

Kline, S.J. and F.A. McClintock. 1953. Describing uncertainties in single-sample experiments. *Mechanical Engineering* January 1953:3.

Kumar, M., and I.N. Kar. 2010. Design of model-based optimizing control scheme for an air-conditioning system. *HVAC&R Research* 16(5):565-597.

Lan, L., P. Wargocki, and Z. Lian. 2011. Quantitative measurement of productivity loss due to thermal discomfort. *Energy and Buildings* 43:1057-1062.

Lavigne, K. 2009. Assisted calibration in building simulation – Algorithm description and case studies. *Proceedings of the Eleventh International IBPSA Conference,* Glasgow, Scotland:1498-1505.

Liu, M., M. Abbas, Y. Zhu, and D.E. Claridge. 2002. Terminal box airflow reset: An effective operation and control strategy for comfort improvement and energy conservation. *Proceedings of the Thirteenth Symposium on Improving Building Systems in Hot and Humid Climates,* Houston, TX.

Mathews, E.H., C.P. Botha, D.C. Arndt, and A. Malan. 2001. HVAC control strategies to enhance comfort and minimize energy usage. *Energy and Buildings* 33:853-563.

Merwin, E. and H. Bynum. 1999. Variable flow – A control engineer's perspective. *ASHRAE Journal* 41(1):26-30.

McQuay International. 2010. *Centrifugal Compressor Water Chillers, Catalog 605-1*. Minneapolis, MN: McQuay International.

Mumma, S.A. 2001. Dedicated outdoor air in parallel with chilled ceiling system. *Engineered Systems Magazine.* October 26, 2001. Accessed at http://www.esmagazine.com/Articles/Feature_Article/1aa5c1d734ca8010VgnVCM100010f932a8c0____ on April 29, 2011.

Ning, M., and M. Zaheeruddin. 2010. Neuro-optimal operation of a variable air volume HVAC&R system. *Applied Thermal Engineering* 30:385-399.

NREL. 2008a. *TMY Data for Houston Bush Intercontinental, Houston, TX.* Golden, CO: National Renewable Energy Laboratory.

NREL. 2008b. *TMY Data for Phoenix Sky Harbor International Airport, Phoenix, AZ.* Golden, CO: National Renewable Energy Laboratory.

OTBD Weather Station. 2011. *Weather history for Doha, Qatar*. Accessed at: http://www.wunderground.com/history/airport/OTBD/2010/8/24/MonthlyHistory.html?MR=1 on February 25, 2011.

Peak Load Management Alliance. 2002. *Demand Response: Principles for Regulatory Guidance*. Jupiter, FL: Peak Load Management Alliance.

Platt, G., J. Li, R. Li, G. Poulton, G. James, and J. Wall. 2010. Adaptive HVAC zone modeling for sustainable buildings. *Energy and Buildings* 42:412-421.

Raftery, P., M. Keane, and A. Costa. 2009. Calibration of a detailed simulation model to energy monitoring system data: A methodology and case study. *Proceedings of the Eleventh International IBPSA Conference,* Glasgow, Scotland:1199-1206.

Shaughnessy, R.J., U. Haverinen-Shaughnessy, A. Nevalainen, and D. Moschandreas. 2006. A preliminary study on the association between ventilation rates in classrooms and student performance. *Indoor Air* 16:465-468.

Shrestha, S.S. 2006. Empirical validation of building energy simulation software: EnergyPlus. M.S. Thesis, Mechanical Engineering, Iowa State University, Ames, Iowa.

Sierra Instruments. 2009. *Innova-Sonic™ Model 205 Dedicated Instruction Manual*. Monterey, CA: Sierra Instruments.

Sterling, E., C. Collett, S. Turner, and C. Downing. 1994. Commissioning to avoid indoor air quality problems. *Proceedings of the ASHRAE Transactions Symposia, January 1994*:867.

TAMUQ. 2010. *Tuition, Fees, and Financial Aid.* Doha, Qatar: Accessed at http://admissions.qatar.tamu.edu/194.aspx on April 30, 2011. Texas A&M University at Qatar.

Tavares, P. and A. Martins. 2007. Energy efficient building design using sensitivity analysis – A case study. *Energy and Buildings* 39(1):23-31.

Thermal Products Corporation. 2007. *HVAC System Designs*. Tucson, AZ: Thermal Products Corporation.

Trane. 2004. *Fan Performance Data for Central-Station Air Handlers*. Davidson, NC: Ingersoll Rand.

Trane. 2010. *Product Catalog: Varitrane™ Products Parallel and Series Fan-Powered*. Davidson, NC: Ingersoll Rand.

Trane. 2011. *Product Catalog: Varitrane™ Products Single Duct/Dual Duct Units*. Davidson, NC: Ingersoll Rand.

Walker, I.S., and M.H. Sherman. 2006. Ventilation requirements in hot, humid climates. *Proceedings of the Thirteenth Symposium on Improving Building Systems in Hot and Humid Climates,* Orlando, FL.

Wasilowski, H.A., and C.F. Reinhart. 2009. Modeling an existing building in DesignBuilder/EnergyPlus: custom versus default inputs. *Proceedings of the Eleventh International IBPSA Conference,* Glasgow, Scotland:1252-1259.

Wemhoff, A.P. 2010. Application of optimization techniques on lumped HVAC models for energy conservation. *Energy and Buildings* 42:2445-2451.

Zhao, Y., B. Erwine, P. Leonard, A. Lee, B. Pease, and A. Dole. 2010. Evaluation of energy efficient measures in hot and humid climates. *Proceedings of the Seventeenth Symposium on Improving Building Systems in Hot and Humid Climates,* Austin, TX.

Zhu, Y., M. Liu, T. Batten, D. Turner, D. Claridge, B. Keeble, C. Cameron, and R. Hirchak. 2000. A simple and quick chilled water loop balancing for variable flow system. *Proceedings of the Twelfth Symposium on Improving Building Systems in Hot and Humid Climates,* San Antonio, TX:158-162.

Zhu, Y., A. Athar, K. Banks, C. Culp, D. Turner, and B. Yazdani. 2001. Continuous commissioning: A valuable partner to retrofit projects. *Proceedings of the First International Conference for Enhanced Building Operations,* Austin, TX.

# APPENDIX A

# NOMENCLATURE

| | |
|---|---|
| $A$ | Floor area [$m^2$, $ft^2$] |
| AC | Alternating Current |
| AHU | Air Handling Unit |
| $b$ | Fan power coefficient |
| BMS | Building Management System |
| $C$ | Cost [$] |
| CHW | Chilled Water |
| COP | Coefficient of Performance |
| $c_p$ | Specific heat [J/kg-°C, BTU/lb-°F] |
| $D$ | Occupant diversity |
| DB | Dry Bulb Temperature [°C, °F] |
| DC | Direct Current |
| DOAS | Dedicated Outside Air System |
| DP | Dew Point Temperature [°C, °F] |
| DX | Direct Expansion |
| ECM | Electronically Commutated Motor |
| $E_v$ | Ventilation efficiency |
| EPW | EnergyPlus Weather |
| ESL | Energy Systems Laboratory |

| | |
|---|---|
| EUI | Energy Use Index [kWh/m$^2$/yr, kBTU/ft$^2$/yr] |
| $f$ | Electrical frequency [Hz] |
| FCU | Fan Coil Unit |
| FPTU | Fan Powered Terminal Unit |
| $h_{fg}$ | Latent heat of vaporization of water [J/kg, BTU/lb] |
| HVAC | Heating, Ventilation, and Air Conditioning |
| IAQ | Indoor Air Quality |
| IDF | Intermediate Distribution Frame |
| $IPLV$ | Integrated Part Load Value [kW/ton] |
| $k$ | Building material thermal conductivity [W/m-°C, BTU/hr-ft-°F] |
| $K$ | Pressure factor |
| $m$ | Minimum VAV flow fraction |
| $N$ | Occupancy |
| $S$ | Fan speed [RPM] |
| $p$ | Pressure [Pa, in. w.g.] |
| $P$ | Electrical Power [W] |
| $Q$ | Cooling load [W, BTU/hr] |
| $R_a$ | IAQ area multiplier [L/s-m$^2$, CFM/ft$^2$] |
| RH | Relative Humidity [%RH] |
| $R_p$ | IAQ occupancy multiplier [L/s-person, CFM/person] |
| RPM | Revolutions per Minute |
| RTD | Resistive Temperature Device |

| | |
|---|---|
| SCR | Silicon Controlled Rectifier |
| $\Delta T$ | Temperature rise [°C, °F] |
| TAMUQ | Texas A&M University at Qatar |
| $t_{avg}$ | Duration of IAQ occupancy average [min] |
| TMY | Typical Meteorological Year |
| $U_{total}$ | Building envelope heat transfer coefficient [W/°C, BTU/hr-°F] |
| $v$ | Voltage [V] |
| $\dot{V}$ | Volume flow rate [L/s, CFM] |
| VAV | Variable Air Volume |
| VFD | Variable Frequency Drive |
| $\dot{W}$ | Fan power [W, hp] |
| WOF | Wide Open Flow |
| WB | Wet Bulb Temperature [°C, °F] |
| $x$ | Outside air fraction |
| $X_s$ | Average outside air fraction |
| $Z_{pz}$ | Primary outside air fraction of a zone |
| $\alpha$ | FPTU regression coefficients |
| $\beta$ | Switchgear power fraction |
| $\delta$ | Building material thickness [m, ft] |
| $\varepsilon_{people}$ | Expected peak occupant density [persons/m$^2$, persons/ft$^2$] |
| $\eta$ | Fan efficiency |
| $\mu$ | Absolute uncertainty |

| | |
|---|---|
| $\rho$ | Density [$kg/m^3$, $lb/ft^3$] |
| $\rho_{solar}$ | Material reflectance of short-wave radiation |
| $\rho_{visible}$ | Material reflectance of long-wave radiation |
| $\tau_{solar}$ | Material transmittance of short-wave radiation |
| $\tau_{visible}$ | Material transmittance of long-wave radiation |
| $\psi(t)$ | Probability of peak occupancy occurring at a given time |
| $\omega$ | Moisture content [$kg_{H2O}/kg_{air}$, $lb_{H2O}/lb_{air}$] |

**Subscripts**

| | |
|---|---|
| $\infty$ | Ambient conditions |
| *air* | Air stream |
| *c* | Cooling |
| *CC* | Cooling coil |
| *cl* | Sensible space cooling load |
| *down* | Downstream |
| *h* | Heating |
| *iav* | Inlet air velocity |
| *lat* | Latent component |
| *mixed* | Mixed return and outside air streams |
| *non* | Non-fan powered VAV box |
| *norm* | Normalized |

| | |
|---|---|
| *OA* | Outside Air |
| *obs* | Observed value |
| *p* | Primary |
| *par* | Parallel FPTU |
| *r* | Return |
| *rh* | Reheat |
| *s* | Supply |
| *ser* | Series FPTU |
| *SP* | Set point |
| *up* | Upstream |
| *w* | Water |
| *X* | Excess |
| *z* | Zone |

# APPENDIX B

# TAMUQ AHU SCHEDULE

Air-handler inputs to the TAMUQ EnergyPlus model were based on HVAC schedules provided by building staff. Table 8 summarizes the academic side AHU design specifications.

Table 8. TAMUQ Air-handler Design Specifications.

| AHU Name | Supply Fan Design Flow (L/s) | Supply Fan Design Outside Airflow (L/s) | Supply Fan External Static (Pa) | Supply Fan Motor Size (kW) | Return Fan Design Flow (L/s) | Return Fan External Static (Pa) | Return Fan Motor Size (kW) | Run-around Coil | Cooling Coil Capacity (kW) |
|---|---|---|---|---|---|---|---|---|---|
| LG/07/0022/AHU | 1155 | 231 | 200 | 3 | 1353 | 200 | 1.5 | N | 11 |
| LG/06/0014/AHU-01 | 3900 | 3900 | 200 | 11 | 2482 | 200 | 4 | Y | 248 |
| LG/06/0014/AHU-02 | 3500 | 3500 | - | 11 | - | - | - | N | 216 |
| 00/07/1028/AHU | 3830 | 651 | 200 | 11 | 2264 | 200 | 4 | N | 74 |
| 00/07/1037/AHU | 2653 | 690 | 200 | 11 | 2264 | 200 | 5.5 | N | 49 |
| 00/04/1045/AHU | 3892 | 1712 | 350 | 11 | 3365 | 250 | 4 | N | 72 |
| 00/04/1052/AHU | 3365 | 505 | 350 | 7.5 | 3226 | 200 | 3 | N | 56 |
| 00/05/1060/AHU | 5213 | 5213 | 100 | 11 | 5845 | 100 | 5.5 | Y | 415 |
| 00/05/1068/AHU | 4052 | 1418 | 200 | 11 | 3753 | 200 | 4 | N | 65 |
| 00/06/1013/AHU | 2870 | 2870 | 200 | 7.5 | 2919 | 200 | 4 | Y | 228 |
| 00/06/1020/AHU | 4463 | 2678 | 200 | 11 | 4674 | 200 | 4 | N | 52 |
| 01/07/2027/AHU | 2265 | 566 | 250 | 5.5 | 1912 | 250 | 2.2 | N | 51 |
| 01/07/2042/AHU | 3390 | 1153 | 300 | 7.5 | 3323 | 300 | 4 | N | 43 |
| 01/04/2049/AHU | 4059 | 1339 | 350 | 11 | 3974 | 350 | 5.5 | N | 53 |
| 01/04/2056/AHU | 2842 | 682 | 300 | 7.5 | 2583 | 300 | 3 | N | 53 |
| 01/05/2064/AHU | 3187 | 3187 | 300 | 11 | 1879 | 300 | 3 | Y | 250 |
| 01/05/2070/AHU | 3187 | 3187 | 300 | 11 | 2850 | 300 | 4 | Y | 250 |
| 01/06/2011/AHU | 3587 | 1148 | 250 | 11 | 2905 | 250 | 4 | N | 85 |
| 01/06/2020/AHU | 3016 | 935 | 300 | 7.5 | 2924 | 300 | 4 | N | 42 |
| 02/07/3019/AHU | 2458 | 418 | 300 | 5.5 | 2189 | 300 | 3 | N | 51 |
| 02/07/3030/AHU | 5200 | 5200 | 250 | 15 | 5800 | 250 | 11 | Y | 414 |
| 02/07/3030/AHU-00 | 7350 | 7350 | - | 18.5 | - | - | - | N | 577 |

Table 8 Continued.

| AHU Name | Supply Fan Design Flow (L/s) | Supply Fan Design Outside Airflow (L/s) | Supply Fan External Static (Pa) | Supply Fan Motor Size (kW) | Return Fan Design Flow (L/s) | Return Fan External Static (Pa) | Return Fan Motor Size (kW) | Run-around Coil | Cooling Coil Capacity (kW) |
|---|---|---|---|---|---|---|---|---|---|
| 02/07/3030/AHU-01 | 7040 | 5843 | 350 | 18.5 | 1700 | 350 | 4 | N | 533 |
| 02/07/3030/AHU-02 | 3600 | 2160 | 350 | 7.5 | 1650 | 350 | 2.2 | N | 162 |
| 02/04/3037/AHU-02 | 5200 | 5200 | 300 | 15 | 5800 | 300 | 11 | Y | 226 |
| 02/04/3045/AHU | 4339 | 4339 | 350 | 15 | 3695 | 350 | 11 | Y | 343 |
| 02/09/3004/AHU | 5300 | 2385 | 500 | 15 | 5000 | 500 | 7.5 | N | 71 |
| 02/09/3007/AHU | 5300 | 2385 | 500 | 15 | 5000 | 500 | 7.5 | N | 71 |
| 02/05/3053/AHU | 5300 | 5300 | 400 | 15 | 5556 | 400 | 11 | Y | 419 |
| 02/05/3059/AHU | 5113 | 5113 | 400 | 15 | 5306 | 400 | 11 | Y | 404 |
| 02/06/3010/AHU | 5150 | 5150 | 250 | 15 | 5550 | 250 | 11 | Y | 122 |
| 02/06/3012/AHU | 3246 | 3246 | 150 | 11 | 3246 | 150 | 7.5 | Y | 80 |
| 02/09/3002/AHU-01 | 4520 | 1808 | 300 | 11 | 4410 | 300 | 7.5 | N | 56 |
| 02/09/3002/AHU-00-01 | 2530 | 961 | 350 | 7.5 | 2430 | 350 | 4 | N | 34 |
| 02/09/3002/AHU-00-02 | 2530 | 961 | 350 | 7.5 | 2430 | 350 | 4 | N | 34 |
| 03/08/3064/AHU | 6000 | 2400 | 400 | 15 | 5400 | 400 | 11 | N | 100 |
| 03/08/3070/AHU | 6000 | 2400 | 400 | 15 | 5400 | 400 | 11 | N | 100 |
| 03/08/3061/AHU | 6000 | 2400 | 400 | 15 | 5400 | 400 | 11 | N | 100 |
| 03/08/3086/AHU | 6000 | 2400 | 400 | 15 | 5400 | 400 | 11 | N | 100 |
| 03/08/5004/AHU-00 | 4610 | 2305 | 400 | 15 | 4610 | 400 | 7.5 | N | 71 |
| 03/08/5004/AHU-01 | 7840 | 1960 | 350 | 18.5 | 7840 | 350 | 11 | N | 227 |
| 03/08/5004/AHU-02 | 4000 | 3200 | 250 | 11 | 1000 | 250 | 1.5 | N | 128 |
| 03/08/5004/AHU-03 | 1120 | 1120 | 200 | 3 | 8000 | 200 | 4 | N | 89 |
| 03/08/5004/AHU-04 | 7000 | 7000 | 250 | 18.5 | - | - | - | N | 550 |
| 03/09/5000/AHU | 660 | 198 | 300 | 2.2 | 520 | 300 | 1.1 | N | 21 |
| 00/1035/PAHU | 15860 | 0 | 125 | - | - | - | - | N | 200 |

# APPENDIX C

# ENERGYPLUS BUILDING MATERIAL PROPERTIES

Table 9 shows the material properties used to define the materials that made up the EnergyPlus constructions summarized in Table 4. Thermal capacitance values of windows are considered negligible in EnergyPlus and unused.

Table 9. EnergyPlus Building Material Properties.

| Name | Roughness | Thickness (mm) | Conductivity (W/m-K) | Density ($kg/m^3$) | Specific Heat (J/kg-K) | Solar Transmittance | Visible Transmittance | Infrared Transmittance |
|---|---|---|---|---|---|---|---|---|
| 1mm metal surface | Smooth | 0.8 | 45.28 | 7824 | 500 | 0 | 0 | 0 |
| 25mm insulation board | Medium Rough | 25.4 | 0.03 | 43 | 1210 | 0 | 0 | 0 |
| 50mm insulation board | Medium Rough | 50.8 | 0.03 | 43 | 1210 | 0 | 0 | 0 |
| 19mm gypsum board | Medium Smooth | 19 | 0.16 | 800 | 1090 | 0 | 0 | 0 |
| 100mm lightweight concrete | Medium Rough | 101.6 | 0.53 | 1280 | 840 | 0 | 0 | 0 |
| Acoustic tile | Medium Smooth | 19.1 | 0.06 | 368 | 590 | 0 | 0 | 0 |
| 100mm brick | Medium Rough | 101.6 | 0.89 | 1920 | 790 | 0 | 0 | 0 |
| 200mm heavyweight concrete | Medium Rough | 203.2 | 1.95 | 2240 | 900 | 0 | 0 | 0 |
| 200mm concrete block | Medium Rough | 203.2 | 1.11 | 800 | 920 | 0 | 0 | 0 |
| 25mm wood | Medium Smooth | 25.4 | 0.15 | 608 | 1630 | 0 | 0 | 0 |
| 4mm air gap | - | 4 | 0.027 | - | - | 1 | 1 | 1 |
| 5mm air gap | - | 5 | 0.027 | - | - | 1 | 1 | 1 |
| Clear 3mm glass | Smooth | 3 | 0.9 | - | - | 0.837 | 0.898 | 0 |

# VITA

Name: Mitchell Ryan Bible

Address: 3123 TAMU

College Station, TX 77843

Email: mbible505@gmail.com

Education: B.S., Mechanical Engineering, Texas A&M University, 2009

M.S., Mechanical Engineering, Texas A&M University, 2011